PHILOSOPHIAE DOCTOR (PHD)

Delivery of Encapsulated Drugs to Cancer Cells and Tissue: The Impact of Ultrasound

Mercy Afadzi

November 2012

Abstract

Abstract

Encapsulated drugs have improved tumor to normal tissue uptake compared to free drugs, however, the concentration of drugs at the tumor site is still low and heterogeneous due to the tumor microenvironment which serves as barriers for the delivery to the target site. Combining ultrasound (US) with encapsulated drugs might enhance the transport of the encapsulated drug across the vasculature and into tumor tissues. US can also increase local drug release and the uptake of the drug into cancer cells. In this thesis, we combined US with encapsulated drug delivery to improve cancer therapy.

We studied the effect of US exposure parameters that maximizes the release of dierucoyl-phosphatidylcholine (DEPC)-based liposomes *in vitro* using low (300 kHz) and medium (1 MHz) frequency US. The mechanism of US-enhanced cellular uptake of nanoparticles (NPs) (DEPC-based liposomes and polymeric NPs) and dextrans was also investigated using low frequency US and microbubbles (MBs, commercial and a novel drug delivery system – air-filled MBs stabilized by polymeric NPs). An *in vivo study was* conducted to investigate the effect of 300 kHz and 1 MHz US on distribution of liposomal doxorubicin and released drug in tumor tissues using tumor bearing nude mice. Lastly, the effect of NPs PEGylation, surfactant and size on cellular uptake and cell viability was studied. *In vitro* drug release was measured with a spectrophotometer whereby flow cytometry was used to measure cellular uptake of released drug and NPs. Confocal laser scanning microscopy was used to image the distribution and internalization of NPs and released drug.

Drug release was demonstrated in *vitro* and *in vivo* with both frequencies. *In vitro* drug release was shown to be caused by inertial cavitation, whereas *in vivo* drug release was suspected to be cavitation, although it is still unclear. Mechanical index and exposure time were found to determine the total drug release from DEPC-based liposomes *in vitro*. The data also suggests that the duty cycle may be used to control the amount of energy deposited and heat generated in tissue during US-mediated drug delivery. The data from the *in vivo* studies showed increased levels of released doxorubicin in US (for both frequencies) exposed tumors compared to control tumors. Also, we observed higher penetration of liposomes and released doxorubicin from blood vessels in tumors exposed to 1 MHz US as compared to 300 kHz US exposure. This might be attributed to the acoustic radiation force generated during US exposure. *In vitro* data shows the dependency of MBs to obtain efficient intracellular uptake of NPs and dextrans, suggesting the mechanism of the improved cellular uptake to be sonoporation and enhanced endocytosis. Although, the percentage of cells internalizing dextran was size-independent (up to 2 MDa), the 4-kDa dextran was internalized in higher quantities than the larger dextrans. Low frequency US did not enhance the cellular uptake of polymeric NPs; neither in the presence nor absence of MBs stabilized by polymeric NPs.

Cellular uptake of polymeric NPs was largely dependent on the surface properties (PEGylation and surfactant) of the particles. Thus, type and length of PEG molecules as well as the type of surfactant used for emulsification of the particles had effect on the cellular uptake of the particles. Polymeric NPs exhibited dose-response toxicity on PC3 cell line and the toxicity was dependent on the type of surfactant.

Altogether, the results show that US can increase the local drug concentration, enhance the penetration depth of drugs for the drug to reach more cancer cells and increase the permeability of the cells for more drugs to enter the cell thereby improving cancer therapy.

Preface

This thesis has been submitted to the Faculty of Natural Sciences and Technology of the Norwegian University of Science and Technology (NTNU) in partial fulfilment of the requirements for the degree of Philosophiae Doctor (PhD). The project has been funded by the Department of Physics, NTNU and Schlumberger Foundation PhD Fellowship (Faculty for the Future). The work has mainly been carried out at the Department of Physics, NTNU from 2008 to 2012 under the supervision of Professor Catharina de Lange Davies at the Department of Physics, NTNU and Professor Bjørn Angelsen at the Department of Circulation and Medical Imaging (ISB), NTNU.

Acknowledgments

Glory to God for His providence and blessings that enabled me complete this thesis. God has really been my solid rock throughout my academic path. I am incredibly blessed to have His unflinching support.

This thesis is the culmination of my research, with support from several people. I wish to hereby acknowledge those who have been instrumental in the creation of this work and who have inspired and enlightened me.

Foremost, I would like to express my profound gratitude to my Supervisor Professor Catharina de Lange Davies, for the continued support, patience and great enthusiasm throughout these years. Your invested time, scientific expertise and valuable guidance added considerably to my research experience and the overall tone of this thesis. You have inspired me a lot with your knowledge and experience in the field of drug delivery.

Very special thanks to my Co-Supervisor Professor Bjørn Angelsen for introducing me to the field of ultrasound. Your enthusiasm in the field of ultrasound is inspiring. I greatly appreciate your encouragement, insightful comments, constructive criticisms and helpful suggestion in shaping my research.

I specially wish to thank my co-authors for their contributions. I have benefited from the technical assistance and the inspiring discussions with the ultrasound Group at ISB; Associate Professor Tonni F. Johansen, Dr. Rune Hansen, Dr. Svein-Erik Måsøy and Øyvind Strandal. Thanks to Dr. Esben A. Nilssen (Epitarget, Oslo), for insightful comments and fruitful collaboration; Dr. Yrr Mørch and Research Scientist Per Stenstad (SINTEF Material and Chemistry), for collaboration, interesting scientific discussions and constructive feedbacks; Siv Eggen and Yngve Hansen (Department of Physics), for interesting experiments and fruitful discussions. It has been a pleasure to work with you all.

Many colleagues including research engineers, and Master students (Silje Flatabø, Simen Barder, Solvieg Haugstad and Sofie Snistad) I had the pleasure to co-supervise provided support throughout my work. Most notably are; Astrid Bjørkøy and Kristin Sæterbo for their technical assistance at the lab, my wonderful office mate Armend Håti, all the Biophysics and Medical Physics Group and my colleagues at ISB for creating such a positive atmosphere at work.

To Bethel Church (Trondheim and Levanger), thank you all for your prayers, advice, support in diverse forms, all these years. You have been more than a family to me in Norway. A big thanks goes to Pastor Jean and Esperance Mbuebue and all the leaders of the church for creating such a loving environment for all of us.

There were many contributions behind the scene. Thanks to all the people who had direct or indirect impact on me during this research. Your assistance and kindness mean a lot to me.

I would like to also thank my family, for their prayers, encouragement, unwavering love and support throughout my academic endeavor. Special thanks go to my parents Mr. S.K Afadzi and Hannah Enchil, my brothers and sisters; Captain Ebenezer Afadzi and his wife Paulina, Abraham Afadzi and his wife Maggie, Sarah Afadzi, Naomi Afadzi, and Paul Afadzi.

Last, but not the least, my sincere thanks goes to my fiancé (Abednego Tetteh), who has been very supportive and patient all these years, and for encouraging me throughout this experience.

November 2012

Trondheim

Mercy Afadzi

List of Abbreviations

AOT	Aerosol OT
CLSM	Confocal laser scanning microscopy
DEPC	Dierucoyl-phosphatidylcholine
DiD	1,1’-dioctadecyl-3,3,3’,3’-tetramethylindoicarbocyanine, 4’chlorobenzenesulfonate salt
DiR	1,1’-dioctadecyl-3,3,3’,3’-tetramethylindotricarbo-cyanine iodine
DLS	Dynamic light scattering
DOPE	Dioleoylphosphatidylethanolamine
DSPE	Disteraoyl-phosphatidylethanolamine
ECM	Extracellular matrix
EPR	Enhanced permeability and retention effect
FITC	Fluorescein-isothiocyanate
IFP	Interstitial fluid pressure
MFI	Median fluorescence intensity
MI	Mechanical index
MPS	Mononuclear phagocyte system
MVP	Microvascular pressure
NP-loaded MBs	Nanoparticle-loaded MBs
PACA	Poly (alkylcyanoacrylate)
PBCA	Poly (butyl cyanoacrylate)
PC	Phosphatidylcholine
PEG	Polyethylene glycol
PI3Ks	Phosphoinositide 3-kinases
PRP	Pulse repetition period

List of Publication

Publications included in this thesis

I. **Mercy Afadzi**, Catharina De L. Davies, Yngve H. Hansen, Tonni Johansen, Øyvind K. Standal, Rune Hansen, Svein-Erik Måsøy, Esben A. Nilssen, Bjørn Angelsen. *Effects of Ultrasound Parameters on the Release of Liposomal Calcein*: US in Medicine and Biology 38 (3), 476–486, 2012.

II. **Mercy Afadzi**, Sabina P. Strand, Esben A. Nilssen, Svein-Erik Masoy, Tonni F. Johansen, Rune Hansen, Bjorn A. Angelsen, Catharina de L. Davies. *Mechanisms of the Ultrasound-mediated Intracellular Delivery of Liposomes and Dextrans*: IEEE Transactions on Ultrasonics, Ferroelectrics and Frequency Control, May 14, 2012.

III. Siv Eggen, **Mercy Afadzi**, Solveig Bjærum Haugstad , Bjørn Angelsen , Esben A. Nilssen and Catharina de L. Davies. *Ultrasound Improves Uptake and Distribution of Liposomal Doxorubicin in Prostate Cancer Xenografts*. Submitted to Ultrasound in Medicine and Biology.

IV. **Mercy Afadzi**, Yrr Mørch, Per Stenstad, Ruth B. Schmid, Bjørn Angelsen, Catharina de Lange Davies. *Multifunctional Particles for Drug Delivery and Imaging: Effect of PEGylation, Surfactant, Size and Ultrasound Exposure on Cellular Uptake.* Manuscript in preparation.

Others Papers (Proceedings)

- **Mercy Afadzi**, Catharina de L. Davies, Yngve Hofstad Hansen, Tonni Franke Johansen, Øyvind Krøvel-Velle Standal, Svein-Erik Måsøy and Bjørn Angelsen. *Ultrasound Stimulated Release of Liposomal Calcein*: IEEE International Ultrasonics Symposium, 2010, 2107-2110.

- **Mercy Afadzi**, Svein-Erik Måsøy, Yngve Hofstad Hansen1, Rune Hansen, Tonni Franke Johansen, Bjørn Angelsen, Catharina de L Davies. *Mechanism of Intracellular Delivery of Nanoparticles using Ultrasound:*IEEE International Ultrasonics Symposium, 2011, 1502-1505.

- **Mercy Afadzi**, Yrr Mørch, Siv Eggen, Per Stenstad, Ruth B. Schmid, Rune Hansen, Yngve Hansen, Bjørn Angelsen, Catharina de Lange Davies. *Multifunctional Nanoparticles for Drug Delivery and Imaging: Effect of Ultrasound on Cellular Uptake and Tumor Tissue Distribution*. IEEE International Ultrasonics Symposium, 2012.

- Siv Eggen, **Mercy Afadzi**, Solveig Bjærum Haugstad, Bjørn Angelsen, Esben A. Nilssen, Catharina de L. Davies. *Ultrasound-Mediated Delivery of Liposomal Doxorubicin in Tumor Tissue*. IEEE International Ultrasonics Symposium, 2012.

- Yngve Hansen, **Mercy Afadzi**, Bjørn Angelsen, Sylvie Lelu, Magnus Lilledahl, Catharina de Lange Davies. *Ultrasonic Drug release: Impact on Liposomal Doxorubicin in Collagen Gels*. IEEE International Ultrasonics Symposium, 2012.

Contributions to papers included in this thesis

The present work is based on collaboration with the Department of Circulation and Medical Imaging (NTNU), SINTEF Material and Chemistry (Trondheim) and Epitarget AS (Oslo). The author's main contribution to the papers are; writing of manuscript, planning, designing experimental setup and all experimental work in Paper I, II and IV. In Paper III, the author was involved in the planning, experimental work and writing of the manuscript. Siv Eggen performed the animal experiments, CLSM and the data analysis in Paper III. The liposomes used in Paper I, II and III were supplied by Epitarget AS, whereas the novel multifunctional drug delivery system used in Paper IV was supplied by SINTEF Material and Chemistry.

Table Contents

List of Figures

1. INTRODUCTION

Cancer is a disease that causes cells to grow out of control to form a tumor. According to the World Health Organization, cancer is the most leading cause of death worldwide, leading to about 7.6 million deaths in the year 2008 with an estimated death of 13.1 million in the year 2030. This calls for an urgent need to improve cancer therapy. Conventional cancer therapy (surgery, radiotherapy and chemotherapy) lacks specificity towards tumor tissues. Thus, normal tissues are also damaged in the treatment process. In chemotherapy for instance, cytotoxic agents have large volume of distribution when administered, which often result in narrow therapeutic index (ratio of therapeutic benefit to side effects) due to high level of toxicity in healthy tissues [1, 2]. This has limited the applied dose in order to spare the normal tissues [1]. To overcome the unwanted effect associated with chemotherapy, the therapeutic index could be enhanced by delivering these agents specifically to tumor cells, whereby keeping them away from non-malignant cells sensitive to the toxic effects of the drug. When the cytotoxic agents are encapsulated in a drug carrier (such as liposomes, polymers, micelles, MBs etc), the antitumor effect is enhanced whereby toxicity is reduced due to the improved pharmacokinetics compared with free drug [3-5]. This is mainly due to the leaky capillaries in tumor tissue. Tumor vasculature differs from the vasculature in normal tissue, *i.e*., it has an irregular morphology, heterogenic blood flow and the endothelial cells lining the capillaries are fenestrated unlike that of the normal tissues [6, 7].

The drug carrier may extravasate through the leaky tumor vessels [8, 9], contributing to selective localisation of drug in tumor tissue (enhanced permeability and retention effect (EPR) [3, 10], a process known as passive targeting. In normal tissue, the intact carrier is confined to the intravascular space, as normal blood vessels are not fenestrated to the same degree as in tumor tissue. Hence, the toxicity to normal tissue is reduced considerably. Although passive targeting improves the tumor uptake compared to free drug, the drug distribution within the tumor tissue is still heterogeneous [11, 12]. Large areas of the tumor are not reached by the drug. However, for successful cancer therapy, the cytotoxic agents need to reach all cancer cells in optimal quantities and deactivate them. To overcome these challenges in drug delivery, development of new cancer specific and effective treatments is required. In the past few decades, lots of studies have focused on the use of an external source (ultrasound (US) or magnetic field, etc.) to trigger the release of drug carriers at the targeted site[13-17], this process is known as physical targeting. This thesis focuses on how to improve the delivery of cytotoxic drugs to cancer tissues by combining passive targeting with the therapeutic effect of US. US may enhance the delivery by; increasing the release of the drug from the carrier, improving the penetration/transport of the carrier and the released drug through the extracellular matrix (ECM) and increasing the cellular uptake of the released drug.

1.1. Barriers Encountered by Cytotoxic Drugs

The drug either encapsulated or free is expected to travel through the bloodstream and cross the capillary wall to its target after it has been administered orally or by systemic injection.

To be able to eradicate the tumor completely, the drug must disperse throughout the tumor in sufficient concentrations to eliminate every deadly cell. Thus, before the drug can attack the tumor cells, it has to make its way through the blood vessels in the tumor, must be able to cross the walls of the vessels into the interstitium and finally, move through the interstitium to the cancer cells and then into the cells [18]. The first barrier to drug delivery is the chaotic blood supply in solid tumor [18, 19], thus, the vasculature is chaotic in terms of spatial distribution, microvessel length and diameter. The poorly developed vascular network is due to the rapid proliferation of the tumor cells compared to the proliferation of the vascular and stromal elements. Due to the uneven distribution of blood vessels, regions lacking vessels will not be able to receive drug directly from circulation and this will result in a decrease in uptake of drug in general. Thus, the average uptake of drug has been shown to decrease with an increase in tumor weight whereas other studies do not find any effect of tumor volume and drug uptake [18, 19]. In addition, the twisted nature of the vessels leads to slow blood flow which also hinders delivery of drugs to poorly perfused regions of the tumor. However, as mentioned above, the permeability of tumor capillaries is shown to be higher than in normal capillaries, and these leaky capillaries thus favour the transport of the therapeutic agents across the blood vessel wall [9, 11].

The second barrier is the mechanism by which the drugs or drug carriers are crossing the capillary wall (*i.e.*, transcapillary transport) and penetrating the interstitium or ECM (*i.e.*, interstitial transport); namely diffusion (driven by the concentration gradient) and convection (driven by the hydrostatic pressure gradient). These transport mechanisms are affected by some important transport parameters namely: transcapillary and interstitial hydraulic conductivity, which relates the velocity of the fluid to the pressure gradient; transcapillary and interstitial diffusion coefficient relating the diffusive flux to the concentration gradients and the permeability across the capillary wall [20]. The lack of a lymphatic network in tumor tissue, and the high capillary permeability which allows molecules and water (by osmosis) to enter the interstitium leads to high interstitial fluid pressure (IFP) in tumor tissues compared to normal tissues. These high pressures are approximately the same as the microvascular pressure (MVP) [21], and so the transcapillary pressure gradient is almost zero. However, it has been shown both experimentally and by mathematical modelling that IPF increases rapidly and reach an elevated level approximately 0.4 – 0.6 mm into the tumor [22, 23], and so there might be a transcapillary pressure gradient at the tumor periphery but not in the centre. This implies that, diffusion will be the most important transport mechanism in the tumor interior where no transcapillary pressure gradient exists. Diffusion is, however, an extremely slow process for large molecules, and the diffusion coefficient decreases with increasing molecular weight. Thus, the high IFP in tumor tissue [21, 23, 24] impedes both transcapillary and interstitial transport of therapeutic agents. Also, the ECM which consists of a protein network of collagen embedded in a hydrophilic gel of glycosaminoglycans and proteoglycans [18] may impede the diffusion of large molecules in tumors due to the collagen content and structure. This in turn contribute to the low concentration of drug molecules in the ECM [18]. Furthermore, studies have shown that interstitial hydraulic conductivity decreases with increasing concentration of glycosaminoglycans [25] and the diffusion coefficient decreases inversely with increasing amount of collagen and sulphated glycosaminoglycans [26, 27]. Therefore, to increase the interstitial hydraulic conductivity and diffusion coefficient, and reduce IFP which depends on hydraulic conductivity, the ECM composition as well as the structure might be modulated.

1.1.1. The cell membrane as a barrier

The interior of the cell is separated from the outside environment by the cell membrane. It allows free diffusion (movement of molecules from a region of higher concentration to a region of lower concentration) of small and non-polar molecules through its semi-permeable membrane. However, it restricts the passage of larger molecules (free or encapsulated drug) and so uptake mechanism like endocytosis is required for the passage of larger molecules. Endocytosis is the active enclosure of an extracellular molecule within a vesicle bound to the membrane, which is in turn transported to intracellular space, and is the most common mechanism for the internalization of larger molecules. Nevertheless, the efficiency of endocytosis is dependent on the surface chemistry and physical properties (size and shape) of the therapeutic molecule or the drug carrier. For effective therapy, the therapeutic agent has to be delivered intracellularly. This calls for new strategies with the aim to increase the efficiency of intracellular delivery of therapeutic molecules.

The mechanism of endocytosis can be categorized as clathrin-mediated or clathrin-independent endocytosis. Clathrin-mediated endocytosis is the best-understood receptor-mediated endocytosis and it involves the internalization of molecules using receptors (clathrin) specific to the molecules being internalized. The main scaffold protein in clathrin-coated pits is clathrin and it occupies the plasma membrane along with the protein complex AP2 and dynamin. Clathrin-independent endocytosis includes several cholesterol-rich pathways. Caveolae-mediated pathway is the most common reported clathrin-independent endocytosis and it consist of subdomains of glycolipid rafts that use the membrane protein caveolin to form stable cell-associated structures[28-30]. Another clathrin-independent pathway is macropinocytosis which involves bulk and non-selective uptake of extracellular fluid through the actin-dependent reorganization of the plasma membrane to form macropinosomes (heterogeneous phase-bright organelles that emanate from ruffles) [31]. To investigate the cellular uptake mechanism of molecules, the various endocytic pathways can be selectively inhibited by using chemical inhibitors [32]. For example, chlorpromazine, inhibits mainly clathrin-mediated endocytosis by reversibly translocating clathrin and its adapter proteins from the plasma membrane to intracellular vesicles [33], genistein, a tyrosine kinase inhibitor, inhibits mainly caveolae-mediated uptake [34, 35]; and wortmannin, an inhibitor of phosphoinositide 3-kinases (PI3Ks), plays a role in the enclosure of ruffles to form macropinosomes [31, 36].

1.2. Types of Carrier used in Drug Delivery

To avoid unwanted effect of cytotoxic drugs with normal tissues, different types of drug carriers have been developed to carry the drug to the tumor tissues. The typical size of drug carriers used in drug delivery is 3 – 1000 nm, hence they are known as NPs [37]. NPs can be designed from various materials like polymer (polymeric NPs and micelles), lipids (liposomes), virus (viral NPs) etc [16, 37]. Although, the drug is protected through encapsulation, the nanoparticle is expected to remain stable in circulation without releasing their content until they reach their targeted site. Thus, the nanoparticle should be designed in such a way to prevent rapid degradation in circulation and opsonization by serum protein or phagocytosis by macrophages. Coating of the NPs with polyethylene glycol (PEG) is shown to reduce the uptake by the mononuclear phagocyte system (MPS) by making them “invisible” to monocytes and macrophages [1, 3]. PEGylation prolongs the circulation time[3] and increases the chance of accumulation at the tumor site compared to normal

tissues due to the EPR effect in tumor tissues. The NPs can also be delivered locally at the target site by attaching a ligand to the drug carrier that binds specifically to receptors at the target site; a method known as active targeting. After localization into the solid tumor, NPs are expected to release the drug in the interstitium followed by uptake of the drug in its free form by the tumor cells or uptake of NPs in tumor cells followed by intracellular release.
In spite of passive targeting, drug release kinetics is still a challenge. Hence, tiggerable release mechanisms are needed to increase the rate of drug release and the local dose. Some of these carriers (liposomes, micelles, polymeric NPs etc.) can been designed to be used in combination with therapeutic US. In this study, liposomes and polymeric NPs were used as drug carriers.

1.2.1. Liposomes for drug delivery

Liposomes are non-toxic biodegradable and ion-immunogenic drug delivery vehicle which was discovered by Bangham [38, 39]. They are spherical vesicles produced from natural phospholipids and cholesterol, which can be used in a lot of applications (clinical, cosmetics etc). They are made up of one or more concentric bilayer of phospholipids with each enclosing an aqueous compartment. The molecular shape of a phospholipid consists of water-loving head and two oil-loving tails (Fig. 1.1). Phospholipids can be classified according to type of polar head group, fatty acid chain length and degree of saturation [40]. The most commonly used phospholipids in liposome formulations are phosphatidylcholines (PCs) and they can be derived from natural sources like egg, soy etc or from synthetic materials. Phospholipids such as disteraoyl-phosphatidylethanolamine (DSPE), dioleoylphosphatidylethanolamine (DOPE) and dierucoyl-phosphatidylcholine (DEPC) with smaller head groups and longer or unsaturated acyl chains can also be used for designing liposomes [14, 41]. When a large number of lipids are placed together, a bilayer will be formed based on hydrophobic interactions in continuous parallel packing, with the hydrophilic head group position towards the aqueous environment (Fig. 1.1). This makes them suitable for delivering both hydrophilic and lipophilic drugs. Hence, they are capable of carrying a great variety of molecules, such as small drug molecules, nucleotides and even plasmids. The size of liposomes ranges from nanometers to micrometers[40] and they can be classified into: small unilamellar vesicles (SUV) which consist of a single bilayer and size range of 10 – 100 nm; large unilamellar vesicles (LUV) consist of single bilayer and size range of 100 – 1000 nm; multilamellar vesicles (MLV) consisting of several bilayers and size range of 100 nm – 20 µm; multivesicular vesicles (MVV) with size range of 100 nm – 20 µm [42]. However, liposomes used for drug delivery are made of single bilayer and are typically of 100 nm in size, for example, Doxil (a PEGylated liposome used in the clinic). The liposomes used in the present work were made from DEPC and are single bilayer with size below 110 nm. Liposomes can be designed to respond either to elevation in temperature (*e.g.*, thermal effect of US) or to the non-thermal effect of ultrasonic waves or both. Liposomes sensitive to the thermal effect of US are called temperature sensitive liposomes (TSL) and the membranes of these liposomes include lipids which have a phase transition temperature in the range of ~ 42–45°C[43, 44]. Liposomes sensitive to the non-thermal effect of US are called sonosensitive liposomes.

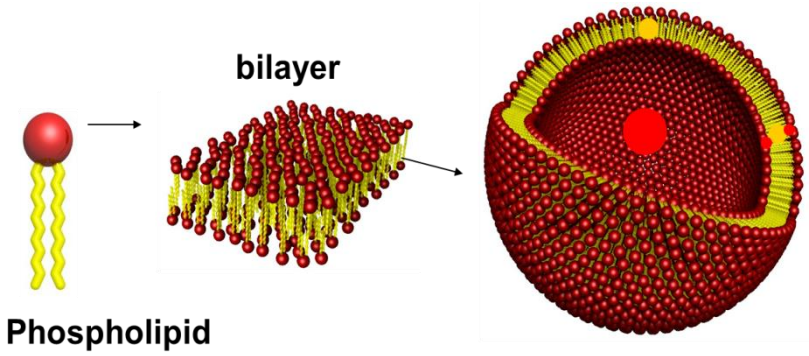

Fig. 1.1: Schematic diagram showing the formation of a liposome. Phospholipid forming a bilayer and then enclosing an aqueous interior. They can carry water soluble (red), fat soluble (yellow) and amphiphilic drugs (red and yellow) and are versatile systems for broad medical applications. Epitarget ©.

1.2.2. Polymeric Nanoparticle for drug delivery

Biodegradable polymeric NPs made for drug delivery application have shown significant therapeutic potential in recent years. This is mainly because; polymer chemistry is a versatile field, where polymers can be used as the backbone for nanoparticle formulation to facilitate the advancement for multiple functionality [45]. Thus, NPs can be formulated to combine tumor targeting (binding small peptides, antibodies or lectins covalently to NPs), tumor imaging (inclusion of metals such as iron oxide, gold, gadolinium etc. for MRI or fluorescence probes for optical imaging) and tumor therapy (inclusion of anti-cancer drug) in one system. Drug release from a polymer NP is normally by the degradation of the nanoparticle or by diffusion of the drug from the polymeric core. The drug can also be attached by a labile linkage to the polymer from which it is released at the target site by degradation of a linker via enzymes or pH at the target site. Non-soluble polymers can form NPs, while soluble or amphiphilic polymers (with attached drugs) can be used to form hydrogel NPs by physically or covalently crosslinking the polymer after the formation of the NP so that it will not dissolve in water (or blood) [16]. Examples of polymers used in designing NPs includes; Poly(lactide-co-glycolides), Poly(methyl methacrylate), Poly(lactic acid), Poly(vinyl alcohol), Polystyrene, Poly(acrylic acid) , Poly(methacrylic acid), Poly (alkyl cyanoacrylate), etc. [46-48].

For drug delivery applications, the polymer must be biocompatible (non-toxic and non-immunogenic) and preferably biodegradable. Poly (alkylcyanoacrylate) (PACA) polymers like poly (butyl cyanoacrylate) (PBCA) are said to be biocompatible and biodegradable and can absorb or entrap bioactive compounds (inorganic crystallites, various drugs, proteins etc.) making them ideal tools for applications like drug delivery where the NPs are administered repeatedly. The polymeric NPs used in this thesis were made from PBCA. Polymeric particles can be stabilized with positively or negatively charged ionic surfactants or the non-ionic polymeric surfactant (Polysorbate 80 (Tween 80)), sodium dodecyl sulphate (SDS), Aerosol OT (AOT), Lutensol AT50, CTMA-Cl, etc.) through physical adsorption or binding chemically to the particle surface[48-50]. Surfactants can also be a source of toxicity to cells if not removed thoroughly after NPs preparation. This is because they can influence cell permeability. Functionalization of NPs with PEG can influence cellular uptake of NPs. Thus, cellular uptake has been shown to be affected by the density and conformation of PEG molecules on the surface of the NPs [46, 51, 52]. In spite of the fact that PBCA particles are

biocompatible, the degradation products *i.e.*, n-butanol and poly (cyanoacrylic acid) are known to be cytotoxic [53-55]. Furthermore, Wessi *et al* [50] also reported that PBCA NPs exhibited cytoxicity which is dependent on the molar mass distribution. However, studies demonstrated that at lower concentration (10-20µg/ml) of PBCA NPs there is little in vivo or in vitro evidence of toxicity on cerebral endothelial cells [56].

1.3. Ultrasound and Drug Delivery

US are sound waves with frequencies above the audible range, that is, above 20 kHz. It is used mainly in the clinic and the industry (including welding and processing and non-destructive evaluation). US waves are mechanical wave and so require a material medium (such as liquid) for its propagation. Thus, there is movement of molecules as the medium is compressed (at high pressures) and decompressed (at low pressures) and can act physically on biomolecules and cells. It can be reflected, refracted (bent), focused and absorbed like light waves. Unlike light waves, US waves can be transmitted through the body at precise location with relatively little absorption. In the clinic, US usually operates in the range of 1 – 40 MHz and is used to image changes in appearance and function of organs, tissues, blood flow or abnormal masses (such as tumors), guide invasive procedures and monitor tissue response to therapy. Currently, US imaging is widespread in clinical use and it accounts for about one in four of all imaging procedures worldwide [57] with a wide range of new therapeutic applications (such as drug delivery, gene therapy, high intensity focused US etc.) currently under consideration [58]. US is of special interest, because it is safe, non-invasive, can be controlled both spatially and temporally, and can penetrate deep into the body without affecting intermediate tissues.

US waves can be transmitted continuously or it can be pulsed. During continuous mode, the ultrasonic transducer is excited continuously with an electrical sine wave at constant amplitude (Fig. 1.2 (a)) which then produces a continuous ultrasonic wave at the same frequency as that of the electrical frequency. Pulsed waved US is generated by exciting the ultrasonic transducer with very short electrical signals and then waiting for some time before repeating the excitation (Fig. 1.2 (b)). US wave is characterized by the amplitude (pressure), wavelength (λ), frequency (f), pulse repetition frequency (PRF), pulse duration (τ), duty cycle (DC), etc. The pulse duration (τ) is given by: $\tau = N/f$ (Fig 1.2 (b)). Where; N is the number of cycles per pulse. The duty cycle is the fractional amount of time that the pulse is activated, and is given by equation 1.

$$DC = \frac{\tau}{PRP} = \tau \times PRF \quad (1)$$

Where; PRP is the pulse repetition period. For a plane harmonic wave, acoustic intensity I of a sound wave can be defined as the average rate of flow of energy through a unit area normal to the direction of propagation (equation 1). Thus, acoustic intensity for plane wave is defined as follows;

$$I = \frac{1}{2}\frac{p^2}{\rho c} \quad (2)$$

Where; p is the amplitude of the pressure, ρ is the density of the medium and c is the velocity of sound in the medium.

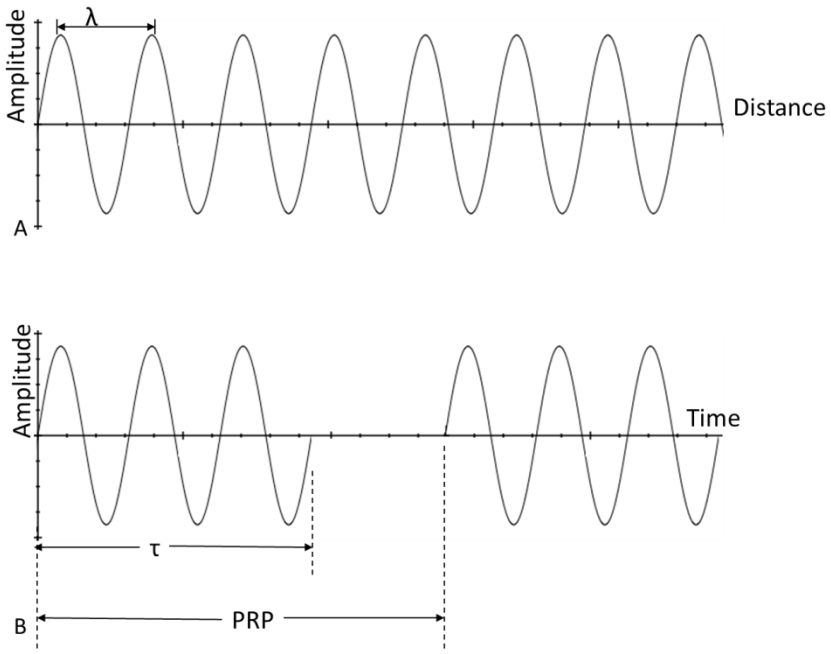

Fig. 1. 2: Schematic presentation of (A) continuous and (B) pulse wave ultrasound. PRP, λ and τ are the pusle repitition period, wavelength and pulse duration respectively.

1.3.1 Biological effect of ultrasound

US-mediated biological phenomena have been grouped into two categories namely: thermal and non-thermal effects. Thermal effects refer to the absorption of acoustic energy by fluids and tissues (heating). The non-thermal effect is associated with acoustic radiation force and cavitation (bubble oscillations). These mechanisms can be used to enhance drug transport, drug release and uptake at the target site. This thesis focuses on the use of non-thermal effect of US to improve drug delivery.

1.3.1.1. Heating

The deposition of acoustic energy into the propagation medium due to absorption leads to heating. When US energy is focused unto a target tissue, the intensity also known as power density (in W/cm^2) of the wave will be absorbed by the tissues, which will then result into heating depending on the magnitude of the intensity. This is directly proportional to the absorption coefficient of the tissue. The thermal effect of US can be used to kill or ablate tissues[59, 60], "melt" or release liposomes to deliver drugs to tissues and also to heat the tissues in order to enhance the uptake of the drugs [61-63]

1.3.1.2. Acoustic Radiation

Propagation of the sound wave can lead to transfer of momentum from the sound wave to the propagating medium, which then generates a unidirectional force called radiation force. When radiation force acts on a fluid medium, it causes formation of a steady flow called acoustic streaming which can be on a large scale or small scale. When small scale acoustic

streaming occurs, it is known as micro-streaming and can lead to small eddy in the vicinity of small vibrating objects like gas bubbles. This phenomenon is related to cavitation and can increase the overall rate of drug transport [64, 65]. The time-average radiation force on a bubble resonating in a travelling-wave is given equation 3 [66].

$$\langle F \rangle = \frac{\langle \dot{W} \rangle}{c} = \frac{I\sigma_e}{c} \quad (3)$$

Where; $\langle \dot{W} \rangle$ is the time-average power loss per bubble, I is the intensity of a plane wave and σ_e is the extinction cross-section which is the sum of the absorption and scattering cross-section of the bubble.

Acoustic streaming has been shown to increase convective heat loss thereby reducing heating from US exposure [67]. Furthermore, radiation force applied to tissues is proportional to the temporal average intensity of the acoustic beam (assuming a plane wave) at a given point in the tissue and the absorption coefficient of the medium, hence the higher the intensity, the higher the radiation force [68-70]. Therefore, depending on the magnitude of the radiation force, tissue displacement at the focal zone can take place and the magnitude of the displacement is inversely proportional to the tissue stiffness [71, 72].

1.3.1.3. Acoustic cavitation

Cavitation is the formation/or oscillation of gas bubbles in a medium upon exposure to ultrasonic pressure waves. It is divided into two main types: stable (non-inertial) and collapse (inertial or transient) cavitation. Stable cavitation is the repeatable oscillation of bubbles (diameters) around some equilibrium size and it occurs at lower intensities (Fig 1.3a). The maximum oscillation occurs at the resonance frequency of the bubble and it depends on equilibrium radius of the bubble (R_o), the ambient pressure (P) and density of the surrounding medium (ρ). For a free bubble, assuming an adiabatic condition, the resonance frequency is given as [73];

$$f_r = \frac{1}{2\pi R_o}\sqrt{\frac{3\gamma P}{\rho}} \quad (4)$$

Where; surface tension is neglected and γ is the adiabatic constant of the gas (air). For an air –filled bubble in water at standard pressures (P = 100 kPa, ρ = 1000 kg/m^3), equation 3 reduces to; $f_r = 3.3/R_0$.

Bubble oscillation can lead to microstreaming (*i.e.*, circulating fluid flow) around the bubble where the amplitude of oscillation is proportional to the velocity and shear rate. It can also induce shear stress in nearby tissues. At higher intensities the bubble oscillates sufficiently that the inertia of the inward moving liquid causes the bubble to collapse violently, producing shock waves, high temperatures, and free radicals (Fig. 1.3) [66, 74, 75]. This phenomenon is called collapse cavitation or inertial cavitation. The transition from stable cavitation to inertial cavitation occurs at a threshold called inertial cavitation threshold [66, 74, 75]. This threshold is dependent on the peak negative pressure, frequency and the initial bubble radius [58, 66, 74, 75]. The likelihood of occurrence of inertial cavitation in a medium exposed to US has

been defined as mechanical index (MI). MI is the ratio between the peak negative pressure (P_{neg} in MPa) and the square root of the US frequency (f, MHz) as given in equation 5.

$$MI = \frac{P_{neg}}{\sqrt{f}} \quad (5)$$

Therefore, inertial cavitation occurs more frequently at lower frequencies than higher frequencies. Theoretically, MIs below 0.7 signifies no occurrence of cavitation [74], thus, even when a broad size distribution of nuclei are present, below 0.7 MI, conditions are still not sufficient to allow significant bubble expansion. However, because there are fewer gas nuclei *in vivo* than *in vitro*, hence, maximum MI in medical US scanners is set to 1.9. Detection of cavitation is accomplished by several methods, including measurement of the acoustic spectra generated by the oscillating or collapsing bubbles, trapping of free radicals, sonoluminescence, etc. [66, 76-78].

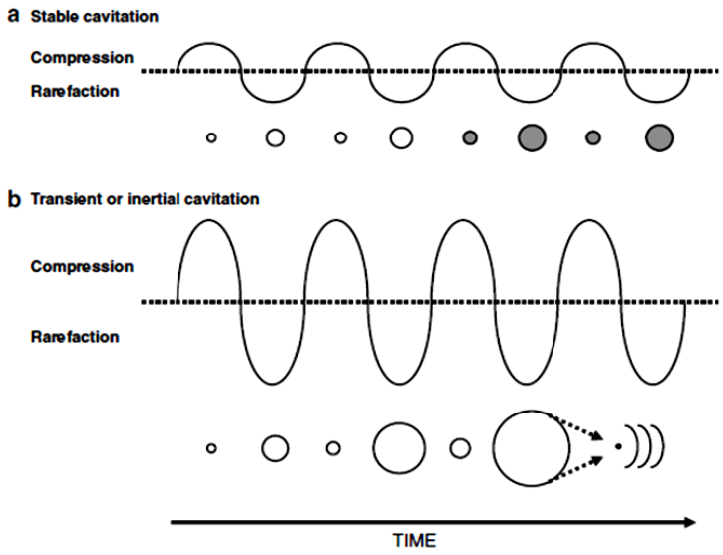

Fig. 1. 3: Schematic representation of cavitation activity with time illustrating the effects of acoustic fields (same frequency but different intensities) on bubble behavior. (a) Stable cavitation: bubble oscillations induced by low-intensity, with a gradual increase in bubble diameter until it reaches a resonant diameter and then stable oscillation occurs (filled circles). (b) Inertial cavitation: the bubble grows rapidly for a few cycles at higher intensities and then collapse violently generating highly localized extremes of temperature and pressure, shock waves and free radicals. This is because the inertial energy of the fluid surrounding the bubble during the compression half cycle becomes so great that it cannot reverse direction when the next rarefaction half cycle arrives [79]

1.4. Acoustic Radiation Force and Drug Delivery

In drug delivery, radiation forces (using MHz-frequency US) can displace gas bubbles (loaded with therapeutic agents) circulating in the blood stream and push them towards the vessel wall which will enhance receptor-ligand contact or induce shear forces and cause gaps in the endothelium of the vessel wall to increase cellular uptake of drugs [80-83]. Acoustic streaming generated by radiation force, might improve the convection of the NPs in the extracellular matrix and enhance the penetration and distribution of the NPs as well as augments the release of the drug from the particle.

1.5. Cavitation and Drug Delivery

Cavitation is one of the important non-thermal US mechanisms in the field of drug delivery. The two main roles of cavitation in drug delivery are: (1) to disrupt the structure of the drug carrier (NPs) and (2) to release the drug and also make the cell membrane and capillaries more permeable to drugs (Fig. 1.4). Cavitation activity increase with increase in the number of gas bubble nuclei, therefore introduction of gas bubbles or MBs (US contrast agents) significantly enhances cavitation activity which in turn facilitates drug delivery.

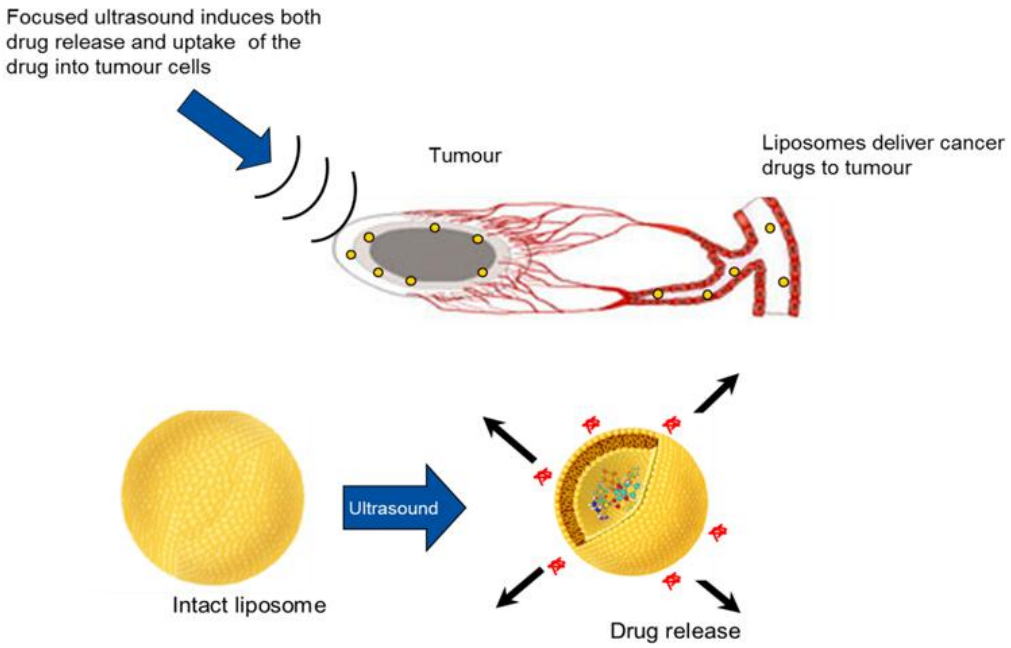

Fig. 1. 4: Schematic illustration of US-mediated drug delivery. The liposomes deliver the cancer drug to the tumuor and then application of focused US will disrupt the structure of the lipsomes and release the drug and also make the cell membrane and capillaries more permeable to drugs. (Epitarget©).

1.5.1. Cavitation and controlled drug release

Although, the EPR effect has been effective in targeting tumor tissues, there is still a challenge to control drug release kinetics at the tumor site. However, several strategies for triggered drug release have been proposed including the use of US energy to trigger the release of NPs [14, 16, 41, 84]. Drug delivery systems such as liposomes, micelles, MBs etc. can be designed to respond to the mechanical effect of US in order to release the content. For instance, studies have shown that the gas-containing liposomes are more sensitive to US exposure [84], but these gas-containing liposomes are too large (in the micrometer range) to allow effective extravasation into tumor tissues. Ejven and co-worker also demonstrated that lipid composition can influence liposome sonosensitivity [14, 85]. Thus, they showed that, DOPE-based liposomes are more sensitive to US exposure than PC-based liposomes due to the cone-shaped geometry and non-bilayer forming characteristics of DOPE. DEPC-based liposomes were used in this thesis and they also have a cone-shaped geometry which makes

them sonosensitive [14]. Although, the exact mechanism of US mediated release is poorly understood, cavitation have been reported to play a dominant role in the drug release from micelles, liposomes and polyersomes [14, 15, 17, 41, 64, 76, 86, 87]. During bubble oscillations (*i.e*, stable cavitation leading to microstreaming) vesicles denser than the surrounding medium would be pushed (by radiation force) towards the bubble and if the shear stress exceeds the strength of the vesicle, it would rupture or reform into smaller vesicles and then release its content [65]. Again, shock waves and jet streams produced during inertial cavitation can lead to shear stress which can also rupture vesicles to release their content [65]. Release of drug from polymer has also been attributed to free radicals generated from inertial cavitation that react with, rearrange and break the bond connecting the drug and the polymer [65, 88]. US triggered release seems to have great potential to improve drug delivery, however, the interaction of US with drug delivery system and the effect of exposure parameters on drug release are yet to be thoroughly elucidated.

1.5.2. Cavitation and cell membrane permeability

Cavitation can also cause stresses on the membranes of biological cells to render them permeable to molecules which are not permeable to the cell membrane. This process is has been termed as sonoporation, that is, creation of transient pores in the plasma membranes of cells by sound waves to enhance permeability. Sonoporation is said to be transient and reversible and is able to facilitate the transport of macromolecules, therapeutic drugs, and small compounds [89-97]. Combination of US with artificial MBs (US contrast agents) has been shown to enhance cell membrane permeability than US or MBs alone [98, 99]. This is because sonoporation occurs as a result of bubble oscillations or collapse, so the presence of MBs will enhance the cavitation activity and therefore enhance cell membrane permeability. During cavitation, cells in the vicinity of cavitation event are subject to shear stresses from microstreaming originated from oscillating bubbles [96] as well as shock waves and microjet from collapse of bubbles which lead to increase permeability of the membrane [100-103]. Thus, both stable and inertial cavitation has been shown to play crucial roles in the sonoporation activity [104-106]. This can lead to enhanced extravasation of NPs or maromolecules into tumor tissues. Although, US offers compelling opportunities to enhance cancer therapy, mechanism of sonoporation is still unclear, thus, full understanding of how molecules enter cells and how cavitation facilitates intracellular uptake is still lacking[107, 108]. However, studies have shown pore formation and enhanced endocytosis to be the main mechanism of sonoporation [94, 97, 101-103, 109, 110].

In addition, US-mediated intracellular uptake has been found to be more efficient with low molecular weight entities than higher molecular weight entities [97]. This is because endocytosis is size dependent and the pore size (30nm to 400nm) distribution on the plasma membrane is said to be heterogeneous with smaller sizes than bigger sizes [94, 97, 102, 103]. Even though, sonoporation is said to be reversible, that is, pores last from milliseconds to minutes [101, 111], cavitation activity (especially inertial cavitation) is non-uniform and difficult to control, as some of the exposed cells will experience irreversible damage which would render them non-viable. That is, cells very close to the oscillating or collapsing microbubble will be killed whereas those too far away will be unaffected; so it is only cells within a certain range from the cavitating bubble that will be reversibly permeabilized[112]. Hence, irreversible permeabilization limits the sonoporation efficiency (percentage of cells with reversible permeability). Therefore, to develop safe and effective protocols for successful cancer therapy, the mechanism of sonoporation needs to be elucidated. However,

sonoporation-mediated therapeutic applications would only be limited to cellular uptake in the vessel wall since MBs can only be exposed to the vasculature and adjacent cells, whereas the tumor cells embedded in the extracellular matrix will not be exposed to microbbubles.

1.6. Ultrasound Contrast Agents – Microbubbles

MBs are US contrast agents used for enhancing ultrasonic contrast imaging. MBs consist of a gas core encapsulated in a shell. The shell of MBs are made up of albumin, lipid, surfactant or polymer whereas the gas core is normally filled with either air (Levovist) or octafluoropropane (Optison™ and Definity®) or perfluorobutane (Sonazoid) or sulfur hexafluoride (SonoVue). They are typically in micrometer (1-10μm) range with a shell thinkness of 2 to 200-nm and can only stay in the vascular system due to their size [113], hence, they are blood pool agents. MBs with hydrophobic gas are more stable than those with normal air since hydrophobic gas have low solubility in blood. The shell also prevents the bubbles from dissolving in the blood and it also determines the rigidity of the microbubble, which in turn affects the collapse threshold. Thus, stability and acoustic response of a microbubble depends not only on the exposure parameters of the US but also on the physical properties (e.g. size, gas and shell) of the MBs [114, 115].

1.6.1. Microbubbles and drug delivery

In drug delivery, microbubbules can be used for imaging of the tumor vasculature, *e.g*., conjugating ligands on the surface of MBs to target specific vascular receptor sites. The oscillations or collapse of these bubbles (cavitation) can also cause changes in the cell membrane and vascular permeability (*i.e.* sonoporation), which can enhance cellular uptake and the distribution of NPs or drugs. In other words, NPs or drugs can be co-administered with MBs while the collapse of the bubble can increase the permeability of the cells to enhance cellular uptake. Drugs can also be loaded onto the MBs in several ways, and application of US can release the drug and the collapse of the bubble can increase the permeability of the cells to enhance cellular uptake. Some strategies for designing multifunctional MBs for US image-guided therapy are; loading therapeutic drugs in the shell (phospholipid-based or polymer-based) [83, 116-118] of the microbubble or attaching NPs directly to MBs [95, 119].

Microbubble with polymer shell is said to be more stable, than those with lipid shell, and it has an advantage of having longer circulation time and higher ligand density for efficient targeting of tissues [47, 117]. In addition, polymeric NPs made from PACA are biocompatible and biodegradable [47, 50] and this makes them ideal systems for drug delivery applications. Fokong and others [118] demonstrated recently that, high amount of chemotherapy drugs can be encapsulated into the shell of polymeric MBs than lipid shell MBs. However, the loading capacity of drugs into the shell of MBs is generally limited by the thickness of the MBs, hence there is a need to increase the drug payload for each microbubble. This can be done by attaching or stabilizing MBs with NPs containing drugs. Loading MBs with NPs (NP-loaded MBs containing contrast agents for MRI or fluorescent probes for optical imaging) can provide contrast imaging for multiple modalities with additional spatial, temporal and depth resolution for improvement in accuracy of disease diagnosis and local treatment of diseases [120]. Furthermore, it has been shown theoretically and experimentally that NP-loaded MBs increases the contrast in US imaging due to the enhanced asymmetric bubble oscillations even at low excitation amplitudes [47, 119-121].

This is because; close packing of the NPs restricts bubble compression. NP-loaded MBs disruption can be done controllably to release the NPs at the targeted site under US image guidance. This may also minimize the destructive effect on nearby cells caused by the acoustic cavitation while maintaining the uptake of NPs in the cells. The reason is that, the presence of NPs around the bubbles will increase the stiffness and attenuation compared with MBs without NPs [47]. Hence, with adequate amount of NPs, NP-loaded MBs might reduce cell death whilst improving delivery efficiency. NP-loaded MBs (air-filled MBs with a shell of NPs) were used in this thesis to study the effect of US on cellular uptake.

2. OBJECTIVES OF THE STUDY

The overall aim of this thesis is to improve the delivery of drugs by combining US and NPs. US may increase the delivery of NPs or cytotoxic agents to cancer tissues in various ways; facilitating the transport across the capillary wall, enhancing the release of the drug from the nanoparticle at the tumor site, enhancing the transport through the ECM and finally enhancing the cellular uptake by making the cell membrane more permeable [93, 94, 112]. However, to develop safe and effective strategies for drug delivery with US, the mechanisms involved in US-mediated drug delivery needs to be understood.

Five specific aims have been addressed to achieve this goal and they are;

- To investigate the effect of various US exposure parameters (frequency, peak negative pressure, duty cycle, PRF, pulse duration and exposure time) that maximize drug release from liposomes in solution, with focus on the impact of MI on drug release. The release mechanism was also investigated.

- To investigate the impact of low US and MBs (commercial micobubbles and NP-loaded MBs) on the cellular uptake of marcomolecules and NPs (liposomes and PBCA NP) and also whether the encapsulated drug was released extracellularly before taken up by the cells.

- To investigate whether the mechanism responsible for cellular uptake of macromolecule is related to pore formation or US enhanced endocytosis.

- To characterize a newly developed multifunctional drug delivery system by investigating the effect of nanoparticle PEGylation, surface chemistry and size on cellular uptake of PBCA NP. The cytotoxic effect of the NPs was investigated as well.

- To investigate the effect of different US exposures (1 MHz and 300 kHz) on delivery and distribution of liposomal doxorubicin in Balb/c nude mice bearing prostate cancer xenografts, *i.e,* the micro-distribution of liposomes and released drug in the ECM after US exposure.

3. MATERIALS AND METHOD

This section comprises the various techniques and models applied in the present work. More information about how the techniques were used in the present study can be found in the original papers.

3.1. Particles and Molecular Tracers

3.1.1. Sonosensitive liposomes

Sonosensitive DEPC-based liposomes containing calcein or doxorubicin were supplied by Epitarget AS (Olso, Norway). DEPC- based liposomes were used to study the effect of US exposure parameters on the release of drug (calcein) from liposomes (Paper I), mechanism of sonoporation (Paper II) and the distribution of liposomal doxorubicin and the released drug in prostate cancer xenografts after US exposure (Paper III).

3.1.2. Dextrans

Dextrans are neutrally charged, complex hydrophilic polysaccharides with low toxicity, and moderate to high molecular weight. They can fluorescently be labeled with fluorescein-isothiocyanate (FITC) and are frequently used as tracers, as well as drug carrier and has been used as model drug in sonoporation experiments [94, 97]. FITC- dextran (Sigma-Aldrich, Oslo, Norway) with various molecular weights (4, 40, 150, 500 and 2000 kDa) were used to study the mechanism of sonoporation in Paper II.

3.1.3. Multifunctional particles

A newly developed multifunctional drug delivery system (manuscript in preparation), *i.e.*, MBs stabilized by PBCA NPs (SINTEF Material and Chemistry, Trondheim, Norway) were used for cellular uptake experiment (Paper IV). This system can be used for both US contrast imaging (diagnosis) and drug delivery (therapy). PBCA NPs labeled with Nile red (small fluorescent molecule) were prepared from miniemulsion polymerization and coated with PEG in a single step. The NPs were PEGylated with three types of PEG (Tween80, long and short Jeffamine chain), 3 types of surfactant (SDS, Tween80 and AOT) with five different sizes (109 – 228 nm). The Jeffamine PEGs are linear whereas Tween80 is a branched polymer. The particles were then used to form the MBs by mixing the NPs dispersion with proteins and air, using an ultra turrax. It should be noted that these PBCA NPs are not US sensitive; thus, they cannot be degraded by neither the thermal nor mechanical effect of US.

3.1.4. Microbubbles

Two types of MBs were used in this thesis, *i.e.*, Definity® MBs (Lantheus Medical Imaging, Billerca, MA) and the multifunctional delivery system (NP-loaded MBs). These MBs were used to study the effect of US on cellular uptake of NPs (Paper II and IV) and macromolecules (Paper II), as well as to investigate the mechanism of US enhanced cellular uptake (Paper II). Definity® consists of octafluropropane (C_3F_8) gas core encapsulated by an outer phospholipid

shell. After activation of the bubbles (as prescribed by the manufacturer) the suspension contains approximately 1.2×10^{10} MBs/ml and the mean diameter ranges from 1.1 to 3.3 μm. The multifunctional delivery system consists of air-filled (O_2) MBs stabilized by PBCA NPs. Three types of PBCA NPs with different sizes and PEGylation were used to form these NP-loaded MBs. Concentration of the NP-loaded MBs were approximately 1×10^{8} to 3×10^{8} MBs/ml and the size ranges from 1 to 2.4 μm

3.2. Characterization of Transducers

Two focused transducers (custom-made) were used in this project. These were supplied by Imasonic (Besancon, France). Detailed description of these transducers (that is diameter, focal length, focal depth etc.) can be found in Table 1. The transducers were focused single-element with frequencies of 300 kHz and 1 MHz, and were made of piezoelectric composite, having matching layers as well as a thick backing. Each transducer had a thermo coupler in the backing for monitoring of the temperature in the transducer. The transducers were characterized in a water tank using a home-built program (ProbeLab) at the Department of Circulation and Medical Imaging. A hydrophone (Onda HGL-0200, Onda Corporation, Sunnyvale, CA, USA) with a tip diameter of 200 μm, connected to a 20-dB pre-amplifier (Onda AH-2020) in a rectangular Plexiglas water tank was used to characterize the acoustic field. The -3dB beam width along the lateral direction was measured (see Table 1) by recording two-dimensional beam profiles. Also, the range (L_m) at which the pressure was -1dB compared to the pressure at the maximum intensity was determined (see Table 1). Equations 5 and 6 were used to calculate temporal average intensities and MIs from the experimental data.

$$I_{TA} = PRF \int_0^T \frac{p^2}{\rho c} dt \qquad (6)$$

Where; p is the acoustic pressure, ρ is the mass density, c is the speed of sound in the medium, T is the repetition period, and PRF is the pulse repetition frequency.

Generally the 1 MHz probe was found to produce higher pressures and intensities than the 0.3 MHz, but the MIs of the two probes are very much comparable. The 1 MHz transducer was also found to have higher nonlinear pulse distortions than the 300 kHz transducer (see Fig.3.1).

Table 1: Specification of transducers

Parameter	Frequency	
	0.3 MHz	1 MHz
Diameter (active)	55 mm	50 mm
Radius of curvature	90 mm	131mm
Location of maximum intensity	69 mm	125 mm
Relative bandwidth	47 %	62 %
- 3dB Beam diameter at location of maximum intensity	6.6 mm	3.0 mm
L_m, range where the pressure is -1dB compared to the pressure at the maximum intensity	32.6 mm	33.0 mm

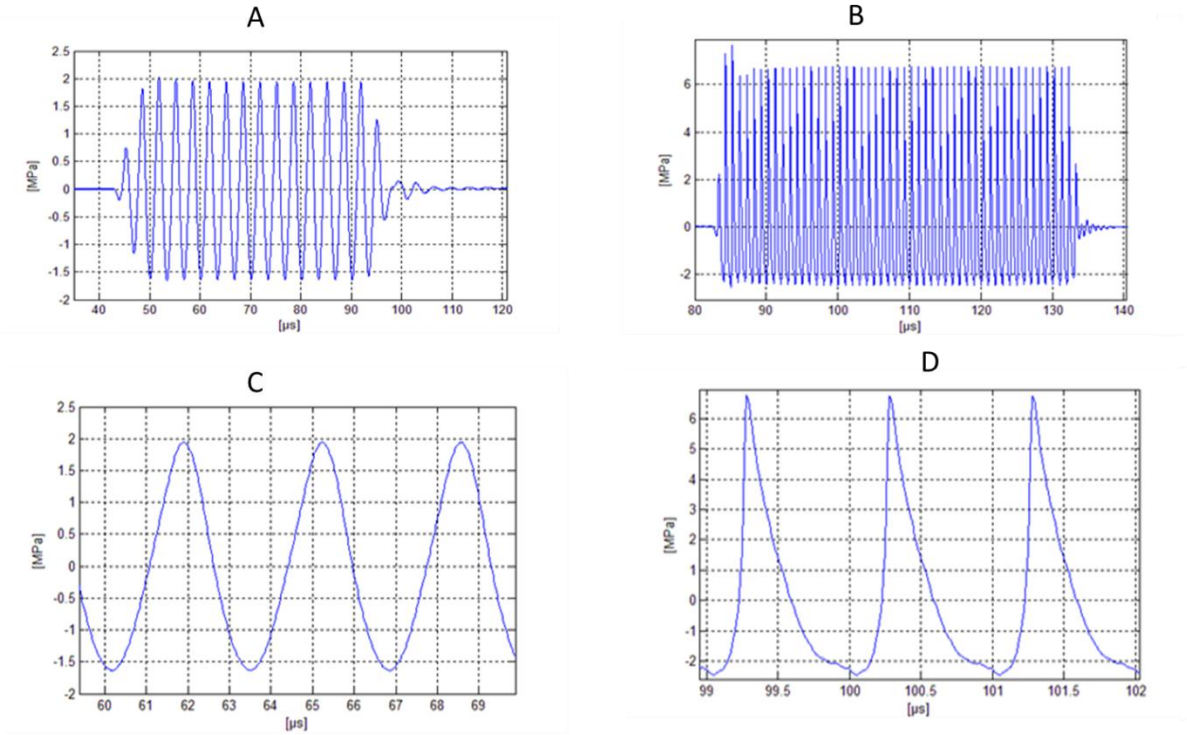

Fig. 3.1: An example of point scans for 0.3 MHz (A and C) and 1MHz (B and D) transducers at 69 and 125 mm respectively. C and D are zoomed version of A and B respcetively showing nonlinear pulse distortion.

3.3. Ultrasound Exposure Set-up

Similar exposure set-ups were used in all the experiments with little modifications based on the type of experiment, *i.e.*, *in vitro* or *in vivo* (see Fig 3.2). Basically, the set-up consisted of a signal generator (Hewlett Packard 33120A, San Jose, CA, USA), an oscilloscope (Lecroy waverunner, LT262, Long Branch, NJ, USA), a power amplifier (ENI 2100L, Rochester, NY, USA), the two custom-made transducers and an insonication chamber. The insonication

chamber for Paper II and Paper IV were the same (Fig. 3.2 B) whereas those of Paper I (Fig. 3.2 A) and III (Fig. 3.2 C) were different due to the nature of samples used in the different experiments. Furthermore, because of the power limitations of the ENI amplifier, in Paper I, an additional eight-channel PC-controlled arbitrary waveform generator board (DA4300, Acquitek, Massy, France) connected to a custom-made eight channel power amplifier (E&I 90AB8, Rochester, NY, USA), (where the eight channels were combined) was used to drive the transducer. Detailed descriptions of the various insonication chambers can be found in the original papers.

3.4. Spectroscopy

3.4.1. Drug release

The release of the model drug calcein (a small fluorescent molecule) was monitored by measuring the fluorescence intensity of the released drug with a spectrophotometer (Perkin Elmer, LS-50B, UK) (Paper I). The destruction of liposomes by the US releases the drug (calcein) into the medium, and by measuring the fluorescence intensity of emitted light, the effect of US on release was investigated. Calcein release during US exposure was determined (according to Düzgünes and coworkers, [122, 123]) by monitoring relief of self-quenching. The percentage of drug release was then estimated from equation 7.

$$\%\, Release = \frac{(F_u - F_b)}{(F_T - F_b)} \times 100 \qquad (7)$$

Where; F_u, F_b, and F_T are the peak fluorescence intensities of calcein released by US, before US exposure and after addition of Triton X-100 (100% release), respectively.

3.4.2. Validation of inertial cavitation

Validation of inertial cavitation was done using a terephthalate dosimeter [124-126] (Paper I). In brief, when inertial cavitation occurs, the produced OH radicals react with the non-fluorescent terephthalate (TA) to form fluorescent 2-hydroxyterephthalic acid (HTA) which can then be measured by spectroscopy.

Paper I

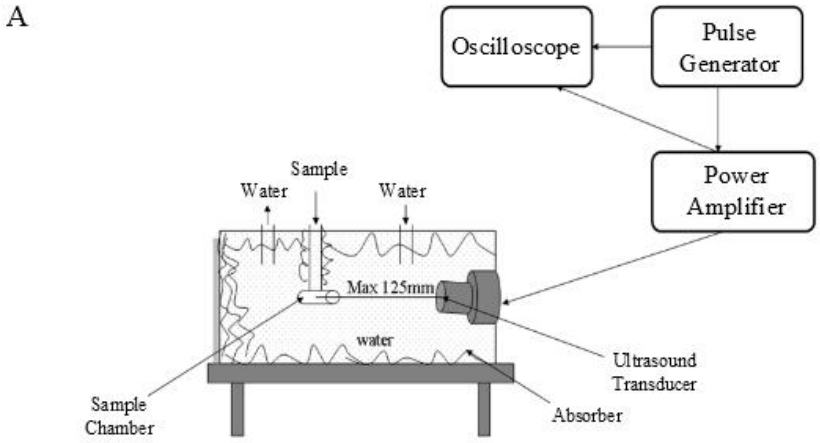

Paper II and IV

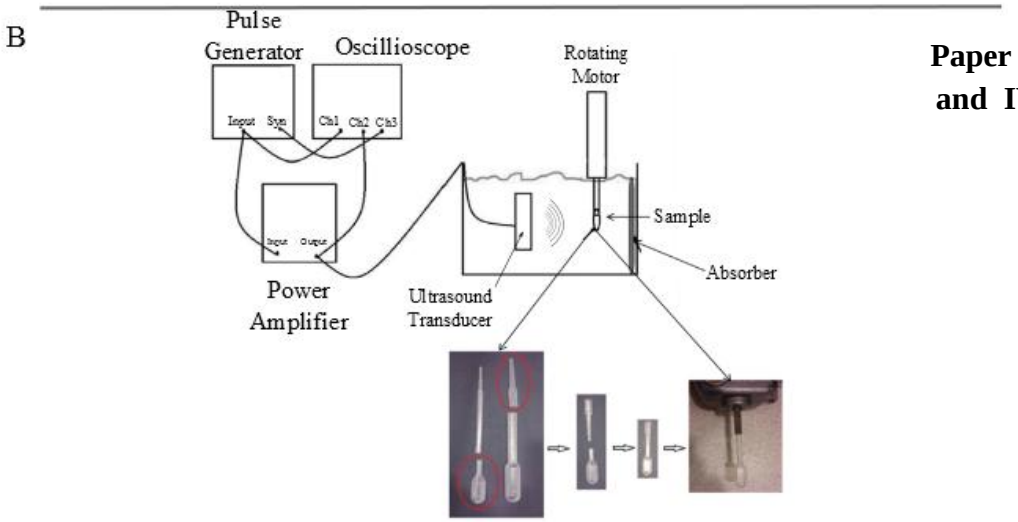

Paper III

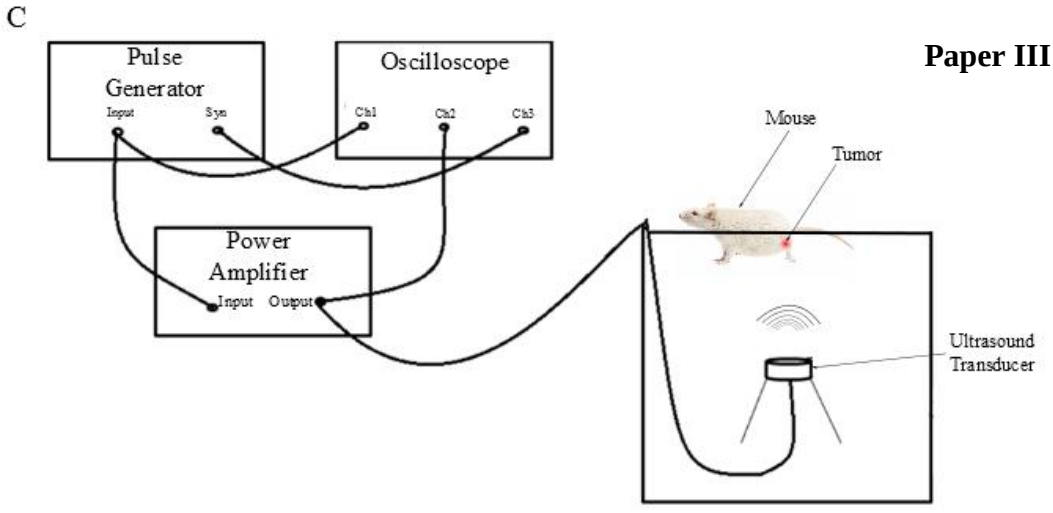

Fig. 3.2: Ultrasound exposure set-ups for *in vitro* ((A) drug release and (B) cellular uptake), and (C) *in vivo* experiments.

3.4.3. Cytotoxicity of Nanoparticles

In paper IV, the cytotoxic effect of PBCA NPs was measured using fluorescent based method of Alamar blue cell viability reagent. The fluorescence intensity of Alamar blue was measured with a microplate reader from the bottom (Tecan Group Ltd. Seestrasse, Männedorf, Switzerland). Alamar blue is a cell health indicator which uses the reducing power of living cells to quantitatively measure the proliferation of cells. Viable cells are able to convert resazurin (active ingredient of Alamar blue which is non-fluorescent) to resorufin (red compound which is highly fluorescent) continuously thereby increasing the overall fluorescence and colour of the cell media. Thus, Alamar blue measures the metabolic activity of cells. Percentage of viable cells was calculated from equation 8;

$$Cell\ viability\ (\%) = \frac{(FL_{NP} - FL_B)}{(FL_C - FL_B)} \times 100 \quad (8)$$

Where; FL_{NP} is the fluorescence intensity of samples treated with NPs, Fl_C is the fluorescence intensity of untreated samples (control) and FL_B is the fluorescence intensity of only the medium (blank).

3.5. Flow Cytometry

Flow cytometry is a technique used for analysis of single cells within heterogeneous populations by recording two physical parameters (*i.e.*, fluorescence and light scattering from each cell). Cells are hydro-dynamically focused to a laser beam and then the light that emerges from each cell as it passes through the laser is captured and the result is grouped based on the individual characteristics. It has the ability to sort cells based on cellular characteristics such as complexity, size, viability and phenotype. It can also distinguish viable cells from dead cells and cell debris. In Paper II and IV, flow cytometry (Gallios, Beckman Coulter, Inc., Indianapolis, IN, USA) was used to measure cellular uptake of NPs (liposomes and PBCA NPs), as well as cell viability before and after US exposure. It was also used to investigate the mechanism of US enhanced cellular uptake by measuring the uptake of FITC-dextran before and after US exposure. To eliminate any spectral cross talk between the fluorochromes (doxorubicin, Nile red, FITC-dextrans etc.) used in the experiments; single-labeled samples were used to determine the necessary percentage of electronic spectral compensation. Cellular uptake was calculated both as the percentage of fluorescent cells (positive cells) and as the amount of internalized fluorochrome, which was estimated based on the median fluorescence intensity (MFI) of the positive cell population. Relative MFI was then calculated as the ratio of MFI of treated and untreated cells. The forward-angle light-scatter signal was used to identify cell fragments and debris. The lowest size possible to detect was approximately 400 nm according to the producer.

3.6. Confocal Laser Scanning Microscopy

Confocal laser scanning microscopy (CLSM) is a high resolution technique which can be used to obtain optical images with depth selectivity from a thick specimen and can also allow

3D reconstruction of the optical sections [127]. A beam splitter directs a laser beam towards the specimen and then focuses the light at a small point at the focal plane of the specimen. The beam is then scanned across the specimen in x-y-direction by a computer controlled scanning mirrors. Spatial filtering techniques are used to eliminate out-of-focus fluorescence emission from reaching the photomultiplier. With CLSM, one can take a number of images at different positions from the same sample (the "tiles") and then merge them digitally to have the whole view of the sample. Thus, specimen larger than the current field of view can be viewed by merging multiple smaller images form the sample together and this method is called tile scanning. CLSM (LSM510, Carl Zeiss Jena GmbH, and Germany) was used to study the internationalization of PBCA NPs in cells (Paper IV) and the distribution of liposomes, released drug and blood vessels in tumor section (5µm) after US exposure (Paper III). Tile scan function was used to analyse tumor section along the radial track from the periphery through the centre and to the other periphery. CLSM (SP5, Leica microsytems CMS GMH, Wetzlar, Germany) was also used to confirm internalization of NPs in cells (Paper II).

3.7. Whole Animal Optical Imaging

Whole animal optical imaging can be based on fluorescence or bioluminescence, and it has an advantage of being fast, easy to perform, cost-effective, very sensitive and also, can be used in studying disease process and biology *in vivo* [128, 129]. This technique is well suited for imaging of small animals and subcutaneous cancer models due to the short penetration depth. Notwithstanding, one of the major challenges in optical imaging in *in vivo* is tissue autofluorescence, which increases the background signal leading to decreased signal to noise ratio [128, 129]. Fluorochromes in the near-infrared and infrared (700 nm – 800 nm) has been shown to have much lower autofluorescence of tissues and deeper tissue penetration. In Paper III, macroscopic distribution of liposomes in normal and tumor tissues were compared before and after US exposure using a Pearl Impulse small animal imaging system (LI-COR Biosciences, Lincoln, NE, USA). PearlCam software was used to analyse the images by drawing a background shape and regions of interest (ROIs) along the tumor margins. Equation 9 was used to calculate the fluorescence signal in the ROI.

$$S = TI - (\mu_B \times Pc_B) \tag{9}$$

Where; S is the fluorescence signal, TI is the total intensity calculated as sum of individual pixel intensities, μ_B is the mean background signal and Pc_B is the pixel count for the background.

3.8. Dynamic Light Scattering (DLS)

Dynamic light scattering is a technique that can be used to determine the size of small particles (proteins, polymers, micelles, carbohydrates, and NPs) in suspension by illuminating the sample with a laser light and then the scattered light is detected at a given scattering angle. The intensity of the fluctuations is due to the fact that the particles are undergoing

Brownian motion and is dependent on size of the particle. The hydrodynamic radius (r) of the particles can then be determined from the Stokes-Einstien relation in equation 10.

$$D = \frac{k_B T}{6\pi\eta r} \quad (10)$$

Where; D is the diffusion constant, k_B is Boltzmann's constant, η is the viscosity of the solvent and T is the absolute temperature. DLS (Nanosizer, Malvern Instruments, Malvern, UK) was used to determine the mean intensity-weighted hydrodynamic diameter, zeta potential and polydispersity index (pdi) of all the NPs (liposomes and PBCA NPs) used in this thesis. In Paper II and III, DLS was a used to measure the size of liposomes before and after labeling with 1,1'-dioctadecyl-3,3,3',3'-tetramethylindo-dicarbocyanine,4'chlorobenzenesulfonate salt (DiD, Molecular Probes, Eugene, OR, USA) and 1,1'-dioctadecyl-3,3,3',3'-tetramethylindotricarbo-cyanine iodine (DiR, Molecular Probes, Eugene, OR, USA) to ensure no significant change in size or pdi after labelling.

3.9. Scanning Electron Microscopy (SEM)

Scanning electron microscope (SEM) is a type of microscope that uses 2 to 3 nm spot of electrons to scan the surface of a sample in a raster scan pattern to produce an image. The interaction of the electrons with the sample produces secondary electrons that can give information about the surface topography and composition of the sample. The morphology of the PBCA-NPs was characterized by Hitachi S-5500 scanning electron microscope (Hitachi GmbH, Krefeld Germany) (Paper IV).

3.10. Coulter Counter

A Coulter counter is an instrument used for counting the number of particles, and can also be used to measure the size of the particles suspended in electrolytes. The coulter counter is based on the principle that, particles moving in an electric field cause some disturbance and the magnitude of the disturbance is proportional to the size of the particles in the field. In Paper IV, Beckman Multisizer 3 coulter counter was used to measure the number and size of the NP-loaded MBs used in cellular uptake experiment.

3.11. Model Systems

3.11.1. Cell lines

Cellular experiments (spectroscopy, flow cytometry, CLSM) of liposomes in Paper II were performed with human cervical carcinoma cells (HeLa) whilst that of PBCA NPs in Paper IV was performed with human prostatic carcinoma cell lines (PC3). HeLa or PC3 cells were grown in Dulbecco's Modified Eagle Medium (DMEM) supplemented with 10% fetal bovine serum (FBS) (Sigma-Aldrich, Oslo, Norway), 2 mM non-essential amino acids and 1 mM L-glutamine (Sigma-Aldrich, Oslo, Norway). The cell cultures were grown at 37°C and in 5% CO_2. Exponentially growing cells were harvested with 3 ml of trypsin (0.25%) and resuspended in growth medium just before experiments.

3.11.2. Animal

For *in vivo* experiments (Paper III), 6 weeks female Balb/c nude mice (C.Cg/AnNTac-Foxn1nu NE9, Taconic, Denmark) were used. The animals were housed in IVC cages (model 1284L, Techniplast, France) under conditions free of specific pathogens according to Federation of European Laboratory Animal Science Association's [130] recommendations. Thus, they had free access to food and sterile water and the environment was controlled with temperatures kept between 19-22 $^{\circ}$C and relative humidity between 50-60 %. All experimental procedures with animals were in compliance with protocols approved by the Norwegian National Animal Research Authorities.

3.11.3. Tumor model and preparation of tumor sections

PC3 cell line as the one used in intracellular experiment were also used as tumor model in Paper III. Before implantation of the cells, mice were anaesthetized with isoflurane, and then, 3 x 10^6 cells in suspension of 50 µl were slowly injected subcutaneously on the lateral aspect of one hind leg, between the hip and the knee. The tumors were allowed to grow for 3-6 weeks until the diameter of the tumor was between 5 and 10 mm. All animals were euthanized by cervical dislocation and then the tumor was excised, embedded in OTC Tissue Tec (Sakura, Alphen aan den Rijn, The Netherlands) and frozen in liquid N_2. The tumor was cut through into frozen sections (5 µm thick) from three depth levels with 250 µm between each level. The sections with blood vessels were labeled using fluorescin-bound lectin (Lycopersicon Esculentum, 2 mg/ml, Vector laboratories, Burlingame, CA, USA) circulation method.

3.12. Data and Statistical Analysis

Detailed analysis of data in the present work can be found in the original papers.

4. SUMMARY OF RESULTS

Paper I – *Effect of Ultrasound Parameters on the Release of Liposomal Calcein*

In this paper, US exposure parameters that maximize drug release (calcein) from sonosensitive DEPC-based liposomes were studied using two focused US transducers at 300 kHz and 1 MHz. Calcein release was measured using a spectrophotometer by monitoring relief from self-quenching liposomes in isoosmotic sucrose solution, after US exposure. At 300 kHz, drug release was more efficient than at 1 MHz, although the 1 MHz transducer was used at higher intensities and peak negative pressures than the 300 kHz transducer. In order to obtain release greater than 5 %, a minimum threshold of acoustic pressure must be overcome, and the peak negative pressure thresholds for the 300 kHz and 1 MHz transducers were found to be 0.9 MPa and 1.9 MPa respectively. Above this threshold, the release increased with increasing peak negative pressure, MI, and duty cycle. However, a decrease in drug release was observed with the 1 MHz transducer at higher pressures. The amount of calcein release followed first-order kinetics, and it increased with increasing exposure time up to a maximal release, which was dependent on the MI. Hence, the maximal release is dependent on the MI. Besides, drug release correlated with the formation of free radicals (OH) demonstrating that the release mechanism involves inertial cavitation, and only a minor temperature increase was measured in US exposed samples.

Paper II – *Mechanisms of the Ultrasound-Mediated Intracellular Delivery of Liposomes and Dextrans*

The focus of this paper is the mechanism involved in US enhanced intracellular delivery of FITC-dextrans (4 – 2000 kDa) and DEPC-based liposomes containing doxorubicin using HeLa cells. The role of endocytosis was also investigated using endocytic inhibitors; chlorpromazine, genistein and wortmannin that inhibits clathrin-mediated endocytosis, caveolae-mediated endocytosis and macropinocytosis respectively. Cellular uptake of doxorubicin and FITC-dextran was enhanced by US only in the presence of MBs, while the percentage of cells internalizing doxorubicin and dextran increased with increasing MI. Flow cytometric analysis indicated that DEPC-based liposomes released their contents extracellularly during US exposure before cellular uptake of the released drug. Confocal images confirmed that doxorubicin was found mainly in the cytoplasm and nucleus of the cell, whereas DiD (fragments or intact liposomes) were found only in the periphery of cells and cell membranes. Cell death was more prominent when incubating cells with liposomal doxorubicin compared to the rate of cell death with dextran during insonication in the presence of MBs. The percentage of cells internalizing dextran was independent of the molecular weight of dextrans, but the amount of the small 4-kDa dextran molecules internalized per cell was higher than the other dextrans. Inhibition of the endocytic pathways resulted in significant decrease in the cellular uptake from approximately 60% when no inhibitors were added to approximately 30%, 22%, and 14% upon addition with genistein, wortmannin, and chlorpromazine respectively. However, complete inhibition of endocytosis did not result in the complete blockage of cellular uptake, suggesting that pore formation is a part of the mechanism. Hence, both sonoporation and endocytosis played a role in the US-enhanced cellular uptake.

Paper III – *Ultrasound Improves Uptake and Distribution of Liposomal Doxorubicin in Prostate Cancer Xenografts*

This paper shows how optical imaging methods were used to study the effect of different US exposures (1 MHz and 300 kHz) on delivery and distribution of DEPC-based liposomal doxorubicin in Balb/c nude mice bearing prostate cancer xenografts. The effect was examined microscopically (micro-distribution in tumor tissue) with confocal laser scanning microscope (CLSM) and macroscopically using whole animal optical imaging (biodistribution). CLSM images showed that the amount of doxorubicin fluorescence in the control group was highest at the periphery of the tumor sections and decreased towards the central areas, whereas the amount in the insonicated groups was high both in the periphery and central areas of the tumor. Thus, the amount of doxorubicin in tumor tissue increased approximately 4-fold in the 1 MHz group and 5-fold in the 300 kHz group as compared to the non-exposed group. However, there was no significant difference between the 1 MHz group and the 300 kHz group. Displacement of liposomes and doxorubicin away from blood vessels increased with both exposure groups. Considering the animals that received 1 MHz insonication, the degree of doxorubicin and liposomal penetration increased approximately twice for both central and peripheral blood vessels as compared to control tumors. Meanwhile, there was no significant increase in liposome penetration (both central and periphery) for those that received 300 kHz insonication and the control group. Furthermore, in the 300 kHz exposure group, there was about 20 % increment in the degree of doxorubicin displacement for both central and peripheral blood vessels as compared to control tumors. However, there was no significant increase in doxorubicin displacement between exposed and control groups in the peripheral areas of the tumor. Additionally, there was no significant difference in the biodistribution of liposomes in normal versus tumor tissues after US exposure.

Paper IV – *Multifunctional Particles for Drug Delivery and Imaging: Effect of Nanoparticle PEGylation, Size and Ultrasound on Cellular Uptake*

The last paper focuses on a newly developed multifunctional drug delivery system *i.e.,* MBs stabilized by NPs. The effect of NP size (109 – 228 nm), PEGylation (Tween80, long and short Jeffamine) and surfactant (SDS, AOT and Tween80) on the kinetics of internalization of the PBCA NPs in prostate cancer cells was investigated. The effect of low frequency US on cellular uptake of the NPs in the presence and absence of NP-loaded MBs were also studied. Cellular uptake was influenced by the length and type of PEG molecules on the NP surface and the surfactant used for emulsification. Thus, cellular uptake of particles PEGylated with long Jeffamine was higher than particles with short Jeffamine PEG. In addition, NPs with SDS showed higher cellular uptake than those with AOT or Tween80. The rate constant determined from fitting the data to a first-order kinetic curve was higher for particles with SDS than particles with AOT, and Tween80. Within the size range studied in this work, the size of particles did not seem to have a large impact on the uptake of NPs. However, the effect of size on cellular uptake was influenced by effect of PEG and surfactant. Internalization of NPs was confirmed by CLSM, where NPs were found mainly in the cytoplasm of cells with barely any particle in the nucleus. PBCA NPs exhibited dose-response toxicity on PC3 cell line, with extensive morphological changes in cells exposed to concentrations of 40µg/ml and above. The toxicity was dependent on the surfactant used, with Tween 80 giving less toxicity than SDS and AOT. US had no significant effect on cellular uptake of PBCA NPs in live cells in the presence and absence of NP-loaded MBs.

5. GENERAL DISCUSSION

Successful cancer therapy requires that the cytotoxic agents must reach the targeted site in optimal concentrations to eradicate every deadly cell, because one single cell is capable of re-growing the tumor. To achieve localized delivery and increase the therapeutic dose at the targeted site, US can be combined with delivery of encapsulated drugs. The use of US in the delivery of NPs has exceptional advantages because it is safe, non-invasive, can be controlled both spatially and temporally, and can penetrate deep into the body without affecting intermediate tissues. In this thesis, focused US with frequencies of 300 kHz (low) and 1MHz (medium) were used to study the effect of US on release of drug from liposomes in *vitro* and *in vivo* (Paper I and III), cellular uptake of NPs and drug *in vitro* and *in vivo* (Paper II, III and IV) and penetration of released drug and liposomes into tumor tissues (Paper III). In this chapter, effect of US on drug carriers, US treatment strategies to overcome barriers to drug delivery and effects of PBCA surface functionalization on cellular uptake and cell viability are discussed.

5.1. Effect of Ultrasound on Liposomal Drug Release

In the present work, US exposure parameter that maximizes drug release was investigated both *in vitro* and in *vivo* using sonosensitive liposomes (Paper I, II and III). The *in vitro* (in solution) results (Paper I) revealed a linear dependence of drug release (calcein) from DEPC-based liposomes on MI after a certain pressure threshold. OH radicals were also detected to validate the occurrence of inertial cavitation. These observations suggest the released mechanism to be inertial cavitation and our result is in accordance with what has been reported by other investigators [14, 15, 76, 87]. A growing line of evidence suggests that inertial cavitation occurs only above a certain MI threshold, and the threshold is dependent on several factors like the level of dissolved gases, viscosity, purity, etc [74, 75, 99]. Schroeder and others suggested that the mechanism of cavitation-mediated drug release from liposomes might be due to increased permeability of the liposomes membrane caused by oscillations of gas nuclei (formed by US) in the hydrophobic region of liposome bilayer [87, 131]. Other suggestions include shear stress from oscillating or collapsing bubbles (close to the liposomes), rupturing or reforming liposomes into smaller vesicles to release the content [65]. DOPE-based liposome which has a cone-shaped geometry has been shown to release drug by destabilization of the lipid bilayer[14]. The liposomes used in this thesis might also release drug through a similar mechanism since DEPC (main phospholipid of the present liposomes) also has a cone-shaped geometry.

Drug release was also observed *in vivo* (Paper III) when tumors were treated with liposomes followed by US (300 kHz and 1 MHz) treatment after 24 hour. We observed an increase in the amount of doxorubicin fluorescence in tumor tissues exposed to US compared with non-exposed tumors. This signifies that US triggered the release of doxorubicin from liposomes in the tumor since the fluorescence of doxorubicin in intact liposomes would be quenched by neighboring doxorubicin molecules. This observation was also demonstrated in an *in vitro* study in Paper II where extracellular disruption of the DEPC-based liposomes followed by intracellular doxorubicin uptake was observed after US and microbubble exposure. Thus, we did not observe any significant uptake of intact liposomes, meaning the observed doxorubicin

uptake was from released liposomes. However, in this study (Paper II), MBs were added to the cells before US exposure and low MIs were used to avoid massive cell death unlike the *in vivo* study (Paper III).

The *in vivo* study in Paper III revealed no statistical difference between the amount of doxorubicin fluorescence in the 300 kHz and the 1 MHz exposed groups, although there seems to be higher release in the 300 kHz group than the 1 MHz group. One possible explanation might be the difference in the MIs (comparable) of the two frequencies, since the other exposure parameters were the same. In addition, the MIs used for the two frequencies (300 kHz and 1 MHz) were above the threshold of cavitation observed in the *in vitro* drug release experiment (Paper I). Moreover, the liposomes used in both *in vitro* and *in vivo* experiments are thermally stable because no calcein leakage was found when the liposomes were incubated for 4 hours at 37 °C in sucrose/HEPES solution. Besides, we did not observe any significant increase in temperature before and after US treatment of tumors. It can therefore be deduced that, mechanical effect of US, probably cavitation might be responsible for the *in vivo* drug release as well. However, because of the complexity of the *in vivo* environment, direct translation from *in vitro* to *in vivo* cavitation might not be possible. Thus, there might be some variation in the factors that determine the occurrence of cavitation (mentioned above) *in vivo*. Also, the presence of plasma proteins and cells in the tumor tissue may have influence on the threshold of cavitation *in vivo* [132]. Although, the underlying mechanism of cavitation (especially *in vivo*) is not fully understood, researchers [66, 74, 133] have reported that, cavitation activity increases with increase in the number of gas nuclei. The presence of pre-existing gas nuclei has been suggested on surfaces such as endothelial in capillaries and epithelia in skin, hence, gas bubbles or small gas nuclei that might be present naturally in the tissue could facilitate the occurrence of cavitation in *vivo*. This also shows that the *in vivo* drug release mechanism might be the occurrence of non-thermal effects like cavitation, although it's not very clear.

Determination of overall optimal US exposure parameters (frequency, peak negative pressure, duty cycle, exposure time, etc.) would be desirable for the development of safe and effective protocols for successful cancer therapy. In Paper I, we observed that two exposure parameters are important in determining the total drug release from DEPC-based liposomes using the first-order kinetic model. These parameters are MI and exposure time (*i.e.* effective time of the US defined as the product of the duty cycle and the insonication time). However, more investigations are needed to verify whether this finding (MI and exposure) will be possible in an *in vivo* setting. Since, exposure time is directly proportional to the duty cycle, optimal exposure time may be achieved by using either continuous wave or pulse wave US. For clinical application, the use of pulse wave US in drug delivery will help to reduce rapid tissue heating. Furthermore, the dependence of release on MI implies that, focused US of higher frequencies could be used in drug delivery to deposit the acoustic energy at a local spot due to the higher focusing ability than low frequency US [66, 99].

Paper I, II and III points to the fact that in US mediated drug delivery, US may increase the concentration of the drug at the target site by inducing drug release of drug carriers (liposomes) before the occurrence of cellular uptake.

5.2. Ultrasound Treatment Strategies to Overcome Barriers to Drug Delivery

Another challenge in drug delivery is the tumor microenvironment, which inhibits uniform and adequate delivery of cytotoxic drugs. To ensure penetration into the tumor ECM and homogenous distribution of the NPs, these barriers (Section 1.1) have to be lifted or opened.

5.2.1. Effect of Ultrasound on the transport of Nanoparticles/drugs through the ECM

The data in Paper III shows an enhancement in the penetration (with respect to central and periphery blood vessels) of both released drug (doxorubicin) and liposomes in tumor tissues after 300 kHz and 1 MHz US exposure, but 1 MHz exposure was more effective than 300 kHz exposure. Acoustic radiation force might be responsible for the enhanced microdistribution of doxorubicin and liposomes in the insonicated tumor tissues. Radiation force is proportional to the temporal average intensity and the absorption coefficient of the tissue [68-70] and increases with increasing US frequency. Also, Nightingale and others [134] have reported that, an increase in non-linearity can increase the radiation force by a factor of 2.6 in breast application *in vivo*. The 1 MHz transducer used in this thesis had higher peak negative pressure (2.2MPa), temporary average intensity (13 W/cm^2) and nonlinear pulse distortions than the 0.3 MHz (pressure 1.3 MPa and intensity of 3 W/cm^2). This might explain why enhanced penetration of drugs in tumor tissues was observed in the 1MHz exposed group more than the 300 kHz exposed group. This displacement is very relevant for clinical applications because the displacement would make drugs available to more cancer cells to eradicate every deadly cell, and focused US of high frequencies can be used for that purpose.

The possibility of using US to cause induction of apoptosis of cancer cells has been shown. For instance, the induction of apoptosis in glioma cells exposed to low frequency US has been demonstrated by Zhang and others [135]. They showed alterations in the regulation of apoptosis-related proteins in cancer cells exposed to US. Guo and coworkers [136] also reported that apoptosis of pancreatic cancer cells increased during the first hours after US exposure and peaked at 24 hour. Apoptotic cells shrink in size and this can induce remodeling of the ECM. Alterations in ECM would also make more space in the ECM to facilitate transport of drugs and particles to target cells. Although, we observed (Paper III) an enhancement in the penetration of released drug and liposomes in tumor tissues after US exposure, the possibility of US induced apoptosis has not been validated in this experiment.

Macroscopic biodistribution of liposomes in tumor and normal tissues was studied with whole animal optical imaging before and after US exposure. US exposure did not increase the accumulation of liposomes in the tumor 24 hour post-injection. This is because, its only about 10 % of the liposomes that will still be in circulation (Cyril Lafon, personal communication) after 24 hour of administration, thus, any contribution of liposomes from the vasculature during US exposure would be insignificant considering the small amounts of circulating liposomes 24 hour after injection. Also, accumulation of liposomes in normal tissues (liver, spleen and kidneys) was observed as reported by others [137, 138]. This might be as a result of MPS in these organs, which might have taken up the liposomes despite the fact that these liposomes were PEGylated. Liposomal formulation should therefore be designed to reduce this effect if not eliminated completely.

In drug delivery, it would be desirable if the NPs can accumulate at the tumor sites by the EPR effect, then US can be applied to release the drug in order to increase local drug

concentration, enhance the distribution and the cellular uptake. However, the EPR effect can be highly heterogeneous [139, 140], and even the vessels in the same tumor may not be fenestrated to the same degree, so depending on the size of the NPs, extravasation may not be uniform. The application of US at the tumor site few minutes after liposome administration to increase the extravasation of NPs or released drug from microcirculation into tumor tissues might also help to overcome this challenge. In addition, accumulation of NPs at the tumor site can also be monitored with imaging modalities like MRI or optical or US to ensure adequate extravasation of NPs [119, 120, 141, 142].

5.2.2. Effect of ultrasound on cellular uptake

Studies have shown that US have the potential to enhance cancer therapy response, by increasing the permeability of cell membrane reversibly to allow the passage of cytotoxic drugs into the cell. The use of US to inflict stress on cells and tissue is the third major contribution of US to drug delivery. In Paper II and IV, we did not see an enhancement in the cellular uptake of DEPC-based liposomes or released doxorubicin or PBCA NPs in the absence of MBs *in vitro*. Thus, to obtain efficient intracellular uptake of NPs and FITC-dextrans, microbubble should be present during US exposure. In the presence of MBs, cellular uptake was enhanced after MI of 0.53 which signifies a threshold effect. These observations indicates the major role played by cavitation in the cellular uptake enhanced by US and this has been shown by other studies as well [64, 65, 91, 93-95, 110, 143, 144].

In Paper III, cellular uptake of released doxorubicin and liposomes was enhanced in US exposed tumors compared to non-exposed group regardless of the fact that no MBs were added during US exposure. Interestingly, in Paper II, with the same frequency (300 kHz), cellular uptake of released doxorubicin or liposomes was not enhanced in the absence of MBs. This confirms the difficulty in translating *in vitro* data to *in vivo*[133]. Perhaps the type of cell lines used (*i.e.*, PC3 tumor model for in *vivo* work whereas HeLa cells were used for the *in vitro)* contributed to this difference. Also differences in exposure set-up might be a contributing factor, thus, the tumor used in the animal studies are superficial and was easy to access by US as compared to the cells in the polyethylene transfer pipette used in the *in vitro* experiment.

The efficiency of sonoporation has been shown to be heterogeneous [112]. That is, in the same experiment, some of the cells, may be permeabilised, killed or appeared to be unaffected even though they received the same US treatment[112, 145]. This was also observed in our *in vitro* cellular uptake experiment in Paper II. Thus, Flow cytometric analysis and confocal images showed cells that have internalized both doxorubicin and DiD, but the majority of the cells showed no doxorubicin or DiD fluorescence. The difference in cell populations was attributed to the distance between the cells and the MBs by Guzman and others [112]. Our *in vitro* data showed higher cell death when cells were treated with liposomal doxorubicin and US in the presence of MBs than when they were treated with liposomal doxorubicin and US in the absence of MBs. This indicates cell damage caused by the collapse of the MBs [65, 94]. However, lower cell death was recorded with cells treated with FITC-dextran but with the same US exposure parameter as those with liposomes and US in the presence of MBs. Hence, the cytotoxic effect of doxorubicin might have contributed to the observed cell death [95]. In cancer therapy, cell killing by too high US exposures may not be desirable because, too high US exposures might also destroy some normal tissues and also increase the occurrence of metastasis (tumor cell detachment). Too low exposures may also not be adequate to effectively enhance cellular uptake even though it would not kill too many cells. It is therefore important

to find cavitational levels that produce bubble activity sufficient to permeabilize cell membranes without killing the healthy cells since both cellular uptake and cell viability are dependent on US exposure parameters. Karshafian and his colleagues [94] defined this optimal exposure parameter as therapeutic ratio, *i.e*., ratio of permeabilised to nonviable cells.

Full understanding of how US and MBs improve cellular uptake of NPs is lacking, although, MBs have been used clinically to enhance US contrast imaging for more than two decades. To have successful sonoporation-mediated therapeutic applications, the mechanism and the effects of US and microbubble exposure conditions need to be understood. A growing line of evidence suggests pore formation caused by bubble oscillation or rupture to be the biological mechanism underpinng sonoporation [100-103, 111, 145, 146]. In paper II, we investigated the mechanism of US-mediated intracellular uptake using US and MBs with FITC-dextrans and endocytic inhibitors. We observed that endocytosis plays an important role in the enhanced cellular uptake caused by US and MBs using 500 kDa. However, complete inhibition of endocytosis did not result in the complete blockage of cellular uptake, suggesting that pore formation is part of the mechanism.

The result also revealed that the percentage of cells that has internalized dextrans is independent on the size of dextran (4 kDa to 2 MDa). Nevertheless, a higher amount of the smallest dextran (4 kDa) was internalized per cell; meaning US-mediated intracellular uptake was more efficient with low molecular weight entities. The implication is that, the use of drugs with a lower molecular weight (*e.g*., Dox) would be more desirable in US-mediated cancer therapy than drugs with a higher molecular weight. This has also been demonstrated by Meijering and colleagues [97] using dextrans and confocal microscopy. They observed that not only pores are created during sonoporation but US and MBs also enhances endocytosis. That is, smaller dextrans (4.4 and 70 kDa) were shown to be taken up throughout the cytosol by transient pores created in the endothelial cells whilst larger dextrans (155 and 500 kDa) were found in distinct vesicles (endocytotic vesicles) after sonoporation. Additional study is needed to understand the dependence of US-enhanced endocytosis on the molecular weight of NPs and also whether different US parameters favours one over the other mechanism. Furthermore, an increased number of endocytic vesicles have been observed in insonicated cells, which also support the hypothesis of US enhanced endocytosis[109]. However, little is known about how US can stimulate endocytosis. Possibly, US trigger stable or transient cavitation, which causes shear stress on the cell membrane. Shear stress has been suggested to stimulate endocytosis through a deformation of the plasma membrane, causing a reorganization of the cytoskeleton, which affects endocytosis [147]. In addition, Lawler and cowoker [148] has also reported that shear stress can stimulate endocytosis by inducing the activation, translocation, and clustering of integrins to counteract stress, which triggers endocytosis.

It has been reported in several studies that sonoporation-induced cell membrane pore size ranges from 75 nm to ~ 1 μm [101, 103, 146]. However, the distribution of these pores are said to be heterogeneous; hence smaller pores are created than larger pore leading to higher cellular uptake of smaller macromolecules than larger ones. The resealing time of the pore has been shown to be within milliseconds to minutes [101, 111] but the larger the pore size, the higher the chances of cells not surviving the resealing process. In Paper IV, we investigated whether low frequency US (300 kHz) enhanced the uptake of PBCA NPs (119 nm – 153 nm) attached to an air-filled microbubble. US with or without NP-loaded MBs did not enhance cellular uptake of PBCA nanoparticle in live cells. One possible explanation might be size limitations of the NPs, that is, the size of the pore might be too small for the particles to enter.

Also, there is evidence that the type of MBs may be of crucial importance in sonoporation [149-151]. In the present work (Paper IV), US and 3.3 % of Definity MBs could not enhance the cellular uptake either, which shows that it might not be the type of MBs but probably the size of particles. This study is ongoing, so more experiments would be conducted with smaller NPs. Studies on the acoustic properties of the different NP-loaded MBs are currently under investigation in our laboratory.

5.3. Effect of PBCA Nanoparticle PEGylation, Surfactant and Size on Cellular Uptake and Cell Viability

Understanding the interaction between cells and NPs is crucial when designing NPs for improved drug delivery to intracellular targets. This is because the cell-nanoparticle interactions, and hence, the cellular uptake of NPs, is affected by factors such as surface chemistry, size, shape and morphology of the particles. In Paper IV, effect of particle PEGylation, size and surfactant on cellular uptake was studied with PC3 cells. Generally, all the different types of NPs have a sticky nature; they stick to cell membrane, however, three times washing with PBS was found to be adequate to remove most of the surface bounded particles. For instance, when NPs were added to cells and removed immediately (*i.e.*, without incubation) followed by three times washing with PBS, cells were found to be Nile red positive and the percentage was found to be dependent on the type of PEG on the surface of the particles. To confirm internalization of particles in cells, CLSM was used to image cells after 3 hours incubation with NPs, and revealed internalization of particles in the cytoplasm, but not in the nucleus. The kinetic study points to the fact that cellular uptake is largely dependent on the surface properties (type or length of PEG and surfactant) of the NPs. Thus, NPs functionalized with long chain Jeffamine were taken up to a larger extent compared to particles with short Jeffamine or Tween80 PEG. This might be as a result of the differences in PEG density and conformation on the particle surface. The Tween80 PEG being a branched polymer is likely to form a more compact PEG wherein the PEG will wrap around the NP more than the linear PEG (Jeffamine) [52, 152-154]. Furthermore, the short Jeffamine PEG might be able to form more dense PEG structure on the particle surface than the long Jeffamine PEG, as the long PEG chain might spatially hinder high amounts of this molecule from reacting with the monomer at the droplet surface upon polymerization [153]. Studies have shown that PEG density or conformation have influence on cellular uptake [46, 51]. The conformation and density of PEG on the particle surface is currently being investigated in our laboratory. NP uptake in PC3 cells was also influenced by the type of surfactant used for manufacturing the particles. NPs with SDS (anionic) surfactant demonstrated higher cellular uptake compared with those with AOT (anionic) or Tween 80 (non-ionic). This is consistent with what has been reported by Musyanovych and others [49] where nanoparticle with anionic surfactant were taken up at a higher rate than NPs with non-ionic surfactant.

Regardless of the fact that PBCA NPs are said to be biocompatible and biodegradable, the data on toxicity is somewhat contradictory, and the degradation products of PBCA NPs have in some studies shown to be toxic [48, 50, 56, 155, 156]. The results from this study indicated concentration above 20µg/ml to be toxic for the PC3 cells and this is in agreement with the result obtained by Kreuter and colleagues [56]. However, higher concentration than 20µg/ml might be tolerated in *vivo* due to the protective mechanism in the body. Apart from the degradation products, surfactant can also contribute to the level of toxicity, since they are known to influence cell permeability [48]. Generally, SDS particles were found to be more toxic than AOT or Tween 80 surfactant.

6. CONCLUDING REMARKS

The work presented in this thesis shows that US has a great potential to improve drug delivery and cancer therapy by triggering the release of drug, thereby increasing the drug concentration at the target site. It follows that US can enhance the penetration of the released drug into tumor tissues, as well as enhancing the drug uptake at the tumor site. Conclusions drawn from this study are contained in subsequent paragraphs.

US parameters optimal for drug release from DEPC-based liposomes *in vitro* were characterized and the study shows that both low and medium US frequency can trigger the release of DEPC-based liposomes in *vitro* and *in vivo.* The release mechanism *in vitro* was shown to be inertial cavitation, however, *in vivo* drug release mechanism is unclear but mechanical effect (cavitation) is suspected. The present work points to the fact that MI and exposure time determines the total drug release from liposomes *in vitro*. Future experiment should focus on verifying whether these two parameters can be used to determine the total amount of drug release in *vivo* since the translation from *in vitro* to *in vivo* is not straight forward.

We have demonstrated that US exposure can improve the distribution of release doxorubicin from DEPC-based liposomes in tumor tissue. Medium frequency US was found to be more efficient in displacing drugs away from blood vessels than low frequency US. In clinical implementation, the displacement of drug away from blood vessels will make drugs available to more cancer cells in order to kill every deadly cell. This suggests that the use of high frequency US in drug delivery would be desirable since clinical application may require non-destructive focused US at higher frequencies.

Furthermore, cellular uptake of liposomes and released doxorubicin was enhanced by US *in vivo* and *in vitro*. The study revealed that DEPC-based liposomes released their contents extracellularly during US and MB exposure before cellular uptake took place. Moreover, US combined with MBs were found to be more effective in enhancing the cellular uptake of doxorubicin and FITC-dextran than US alone *in vitro*. The percentage of cells internalizing dextran was size-independent; however, smaller sized dextrans were internalized in higher quantities than larger dextrans, meaning lower molecular weight drugs would be more appropriate for ultrasound-mediated cancer therapy than drugs with a higher molecular weight. Both pore formation and US enhanced-endocytosis were found to be the main mechanisms responsible for the US-enhanced cellular uptake. More studies are therefore required to verify whether acoustic parameters (frequency, pressure, duty cycle etc.) and properties of MBs (size, gas composition, wall thickness and mechanical properties) affect these two mechanisms differently.

The length and the type of PEG, as well as surfactant on the surface of the NPs were found to have impact on cellular uptake. In addition, PBCA NPs exhibited dose-response toxicity on PC3 cell line. Low frequency US and NP-loaded MBs did not enhance the cellular uptake of the PBCA NPs, probably, due to size limitations of the NPs. There is an ongoing study to determine the conformation and density of PEG on the particle surface, as well as the acoustic properties of the shell of the different NP-loaded MBs

Although US-mediated drug delivery seems to be promising, in order to develop safe and effective protocols for successful cancer therapy, the mechanisms behind the observed effects need to be elucidated thoroughly so as to have optimal treatment and also, avoid unwanted effect from US on adjacent healthy tissues. Future experiments will therefore focus on understanding the behaviour of NP-loaded MBs in ultrasonic field in order to determine the optimal exposure parameters for target imaging, bubble destruction and cell membrane permeability. Thus, the acoustic parameters optimal for releasing the NPs from the MBs might not be the same as those for cell membrane permeabilization without cell killing. Hence, *in vitro* and *in vivo* experiments would be conducted to determine these parameters. Currently, *in vivo* experiments are ongoing, where the biodistribution of the NP is being studied with whole animal optical imaging. In addition, studies on the effect of low and high ultrasound exposure with and without NP-loaded MBs on the microdistribution of NP in tumor tissues are also in progress.

In summary, the results show that US has a great potential to improve drug delivery. With additional advantages of US being non-invasive, able to be focused locally at target site and also deep in the body, US-mediated drug delivery proves to be a powerful strategy to improve cancer therapy.

7. REFERENCES

1. Drummond, D.C., et al., *Optimizing Liposomes for Delivery of Chemotherapeutic Agents to Solid Tumors.* Pharmacological Reviews, 1999. **51**(4): p. 691-744.
2. Speth, P.A., Q.G. van Hoesel, and C. Haanen, *Clinical pharmacokinetics of doxorubicin.* Clin Pharmacokinet, 1988. **15**(1): p. 15-31.
3. Gabizon, A. and F. Martin, *Polyethylene glycol-coated (pegylated) liposomal doxorubicin. Rationale for use in solid tumours.* Drugs, 1997. **54 Suppl 4**: p. 15-21.
4. Mayer, L.D., et al., *Influence of Vesicle Size, Lipid Composition, and Drug-to-Lipid Ratio on the Biological Activity of Liposomal Doxorubicin in Mice.* Cancer Research, 1989. **49**(21): p. 5922-5930.
5. Working, P.K., et al., *Pharmacokinetics, Biodistribution and Therapeutic Efficacy of Doxorubicin Encapsulated in Stealth® Liposomes (Doxil®).* Journal of Liposome Research, 1994. **4**(1): p. 667-687.
6. Bae, Y.H., *Drug targeting and tumor heterogeneity.* Journal of Controlled Release, 2009. **133**(1): p. 2-3.
7. Reitan, N.K., et al., *Characterization of tumor microvascular structure and permeability: comparison between magnetic resonance imaging and intravital confocal imaging.* J Biomed Opt, 2010. **15**(3): p. 036004.
8. Wu, N.Z., et al., *Increased microvascular permeability contributes to preferential accumulation of Stealth liposomes in tumor tissue.* Cancer Res, 1993. **53**(16): p. 3765-70.
9. Yuan, F., et al., *Mirovascular Permeability and Interstitial Penetration of Sterically Stabilized (Stealth) Liposomes in a Human Tumor Xenograft.* Cancer Research, 1994. **54**(13): p. 3352-3356.
10. Symon, Z., et al., *Selective delivery of doxorubicin to patients with breast carcinoma metastases by stealth liposomes.* Cancer, 1999. **86**(1): p. 72-8.
11. Davies Cde, L., et al., *Radiation improves the distribution and uptake of liposomal doxorubicin (caelyx) in human osteosarcoma xenografts.* Cancer Res, 2004. **64**(2): p. 547-53.
12. Vaage, J., et al., *Tumour uptake of doxorubicin in polyethylene glycol-coated liposomes and therapeutic effect against a xenografted human pancreatic carcinoma.* Br J Cancer, 1997. **75**(4): p. 482-6.
13. Babincova, M., et al., *AC-magnetic field controlled drug release from magnetoliposomes: design of a method for site-specific chemotherapy.* Bioelectrochemistry, 2002. **55**(1-2): p. 17-9.
14. Evjen, T.J., et al., *Ultrasound-mediated destabilization and drug release from liposomes comprising dioleoylphosphatidylethanolamine.* Eur J Pharm Sci, 2011. **42**(4): p. 380-6.
15. Husseini, G.A., et al., *Factors affecting acoustically triggered release of drugs from polymeric micelles.* J Control Release, 2000. **69**(1): p. 43-52.
16. Husseini, G.A. and W.G. Pitt, *Micelles and nanoparticles for ultrasonic drug and gene delivery.* Advanced Drug Delivery Reviews, 2008. **60**(10): p. 1137-1152.
17. Pangu, G.D., et al., *Ultrasonically induced release from nanosized polymer vesicles.* Macromol Biosci, 2010. **10**(5): p. 546-54.
18. Jain, R.K., *Barriers to drug delivery in solid tumors.* Sci Am, 1994. **271**(1): p. 58-65.
19. Jain, R.K., *Delivery of molecular medicine to solid tumors: lessons from in vivo imaging of gene expression and function.* J Control Release, 2001. **74**(1-3): p. 7-25.
20. Jain, R.K., *Transport of molecules in the tumor interstitium: a review.* Cancer Res, 1987. **47**(12): p. 3039-51.

21. Boucher, Y. and R.K. Jain, *Microvascular pressure is the principal driving force for interstitial hypertension in solid tumors: implications for vascular collapse.* Cancer Res, 1992. **52**(18): p. 5110-4.
22. Boucher, Y. and R.K. Jain, *Microvascular Pressure Is the Principal Driving Force for Interstitial Hypertension in Solid Tumors: Implications for Vascular Collapse.* Cancer Research, 1992. **52**(18): p. 5110-5114.
23. Eikenes, L., et al., *Collagenase increases the transcapillary pressure gradient and improves the uptake and distribution of monoclonal antibodies in human osteosarcoma xenografts.* Cancer Res, 2004. **64**(14): p. 4768-73.
24. Brekken, C., O.S. Bruland, and C. de Lange Davies, *Interstitial fluid pressure in human osteosarcoma xenografts: significance of implantation site and the response to intratumoral injection of hyaluronidase.* Anticancer Res, 2000. **20**(5B): p. 3503-12.
25. Swabb, E.A., J. Wei, and P.M. Gullino, *Diffusion and convection in normal and neoplastic tissues.* Cancer Res, 1974. **34**(10): p. 2814-22.
26. Davies Cde, L., et al., *Comparison of IgG diffusion and extracellular matrix composition in rhabdomyosarcomas grown in mice versus in vitro as spheroids reveals the role of host stromal cells.* Br J Cancer, 2002. **86**(10): p. 1639-44.
27. Netti, P.A., et al., *Role of extracellular matrix assembly in interstitial transport in solid tumors.* Cancer Res, 2000. **60**(9): p. 2497-503.
28. Hayer, A., et al., *Caveolin-1 is ubiquitinated and targeted to intralumenal vesicles in endolysosomes for degradation.* J Cell Biol, 2010. **191**(3): p. 615-29.
29. Mayor, S. and R.E. Pagano, *Pathways of clathrin-independent endocytosis.* Nat Rev Mol Cell Biol, 2007. **8**(8): p. 603-612.
30. Midoux, P., et al., *Polymer-based gene delivery: a current review on the uptake and intracellular trafficking of polyplexes.* Curr Gene Ther, 2008. **8**(5): p. 335-52.
31. Kerr, M.C. and R.D. Teasdale, *Defining macropinocytosis.* Traffic, 2009. **10**(4): p. 364-71.
32. Iversen, T.-G., T. Skotland, and K. Sandvig, *Endocytosis and intracellular transport of nanoparticles: Present knowledge and need for future studies.* Nano Today, 2011. **6**(2): p. 176-185.
33. Wang, L.H., K.G. Rothberg, and R.G. Anderson, *Mis-assembly of clathrin lattices on endosomes reveals a regulatory switch for coated pit formation.* J Cell Biol, 1993. **123**(5): p. 1107-17.
34. Nabi, I.R. and P.U. Le, *Caveolae/raft-dependent endocytosis.* J Cell Biol, 2003. **161**(4): p. 673-7.
35. Parton, R.G., B. Joggerst, and K. Simons, *Regulated internalization of caveolae.* J Cell Biol, 1994. **127**(5): p. 1199-215.
36. Kruth, H.S., et al., *Macropinocytosis is the endocytic pathway that mediates macrophage foam cell formation with native low density lipoprotein.* J Biol Chem, 2005. **280**(3): p. 2352-60.
37. Cho, K., et al., *Therapeutic Nanoparticles for Drug Delivery in Cancer.* Clinical Cancer Research, 2008. **14**(5): p. 1310-1316.
38. Bangham, A.D. and R.W. Horne, *Negative staining of phospholipids and their structural modification by surface-active agents as observed in the electron microscope.* Journal of Molecular Biology, 1964. **8**(5): p. 660-IN10.
39. Bangham, A.D., M.M. Standish, and J.C. Watkins, *Diffusion of univalent ions across the lamellae of swollen phospholipids.* Journal of Molecular Biology, 1965. **13**(1): p. 238-IN27.
40. New, R.R.C., *Liposomes: a practical approach*. 1990, Oxford: IRL Press. xvi, 301 s.
41. Evjen, T.J., et al., *Distearoylphosphatidylethanolamine-based liposomes for ultrasound-mediated drug delivery.* Eur J Pharm Biopharm, 2010. **75**(3): p. 327-33.
42. Kulkarni, S.B., G.V. Betageri, and M. Singh, *Factors affecting microencapsulation of drugs in liposomes.* J Microencapsul, 1995. **12**(3): p. 229-46.

43. Gasselhuber, A., et al., *Comparison of Conventional Chemotherapy, Stealth Liposomes and Temperature-Sensitive Liposomes in a Mathematical Model.* PLoS ONE, 2012. **7**(10): p. e47453.
44. Dromi, S., et al., *Pulsed-high intensity focused ultrasound and low temperature-sensitive liposomes for enhanced targeted drug delivery and antitumor effect.* Clin Cancer Res, 2007. **13**(9): p. 2722-7.
45. van Vlerken, L.E. and M.M. Amiji, *Multi-functional polymeric nanoparticles for tumour-targeted drug delivery.* Expert Opin Drug Deliv, 2006. **3**(2): p. 205-16.
46. Soppimath, K.S., et al., *Biodegradable polymeric nanoparticles as drug delivery devices.* Journal of Controlled Release, 2001. **70**(1–2): p. 1-20.
47. Cavalieri, F., et al., *Methods of preparation of multifunctional microbubbles and their in vitro / in vivo assessment of stability, functional and structural properties.* Curr Pharm Des, 2012. **18**(15): p. 2135-51.
48. Mailänder, V. and K. Landfester, *Interaction of Nanoparticles with Cells.* Biomacromolecules, 2009. **10**(9): p. 2379-2400.
49. Musyanovych, A., et al., *Criteria impacting the cellular uptake of nanoparticles: A study emphasizing polymer type and surfactant effects.* Acta Biomaterialia, 2011. **7**(12): p. 4160-4168.
50. Weiss, C.K., et al., *Cellular uptake behavior of unfunctionalized and functionalized PBCA particles prepared in a miniemulsion.* Macromol Biosci, 2007. **7**(7): p. 883-96.
51. Hu, Y., et al., *Effect of PEG conformation and particle size on the cellular uptake efficiency of nanoparticles with the HepG2 cells.* Journal of Controlled Release, 2007. **118**(1): p. 7-17.
52. Vugmeyster, Y., et al., *Pharmacokinetic, Biodistribution, and Biophysical Profiles of TNF Nanobodies Conjugated to Linear or Branched Poly(ethylene glycol).* Bioconjugate Chemistry, 2012. **23**(7): p. 1452-1462.
53. Kante, B., et al., *Toxicity of polyalkylcyanoacrylate nanoparticles I: Free nanoparticles.* J Pharm Sci, 1982. **71**(7): p. 786-90.
54. Müller, R.H., et al., *Alkylcyanoacrylate drug carriers: I. Physicochemical characterization of nanoparticles with different alkyl chain length.* International Journal of Pharmaceutics, 1992. **84**(1): p. 1-11.
55. Vauthier, C., et al., *Poly(alkylcyanoacrylates) as biodegradable materials for biomedical applications.* Adv Drug Deliv Rev, 2003. **55**(4): p. 519-48.
56. Kreuter, J., et al., *Direct evidence that polysorbate-80-coated poly(butylcyanoacrylate) nanoparticles deliver drugs to the CNS via specific mechanisms requiring prior binding of drug to the nanoparticles.* Pharm Res, 2003. **20**(3): p. 409-16.
57. Wells, P.N., *Ultrasound imaging.* Phys Med Biol, 2006. **51**(13): p. 20.
58. Humphrey, V.F., *Ultrasound and matter—Physical interactions.* Progress in Biophysics and Molecular Biology, 2007. **93**(1–3): p. 195-211.
59. Huber, P.E., et al., *A new noninvasive approach in breast cancer therapy using magnetic resonance imaging-guided focused ultrasound surgery.* Cancer Res, 2001. **61**(23): p. 8441-7.
60. Kennedy, J.E., G.R. Ter Haar, and D. Cranston, *High intensity focused ultrasound: surgery of the future?* Br J Radiol, 2003. **76**(909): p. 590-9.
61. Kong, G., et al., *Efficacy of liposomes and hyperthermia in a human tumor xenograft model: importance of triggered drug release.* Cancer Res, 2000. **60**(24): p. 6950-7.
62. Koning, G.A., et al., *Hyperthermia and thermosensitive liposomes for improved delivery of chemotherapeutic drugs to solid tumors.* Pharm Res, 2010. **27**(8): p. 1750-4.
63. Tacker, J.R. and R.U. Anderson, *Delivery of antitumor drug to bladder cancer by use of phase transition liposomes and hyperthermia.* J Urol, 1982. **127**(6): p. 1211-4.
64. Frenkel, V., *Ultrasound mediated delivery of drugs and genes to solid tumors.* Adv Drug Deliv Rev, 2008. **60**(10): p. 1193-208.

65. Pitt, W.G., G.A. Husseini, and B.J. Staples, *Ultrasonic drug delivery--a general review.* Expert Opin Drug Deliv, 2004. **1**(1): p. 37-56.
66. Leighton, T.G., *The acoustic bubble*. 1994, London: Academic Press. XXVI, 613 s.
67. Wu, J., A.J. Winkler, and T.P. O'Neill, *Effect of acoustic streaming on ultrasonic heating.* Ultrasound Med Biol, 1994. **20**(2): p. 195-201.
68. Nightingale, K.R., et al., *On the feasibility of remote palpation using acoustic radiation force.* J Acoust Soc Am, 2001. **110**(1): p. 625-34.
69. Starritt, H.C., F.A. Duck, and V.F. Humphrey, *Forces acting in the direction of propagation in pulsed ultrasound fields.* Phys Med Biol, 1991. **36**(11): p. 1465-74.
70. Torr, G.R., *The acoustic radiation force.* American Journal of Physics, 1984. **52**(5): p. 402-408.
71. Lizzi, F.L., et al., *Radiation-force technique to monitor lesions during ultrasonic therapy.* Ultrasound Med Biol, 2003. **29**(11): p. 1593-605.
72. Nightingale, K., et al., *Acoustic radiation force impulse imaging: in vivo demonstration of clinical feasibility.* Ultrasound in Medicine & Biology, 2002. **28**(2): p. 227-235.
73. Minnaert, M., *On musical air bubbles and sound of running water.* Philosophical Magazine, 1933. **16**(104): p. 13.
74. Apfel, R.E. and C.K. Holland, *Gauging the likelihood of cavitation from short-pulse, low-duty cycle diagnostic ultrasound.* Ultrasound in Medicine & Biology, 1991. **17**(2): p. 179-185.
75. Young, F.R., *Cavitation*. 1999, London: Imperial College Press. XXII, 418 s.
76. Husseini, G.A., et al., *The role of cavitation in acoustically activated drug delivery.* Journal of Controlled Release, 2005. **107**(2): p. 253-261.
77. Mestas, J.L., P. Lenz, and D. Cathignol, *Long-lasting stable cavitation.* J Acoust Soc Am, 2003. **113**(3): p. 1426-30.
78. Neppiras, E., *Subharmonic and Other Low-Frequency Emission from Bubbles in Sound-Irradiated Liquids.* Acoust Soc Amer, 1968. **46**(3): p. 187- 601
79. Newman, C.M. and T. Bettinger, *Gene therapy progress and prospects: ultrasound for gene transfer.* Gene Ther, 2007. **14**(6): p. 465-75.
80. Dayton, P.A., J.S. Allen, and K.W. Ferrara, *The magnitude of radiation force on ultrasound contrast agents.* J Acoust Soc Am, 2002. **112**(5 Pt 1): p. 2183-92.
81. Lum, A.F., et al., *Ultrasound radiation force enables targeted deposition of model drug carriers loaded on microbubbles.* J Control Release, 2006. **111**(1-2): p. 128-34.
82. Shortencarier, M.J., et al., *A method for radiation-force localized drug delivery using gas-filled lipospheres.* IEEE Trans Ultrason Ferroelectr Freq Control, 2004. **51**(7): p. 822-31.
83. Tartis, M.S., et al., *Therapeutic effects of paclitaxel-containing ultrasound contrast agents.* Ultrasound Med Biol, 2006. **32**(11): p. 1771-80.
84. Huang, S.L. and R.C. MacDonald, *Acoustically active liposomes for drug encapsulation and ultrasound-triggered release.* Biochim Biophys Acta, 2004. **1665**(1-2): p. 134-41.
85. Evjen, T.J., et al., *Lipid membrane composition influences drug release from dioleoylphosphatidylethanolamine-based liposomes on exposure to ultrasound.* International Journal of Pharmaceutics, 2011. **406**(1–2): p. 114-116.
86. Nelson, J.L., et al., *Ultrasonically activated chemotherapeutic drug delivery in a rat model.* Cancer Res, 2002. **62**(24): p. 7280-3.
87. Schroeder, A., et al., *Controlling Liposomal Drug Release with Low Frequency Ultrasound: Mechanism and Feasibility.* Langmuir, 2007. **23**(7): p. 4019-4025.
88. Howard, W.A., Jr., et al., *Sonolysis promotes indirect Co-C bond cleavage of alkylcob(III)alamin bioconjugates.* Bioconjug Chem, 1997. **8**(4): p. 498-502.
89. de Paula, D.M.B., et al., *Therapeutic ultrasound promotes plasmid DNA uptake by clathrin-mediated endocytosis.* Journal of Gene Medicine, 2011. **13**(7-8): p. 392-401.
90. Delalande, A., et al., *Ultrasound and microbubble-assisted gene delivery in Achilles tendons: Long lasting gene expression and restoration of fibromodulin KO phenotype.* Journal of Controlled Release, 2011. **156**(2): p. 223-230.

91. Diaz-Moscoso, A., et al., *Insights in cellular uptake mechanisms of pDNA-polycationic amphiphilic cyclodextrin nanoparticles (CDplexes).* J Control Release, 2010. **143**(3): p. 318-25.
92. Geers, B., et al., *Elucidating the mechanisms behind sonoporation with adeno-associated virus-loaded microbubbles.* Molecular Pharmaceutics, 2011. **8**(6): p. 2244-2251.
93. Guzman, H.R., et al., *Equilibrium loading of cells with macromolecules by ultrasound: effects of molecular size and acoustic energy.* J Pharm Sci, 2002. **91**(7): p. 1693-701.
94. Karshafian, R., et al., *Sonoporation by ultrasound-activated microbubble contrast agents: effect of acoustic exposure parameters on cell membrane permeability and cell viability.* Ultrasound Med Biol, 2009. **35**(5): p. 847-60.
95. Lentacker, I., et al., *Design and evaluation of doxorubicin-containing microbubbles for ultrasound-triggered doxorubicin delivery: cytotoxicity and mechanisms involved.* Mol Ther, 2010. **18**(1): p. 101-8.
96. Marmottant, P. and S. Hilgenfeldt, *Controlled vesicle deformation and lysis by single oscillating bubbles.* Nature, 2003. **423**(6936): p. 153-6.
97. Meijering, B.D., et al., *Ultrasound and microbubble-targeted delivery of macromolecules is regulated by induction of endocytosis and pore formation.* Circ Res, 2009. **104**(5): p. 679-87.
98. Barnett, S.B., et al., *The sensitivity of biological tissue to ultrasound.* Ultrasound Med Biol, 1997. **23**(6): p. 805-12.
99. Nyborg, W.L.M. and J. Wu, *Emerging therapeutic ultrasound*. 2006, Hackensack, N.J.: World Scientific. xvi, 346 s.
100. Collis, J., et al., *Cavitation microstreaming and stress fields created by microbubbles.* Ultrasonics, 2010. **50**(2): p. 273-9.
101. Qiu, Y., et al., *The correlation between acoustic cavitation and sonoporation involved in ultrasound-mediated DNA transfection with polyethylenimine (PEI) in vitro.* J Control Release, 2010. **145**(1): p. 40-8.
102. Zhou, Y., J. Cui, and C.X. Deng, *Dynamics of sonoporation correlated with acoustic cavitation activities.* Biophys J, 2008. **94**(7): p. L51-3.
103. Zhou, Y., et al., *The size of sonoporation pores on the cell membrane.* Ultrasound Med Biol, 2009. **35**(10): p. 1756-60.
104. Schlachetzki, F., et al., *Observation on the Integrity of the Blood-Brain Barrier After Microbubble Destruction by Diagnostic Transcranial Color-Coded Sonography.* Journal of Ultrasound in Medicine, 2002. **21**(4): p. 419-429.
105. Skyba, D.M., et al., *Direct In Vivo Visualization of Intravascular Destruction of Microbubbles by Ultrasound and its Local Effects on Tissue.* Circulation, 1998. **98**(4): p. 290-293.
106. Song, J., et al., *Influence of injection site, microvascular pressureand ultrasound variables on microbubble-mediated delivery of microspheres to muscle.* Journal of the American College of Cardiology, 2002. **39**(4): p. 726-731.
107. Lawrie, A., et al., *Microbubble-enhanced ultrasound for vascular gene delivery.* Gene Ther, 2000. **7**(23): p. 2023-7.
108. Tachibana, K. and S. Tachibana, *The use of ultrasound for drug delivery.* Echocardiography, 2001. **18**(4): p. 323-8.
109. Hauser, J., et al., *Ultrasound enhanced endocytotic activity of human fibroblasts.* Ultrasound Med Biol, 2009. **35**(12): p. 2084-92.
110. Kooiman, K., et al., *Sonoporation of endothelial cells by vibrating targeted microbubbles.* Journal of Controlled Release, 2011. **154**(1): p. 35-41.
111. Gambihler, S., M. Delius, and J.W. Ellwart, *Permeabilization of the plasma membrane of L1210 mouse leukemia cells using lithotripter shock waves.* J Membr Biol, 1994. **141**(3): p. 267-75.
112. Guzman, H.R., et al., *Bioeffects caused by changes in acoustic cavitation bubble density and cell concentration: a unified explanation based on cell-to-bubble ratio and blast radius.* Ultrasound Med Biol, 2003. **29**(8): p. 1211-22.

113. Bouakaz, A. and N. de Jong, *WFUMB Safety Symposium on Echo-Contrast Agents: nature and types of ultrasound contrast agents.* Ultrasound Med Biol, 2007. **33**(2): p. 187-96.
114. Chen, W.S., et al., *A comparison of the fragmentation thresholds and inertial cavitation doses of different ultrasound contrast agents.* J Acoust Soc Am, 2003. **113**(1): p. 643-51.
115. de Jong, N., A. Bouakaz, and P. Frinking, *Basic acoustic properties of microbubbles.* Echocardiography, 2002. **19**(3): p. 229-40.
116. Unger, E.C., et al., *Acoustically active lipospheres containing paclitaxel: A new therapeutic ultrasound contrast agent.* Investigative Radiology, 1998. **33**(12): p. 886-892.
117. Wheatley, M.A., J.D. Lathia, and K.L. Oum, *Polymeric ultrasound contrast agents targeted to integrins: importance of process methods and surface density of ligands.* Biomacromolecules, 2007. **8**(2): p. 516-22.
118. Fokong, S., et al., *Image-guided, targeted and triggered drug delivery to tumors using polymer-based microbubbles.* Journal of Controlled Release, 2012. **163**(1): p. 75-81.
119. Yang, F., et al., *Superparamagnetic iron oxide nanoparticle-embedded encapsulated microbubbles as dual contrast agents of magnetic resonance and ultrasound imaging.* Biomaterials, 2009. **30**(23–24): p. 3882-3890.
120. Park, J.I., et al., *Microbubbles Loaded with Nanoparticles: A Route to Multiple Imaging Modalities.* ACS Nano, 2010. **4**(11): p. 6579-6586.
121. Stride, E., et al., *Increasing the nonlinear character of microbubble oscillations at low acoustic pressures.* J R Soc Interface, 2008. **5**(24): p. 807-11.
122. Duzgunes, N., et al., *Proton-induced fusion of oleic acid-phosphatidylethanolamine liposomes.* Biochemistry, 1985. **24**(13): p. 3091-8.
123. Düzgünes, N., et al., *Fluorescence methods in liposome research*, in *Liposomes.*, V.P. Torchilin, Weissig, V., Editor. 2003, Oxford university press: Oxford
124. Mason, T.J., et al., *Dosimetry in sonochemistry: the use of aqueous terephthalate ion as a fluorescence monitor.* Ultrasonics Sonochemistry, 1994. **1**(2): p. S91-S95.
125. Somaglino, L., et al., *Validation of an acoustic cavitation dose with hydroxyl radical production generated by inertial cavitation in pulsed mode: application to in vitro drug release from liposomes.* Ultrason Sonochem, 2011. **18**(2): p. 577-88.
126. Villeneuve, L., et al., *Assay of hydroxyl radicals generated by focused ultrasound.* Ultrason Sonochem, 2009. **16**(3): p. 339-44.
127. Pawley, J.B., *Handbook of Biological Confocal Microscopy*. 2006, Boston, MA: Springer-Verlag US.
128. Choy, G., P. Choyke, and S.K. Libutti, *Current advances in molecular imaging: noninvasive in vivo bioluminescent and fluorescent optical imaging in cancer research.* Mol Imaging, 2003. **2**(4): p. 303-12.
129. Weissleder, R. and U. Mahmood, *Molecular Imaging1.* Radiology, 2001. **219**(2): p. 316-333.
130. Nicklas, W., et al., *Recommendations for the health monitoring of rodent and rabbit colonies in breeding and experimental units.* Lab Anim, 2002. **36**(1): p. 20-42.
131. Schroeder, A., J. Kost, and Y. Barenholz, *Ultrasound, liposomes, and drug delivery: principles for using ultrasound to control the release of drugs from liposomes.* Chem Phys Lipids, 2009. **162**(1-2): p. 1-16.
132. Deng, C.X., et al., *In vitro measurements of inertial cavitation thresholds in human blood.* Ultrasound in Medicine & Biology, 1996. **22**(7): p. 939-948.
133. Miller, M.W., D.L. Miller, and A.A. Brayman, *A review of in vitro bioeffects of inertial ultrasonic cavitation from a mechanistic perspective.* Ultrasound Med Biol, 1996. **22**(9): p. 1131-54.
134. Nightingale, K.R., P.J. Kornguth, and G.E. Trahey, *The use of acoustic streaming in breast lesion diagnosis: a clinical study.* Ultrasound Med Biol, 1999. **25**(1): p. 75-87.
135. Zhang, Z., et al., *Low frequency and intensity ultrasound induces apoptosis of brain glioma in rats mediated by caspase-3, Bcl-2, and survivin.* Brain Res, 2012. **1473**: p. 25-34.

136. Guo, Q., L.X. Jiang, and B. Hu, *Focused ultrasound induces apoptosis in pancreatic cancer cells.* Chin Med J (Engl), 2012. **125**(12): p. 2089-93.
137. Harrington, K.J., et al., *Biodistribution and pharmacokinetics of 111In-DTPA-labelled pegylated liposomes in a human tumour xenograft model: implications for novel targeting strategies.* Br J Cancer, 2000. **83**(2): p. 232-8.
138. Gabizon, A., H. Shmeeda, and Y. Barenholz, *Pharmacokinetics of pegylated liposomal Doxorubicin: review of animal and human studies.* Clin Pharmacokinet, 2003. **42**(5): p. 419-36.
139. Bae, Y.H. and K. Park, *Targeted drug delivery to tumors: Myths, reality and possibility.* Journal of Controlled Release, 2011. **153**(3): p. 198-205.
140. Jain, R.K. and T. Stylianopoulos, *Delivering nanomedicine to solid tumors.* Nat Rev Clin Oncol, 2010. **7**(11): p. 653-664.
141. Lammers, T., et al., *Nanotheranostics and Image-Guided Drug Delivery: Current Concepts and Future Directions.* Molecular Pharmaceutics, 2010. **7**(6): p. 1899-1912.
142. Sun, D., *Nanotheranostics: Integration of Imaging and Targeted Drug Delivery.* Molecular Pharmaceutics, 2010. **7**(6): p. 1879-1879.
143. Marin, A., et al., *Drug delivery in pluronic micelles: effect of high-frequency ultrasound on drug release from micelles and intracellular uptake.* Journal of Controlled Release, 2002. **84**(1–2): p. 39-47.
144. Tran, T.A., et al., *Effect of ultrasound-activated microbubbles on the cell electrophysiological properties.* Ultrasound Med Biol, 2007. **33**(1): p. 158-63.
145. van Wamel, A., et al., *Ultrasound microbubble induced endothelial cell permeability.* J Control Release, 2006. **116**(2): p. e100-2.
146. Mehier-Humbert, S., et al., *Plasma membrane poration induced by ultrasound exposure: implication for drug delivery.* J Control Release, 2005. **104**(1): p. 213-22.
147. Apodaca, G., *Modulation of membrane traffic by mechanical stimuli.* Am J Physiol Renal Physiol, 2002. **282**(2): p. F179-90.
148. Lawler, K., et al., *Shear stress induces internalization of E-cadherin and invasiveness in metastatic oesophageal cancer cells by a Src-dependent pathway.* Cancer Sci, 2009. **100**(6): p. 1082-7.
149. Blomley, M., *Which US microbubble contrast agent is best for gene therapy?* Radiology, 2003. **229**(2): p. 297-8.
150. Li, T., K. Tachibana, and M. Kuroki, *Gene transfer with echo-enhanced contrast agents: comparison between Albunex, Optison, and Levovist in mice--initial results.* Radiology, 2003. **229**(2): p. 423-8.
151. Ward, M., J. Wu, and J.F. Chiu, *Ultrasound-induced cell lysis and sonoporation enhanced by contrast agents.* J Acoust Soc Am, 1999. **105**(5): p. 2951-7.
152. Park, J.B., et al., *PEGylation of bacterial cocaine esterase for protection against protease digestion and immunogenicity.* J Control Release, 2010. **142**(2): p. 174-9.
153. Sofia, S.J., V.V. Premnath, and E.W. Merrill, *Poly(ethylene oxide) Grafted to Silicon Surfaces: Grafting Density and Protein Adsorption.* Macromolecules, 1998. **31**(15): p. 5059-70.
154. Wu, M., et al., *Poly(n-butyl cyanoacrylate) nanoparticles via miniemulsion polymerization. 2. PEG-based surfactants.* Colloids and Surfaces B: Biointerfaces, 2009. **69**(1): p. 147-151.
155. Olivier, J.C., *Drug transport to brain with targeted nanoparticles.* NeuroRx, 2005. **2**(1): p. 108-19.
156. Olivier, J.C., et al., *Indirect evidence that drug brain targeting using polysorbate 80-coated polybutylcyanoacrylate nanoparticles is related to toxicity.* Pharm Res, 1999. **16**(12): p. 1836-42.

8. PAPERS

Paper I

EFFECT OF ULTRASOUND PARAMETERS ON THE RELEASE OF LIPOSOMAL CALCEIN

Ultrasound in Med. & Biol., Vol. 38, No. 3, pp. 476–486, 2012

0301-5629/$ - see front matter

ELSEVIER

doi:10.1016/j.ultrasmedbio.2011.11.017

● *Original Contribution*

EFFECT OF ULTRASOUND PARAMETERS ON THE RELEASE OF LIPOSOMAL CALCEIN

Mercy Afadzi,*† Catharina de L. Davies,* Yngve H. Hansen,* Tonni Johansen,† Øyvind K. Standal,† Rune Hansen,†‡ Svein-Erik Måsøy,† Esben A. Nilssen,§ and Bjørn Angelsen†

*Department of Physics; †Department of Circulation and Medical Imaging, The Norwegian University of Science and Technology, Trondheim, Norway; ‡Department of Medical Technology SINTEF Technology and Society, Trondheim, Norway; and §Epitarget AS, Oslo, Norway

(*Received* 1 *July* 2011; *revised* 17 *November* 2011; *in final form* 27 *November* 2011)

Abstract—The ultrasound exposure parameters that maximize drug release from dierucoyl-phosphatidylcholine (DEPC)-based liposomes were studied using two transducers operating at 300 kHz and 1 MHz. Fluorescent calcein was used as a model drug, and the release from liposomes in solution was measured using a spectrophotometer. The release of calcein was more efficient at 300 kHz than at 1 MHz, with thresholds of peak negative pressures of 0.9 MPa and 1.9 MPa, respectively. Above this threshold, the release increased with increasing peak negative pressure, mechanical index (MI), and duty cycle. The amount of drug released followed first-order kinetics and increased with exposure time to a maximal release. To increase the release further, the MI had to be increased. The results demonstrate that the MI and the overall exposure time are the major parameters that determine the drug's release. The drug's release is probably due to mechanical (cavitation) rather than thermal effects, and that was also confirmed by the detection of hydroxide radicals. (E-mail: mercy.afadzi@ntnu.no) © **2012 World Federation for Ultrasound in Medicine & Biology.**

Key Words: **Ultrasound parameters, Mechanical index, Drug release, Liposomes, Cavitation.**

INTRODUCTION

The main limitation associated with conventional chemotherapy is the poor therapeutic index caused by the high level of toxicity in healthy tissues (Drummond et al. 1999). Successful cancer therapy requires that cytotoxic drugs reach the tumor cells and inactivate them with minimal damage to normal tissue. To reduce the exposure of normal tissue, cytotoxic drugs should be selectively delivered to tumor tissue. This may be achieved by encapsulating the drug in a particulate carrier, such as a liposome, micelle, or other nanoparticle (Allen 1997; Barenholz 2001, 2007; Torchilin 2005; Liu et al. 2006). For an effective therapeutic effect, the carrier should remain stable in the circulatory system with an adequate amount of drug and then release the drug at a sufficient rate once the nanoparticle is at the tumor site (Huang and McDonald 2004). Because of the hyperpermeable, fenestrated nature of tumor vessels (Yuan et al. 1994; Bae 2009), nanoparticles with diameters of approximately 100 nm are typically able to cross the capillary wall and accumulate in the tumor interstitium. However, the distribution of the nanoparticles and the drug is heterogeneous within the tumor tissue (Vaage et al. 1997; Davies et al. 2004; Bae 2009). Large areas of the tumor are not reached by the drug because of the heterogeneous fenestration of the tumor blood vessels and poor penetration through the extracellular matrix.

There is also a challenge in controlling the localization and drug-release kinetics of intravenously injected nanoparticles so as to obtain sufficient drug concentrations at the target site. Triggered mechanisms, both chemical and physical, for controlling the release of the drug may be used to overcome this challenge. Ultrasound has been shown to improve both the release and the biodistribution of the drug (Huang and McDonald 2004; Rapoport 2007; Steinberg et al. 2007; Schroeder et al. 2007, 2009;). Ultrasound is of special interest because it is noninvasive, can be controlled both spatially and

Address correspondence to: Mercy Afadzi, M.Sc., Department of Physics, The Norwegian University of Science and Technology, Høgskoleringen 5, 7491 Trondheim, Norway. E-mail: mercy.afadzi@ntnu.no

temporally, and can penetrate deep into the body without affecting intermediate tissue. Furthermore, it has been shown that ultrasound increases the permeability of blood-tissue barriers and cell membranes (Bednarski et al. 1997; Price et al. 1998; Guaman et al. 2001; Kost and Langer 2001). Several animal studies combining ultrasound and liposomal drugs have demonstrated a reduced tumor growth rate when ultrasound and liposomal drugs are combined, compared to liposomal drugs alone (Myhr and Moan 2006; Schroeder et al. 2009; Hagtvet et al. 2011; Pitt et al. 2011).

Although the mechanism of ultrasound-mediated drug release is not fully understood (Pitt et al. 2004; Steinberg et al. 2007), it is generally divided into thermal and nonthermal effects. Acoustic cavitation is the most important nonthermal mechanism; it involves the creation, oscillation, growth, and collapse of gas bubbles in a fluid exposed to a sound wave (Leighton et al. 1994, 1998; Young 1999). The effect of the sound wave on the bubbles can lead to stable oscillations (stable cavitation) or to total collapse (transient or inertial cavitation) of the bubbles. The transition from stable cavitation to inertial cavitation occurs at a threshold called the inertial cavitation threshold (Apfel and Holland 1991; Leighton 1994; Young 1999; Miller 2007), which is dependent on the peak negative pressure, the frequency, and the initial bubble radius (Leighton 1994, 2007; Young 1999; Humphrey 2007). During inertial cavitation, the collapse of the bubbles can be very violent, and the bubbles often disintegrate into a mass of smaller bubbles, which can produce shock waves, jet streams, high temperatures, and free radicals (Apfel and Holland 1991; Leighton 1994; Young 1999; Miller 2007). The mechanical index (MI) (i.e., the ratio between the peak negative pressure [megapascal] and the square root of the frequency [megahertz]) indicates the occurrence of inertial cavitation; an MI below 0.7 (with a broad range of bubbles sizes) theoretically signifies no occurrence of cavitation (Apfel and Holland 1991).

Husseini et al. (2000) used 70 kHz ultrasound, varied the intensity, and showed that the release of drug from the micelles was caused by cavitation, that is, the structure of the micelles was perturbed by cavitation. Liu et al. (1988) also reported that inertial cavitation played a dominant role in the drug release from micelle cores. Schroeder et al. (2007) and Pangu et al. (2010), using 20 kHz ultrasound and varying the intensity and exposure time, suggested that the increased release was caused by cavitation-inducing transient pore formation in liposomes and polysomes, respectively. However, most of these studies were based on nonfocused low-frequency (20 to 90 kHz) ultrasound, which is not compatible with frequencies used in the clinic; only a few different exposure regimes were compared; and the transducers used were often ultrasonic mixers, limiting user control over exposure parameters. Thus, only a limited number of exposure parameters have been studied. For the effective release of drug from liposomes, determination of optimal ultrasound exposure parameters, such as frequency, negative pressure, intensity, duration, and duty cycle, have to be determined in order to develop protocols for improved cancer therapy.

The lipid composition of liposomes has been reported to be of importance for ultrasound-induced drug release (Lin and Thomas 2003, 2004; Schroeder et al. 2009). Traditional and clinically used liposomes consisting of hydrogenated soy phosphatidylcholine (HSPC); cholesterol; and polyethylene glycol–conjugated phosphatidylethanolamines (DSPE-PEG) are reported to have reduced sonosensitivity compared to liposomal formulations comprising phospholipids with smaller head groups and longer and/or unsaturated acyl chains (Evjen et al. 2010, 2011). The latter liposomes may be based on, for example, distearoyl-phosphatidylethanolamine (DSPE); dioleoylphosphatidylethanolamine (DOPE); or dierucoyl-phosphatidylcholine (DEPC) without nondissolved gasses. In the present work we used DEPC-based liposomes.

The aim of this work was to investigate the effects of the various ultrasound exposure parameters that maximize drug release from DEPC-based liposomes. We hypothesized that cavitation was the primary mechanism of drug release, and the impact of MI on drug release was studied, as was the overall exposure time determined by the duty cycle and insonication time. The liposomes were placed in solution and exposed to a focused ultrasound beam using frequencies of 300 kHz and 1 MHz. Such frequencies allow adequate focusing of the ultrasound beam, hence facilitating spatially confined drug delivery. The release of the model drug calcein (a small fluorescent molecule) was monitored by measuring the fluorescence intensity of the released drug spectrophotometrically at increasing acoustic pressures and exposure times.

MATERIALS AND METHODS

Materials

Distearoylphosphatidylcholine (DSPC) and distearoylphosphatidylethanolamine-(methoxy(polyethyleneglycol)2000) (DSPE-PEG) were purchased from Genzyme Pharmaceuticals (Liestal, Switzerland). Calcein, cholesterol, 4-(2-hydroxyethyl)-1-piperazineethanesulfonic acid (HEPES), Triton X-100 solution, and sucrose were obtained from Sigma Aldrich (Oslo, Norway). Dierucoylphosphatidylcholine (DEPC) was supplied by Avanti Polar Lipids (Alabaster, AL, USA).

Table 1. Specification of transducers

Parameter	Frequency	
	0.3 MHz	1 MHz
Diameter (active)	55 mm	50 mm
Radius of curvature	90 mm	131 mm
Location of maximum intensity	69 mm	125 mm
Relative bandwidth	47%	62%
−3 dB beam diameter at location of maximum intensity	6.6 mm	3 mm
L_m, range where the pressure is −1 dB compared to the pressure at the maximum intensity	32.57 mm	33 mm

Liposomes

The liposomes had a lipid composition of 52 mol% DEPC, 5 mol% DSPC, 8 mol% DSPE-PEG, and 35 mol% cholesterol. The intraliposomal phase consisted of 50 mM calcein in a 10 mM HEPES solution (osmolality of 313 mOsm/kg and a pH of 7.4). The extraliposomal phase consisted of an isosmotic sucrose solution in 10 mM HEPES and 0.02% (w/v) sodium azide (pH 7.4). The liposomes were produced according to the thin film method (Lasic 1993). Briefly, the lipids were dissolved in a chloroform/methanol mixture (9/1 v/v) at 60°C and rotary-evaporated to dryness under vacuum for 6 h. The resulting dried lipid films were hydrated with the 50 mM calcein solution for 2 h followed by 3 freeze-thaw cycles in a dry ice/acetone/methanol mixture and water, respectively. The liposomes at a lipid concentration of 16 mg/mL were downsized by stepwise extrusion (Lipex extruder, Biomembrane, Vancouver, BC, Canada) through Nucleopore polycarbonate filters with pore sizes of 800, 400, 200, 100, and 100 nm (Nuclepore, West Chester, PA, USA). The lipid hydration, liposome extrusion, and thawing processes were performed at 25°C, which is above the gel-to-liquid crystalline phase transition temperature of the phospholipids. Extraliposomal calcein was removed by dialyzing 10 mL liposome dispersion against 0.5 L isotonic sucrose solution containing 10 mM HEPES and 0.01% (w/v) sodium azide. The latter dialysis buffer was changed 10 times. The liposome diameter was determined to be 105 nm (polydispersity index of 0.18) by photon correlation spectroscopy (Nanosizer, Malvern Instruments, Malvern, UK). Stability studies showed 1% or less liposome leakage after 4-hour incubation at 37°C or 6-month incubation at 5°C in HEPES sucrose buffer.

Characterization of transducers

Two custom-made, single-element ultrasound transducers (Imasonic, Besançon, France) with frequencies of 300 kHz and 1 MHz were used. The transducers were of piezoelectric composite and had matching layers and a thick backing. Each transducer had a thermocoupler in the backing to monitor the temperature in the transducer. The specifications of the transducers can be found in Table 1. The acoustic field was characterized using a capsule hydrophone (Onda HGL-0200, Onda, Sunnyvale, CA, USA) with a tip diameter of 200 μm, connected to a 20-dB preamplifier (Onda AH-2020) in a rectangular Plexiglas water tank. The 2-dimensional beam profiles were recorded and the -3-dB beam width along the lateral direction was measured (see Table 1). Also, the range (L_m) at which the pressure was -1 dB compared to the pressure at the maximum intensity was determined (see Table 1). Generally, the 1-MHz transducer was found to exhibit more nonlinearity than the 300-kHz transducer at the peak maximum intensity. That is, the ratio of the second to the first harmonic component for the 1-MHz transducer was -17.6 dB and -7.6 dB for, respectively, the lowest and highest pressures measured, whereas that of the 300-kHz transducer was -36.6 dB (lowest pressure) and -22.9 dB (highest pressure measured). The maximal pressures and their corresponding temporal average intensities (I_{TA}) and MIs were calculated from the experimental data using Equations 1 and 2:

$$I_{TA} = PRF \int_0^T \frac{p^2}{\rho c}\, dt \tag{1}$$

$$MI = \frac{P_{neg}}{\sqrt{f}} \tag{2}$$

where p is the acoustic pressure, ρ is the mass density, c is the speed of sound in the medium, T is the repetition period, PRF is the pulse repetition frequency, P_{neg} is the peak negative pressure in MPa, and f is the frequency in MHz. However, the levels of the pressure were measured in free space (inside the water tank), not inside the sample chamber.

Ultrasound exposure set-up

The exposure set-up consisted of a signal generator (Hewlett Packard 33120A, San Jose, CA, USA); an oscilloscope (Lecroy waverunner, LT262, Long Branch, NJ, USA); a power amplifier (ENI 2100L, Rochester, NY, USA); the two custom-made transducers, and an insonication chamber. However, because of the power limitations of the ENI amplifier, in addition, an 8-channel PC-controlled arbitrary waveform generator board (DA4300, Acquitek, Massy, France) connected to a custom-made 8 channel power amplifier (ENI 90AB8, Rochester, NY, USA), (in which the 8 channels were combined) was used to drive the transducer. A cylindrical PVC water tank (200 mm in diameter and 300 mm long) was designed for the insonication of the sample. The inside of the water tank was coated with regular sponge

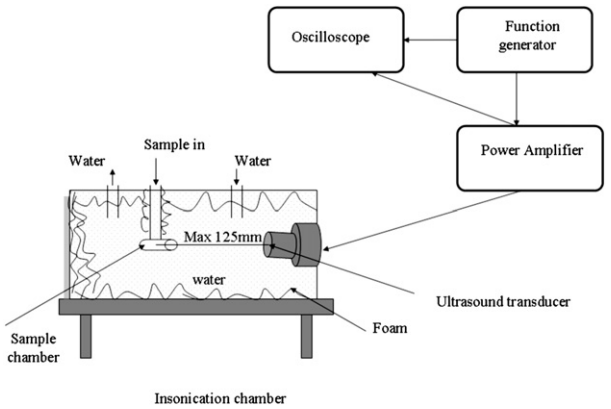

Fig. 1. Schematic presentation of the insonication chamber and the exposure set-up for ultrasound-triggered release.

(15 mm thick) to avoid reflections of the sound waves. A cylindrical Plexiglas tube (8 mm in diameter and 20 mm long) with a 23 μm-thick Mylar membrane glued on both the front and back openings was used as the sample chamber. The center of the sample chamber was placed at a position equivalent to the maximum intensity of the transducer (69 mm for the 300-kHz transducer and 125 mm for the 1-MHz transducer). The PVC tank was filled with deionized and partially degassed water at room temperature. The transducer was connected to the insonication chamber through the end piece, as shown in Figure 1. The sample was introduced into the chamber through a 10-mm hole on the top of the insonication chamber.

Experimental procedure

The liposomes were diluted to 1:500 v/v in a 10 mM HEPES-buffered iso-osmotic sucrose solution (made of deionized water) prior to ultrasound exposure. The liposome solution was exposed to ultrasound with varying pressures, pulse lengths, PRFs and insonication times (i.e., times for treating the sample with ultrasound), and each parameter condition was repeated 2 to 5 independent times. Calcein release during ultrasound exposure was determined according to Düzgünes and coworkers (Düzgünes et al. 1985, 2003) by monitoring relief of self-quenching. The fluorescence intensity of the liposome solution was measured with a spectrophotometer (Perkin Elmer, LS-50B, Waltham, MA, USA) using excitation wavelengths of 494 nm and measuring the emission peak intensity at 520 nm. To obtain the total drug release, 5 μL of 10% Triton X-100 was added to 1 mL of the solution, and the fluorescence intensity was measured. Separate titration experiments were performed to determine amount of Triton X-100 required to obtain total drug release. The percentage of calcein released as a result of ultrasound exposure was calculated using Equation 3:

$$\%release = \frac{F_u - F_b}{F_T - F_b} \times 100 \quad (3)$$

where F_u, F_b, and F_T are the peak fluorescence intensities of calcein released by ultrasound, before ultrasound exposure and after addition of Triton X-100 (100% release), respectively.

Ultrasound exposure parameters

Peak negative pressure and frequency. To investigate the effect of the peak negative pressure on drug release, the liposomes were exposed to 2 frequencies (300 kHz and 1 MHz) and a range of peak negative pressures with a constant pulse length of 0.2 ms, a PRF of 500 Hz, and an insonication time of 3 min. At 300 kHz, the peak negative pressure was varied from 0.29 to 1.7 MPa (i.e., I_{TA} of 0.26 to 10 W/cm^2 and MI values of 0.52 to 3.1), whereas at 1 MHz, the peak negative pressure varied from 0.68 to 3.58 (i.e., I_{TA} of 1.64 to 57.24 W/cm^2 and MI values of 0.68 to 3.58).

Exposure time. The effect of the exposure time (see Eq. 4) on drug release was investigated, and the following parameters were kept constant: pulse length (0.2 ms); PRF (500 Hz); and peak negative pressure (1.3 MPa for the 300-kHz transducer and 2.2 MPa for the 1-MHz transducer). The overall exposure time is given by:

$$\tau = PL \times PRF \times T \quad (4)$$

where τ is the exposure time (i.e., actual duration that the ultrasound is on), PL is the pulse length, and T is the insonication time.

To investigate the effect of the MI on drug release as a function of the exposure time, the liposomes were exposed to ultrasound for a range of insonication times (T), 0 to 20 min, which corresponds to exposure times (τ) of 0 to 120 s (see Eq. 4) at 5 MI values (1.05 to 2.7), with a constant duty cycle (10%) and frequency (300 kHz).

Duty cycle at a constant frequency. The effect of the duty cycle on drug release was studied by varying either the pulse length (0 to 0.4 ms) or the PRF (0 to 1000 Hz) at a constant frequency (300 kHz), with an insonication time of 3 min and a peak negative pressure of 1.3 MPa.

Temperature measurements. To verify whether ultrasound exposure produced any thermal effects, the temperature of the samples were measured before and immediately after each ultrasound exposure (i.e., at all MI values) using a hand-held digital thermometer (VWR International, LLC, Radnor, PA, USA). Another temperature verfication was done by measuring the temperature of the sucrose/HEPES buffer solution before

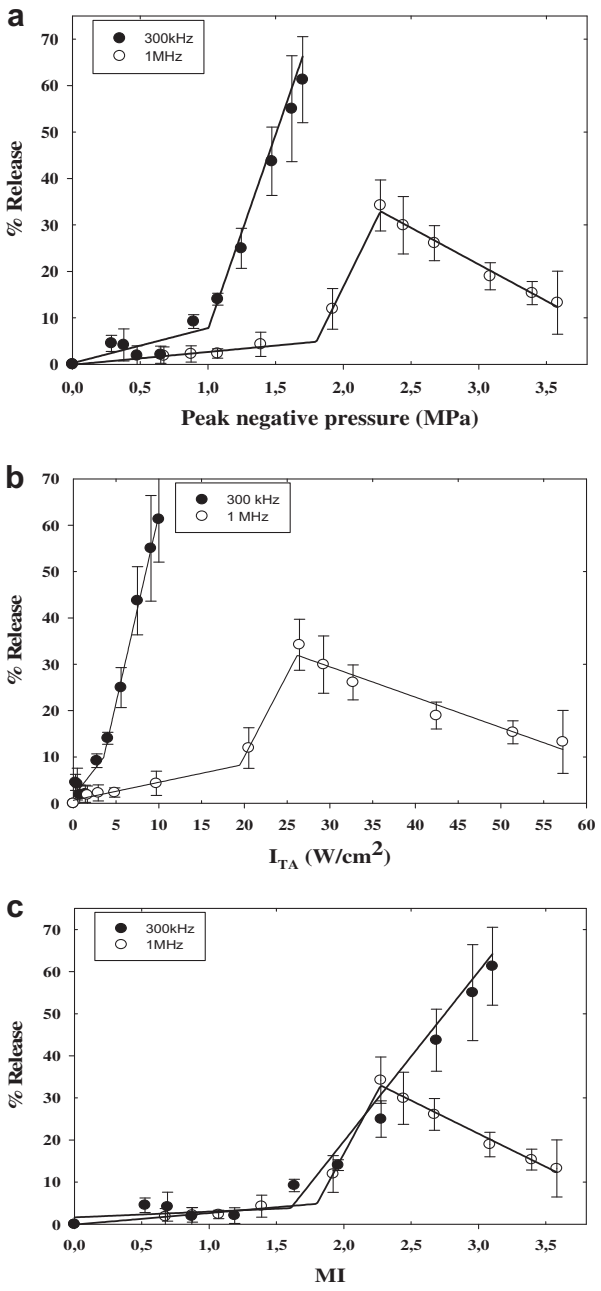

Fig. 2. Effect of the acoustic parameters on the release of calcein from liposomes with a 10% duty cycle and a 3-min insonication time for the 300 kHz (●) and 1 MHz (○) transducers. The error bars show the standard deviation (n = 5) from the mean of the percentage release. The percentage release is shown as a function of peak negative pressure (a), intensity (b), and MI (c), R^2 value > 0.9886; $p < 0.0001$ for all fits.

and continuously during ultrasound exposure, using a thermocouple placed inside the sample chamber. The buffer solution was exposed to ultrasound with MI values of 2.6 and 2.2 for, respectively, the 300-kHz and 1-MHz transducers, and a duty cycle of 10% and 20 min of insonication time (i.e., 120 s of exposure time).

Validation of inertial cavitation. To study whether the ultrasound treatment generated inertial cavitation, a terephthalate dosimeter was used (Mason et al. 1994; Villeneuve et al. 2009; Somaglino et al. 2010). In brief, when inertial cavitation occurs, the produced hydroxide (OH) radicals react with the nonfluorescent terephthalate (TA) to form fluorescent 2-hydroxyterephthalic acid (HTA). Solutions of 2 mM TA (Sigma Aldrich, Oslo, Norway) and HTA (Mole's Science & Technology, Hangzhou, China) were prepared (with deionized water) and maintained at pH 7.3. The HTA solution was diluted to concentrations between 0.01 μM and 1 μM, and the fluorescence intensity of each concentration was measured to obtain a standard curve. A spectrophotometer (Olis RSM 1000, Conway, SC, USA) with excitation and emission wavelengths of 320 and 425.5 nm (i.e., peak intensity value), respectively, was used for the fluorescent measurement. A 1-mL TA solution was placed in the sample chamber and exposed to various acoustic pressures using the same set-up as previously described. The fluorescence intensity of the TA solution before and after ultrasound exposure was measured with the same settings as the HTA standard curve. The background fluorescence intensity of TA was subtracted from the fluorescence intensity of the HTA that was generated as a result of cavitation.

Mathematical fitting and statistical analysis. The relationship between the release of calcein and the ultrasound exposure parameters (peak negative pressure, I_{TA} and MI) was described mathematically by fitting a linear function of 2 or 3 segments to the experimental release data. A first-order exponential model was used to fit the data describing drug release as a function of time. SigmaPlot (Systat Software, Chicago, IL, USA) was used for all fits. These models were selected because they gave the best fit. The goodness of the fit was determined by the square coefficient of correlation (R^2) and the p value of the fit.

RESULTS

Effect of I_{TA}, peak negative pressure, MI, and exposure time on calcein release: Comparison of 300-kHz and 1-MHz frequencies

The effect of the peak negative pressure and exposure time on the release of calcein from liposomes was investigated at the same duty cycle (10%) for the 2 frequencies using a 500-Hz PRF and a pulse length of 0.2 ms. The release was plotted as a function of the peak negative pressure and the corresponding I_{TA} and MI values (Fig. 2). Generally, the 300-kHz transducer released more calcein than did the 1-MHz transducer, although the 1-MHz transducer was used at higher intensities and peak negative pressures than was the 300-kHz transducer (Fig. 2). A minimum threshold of acoustic

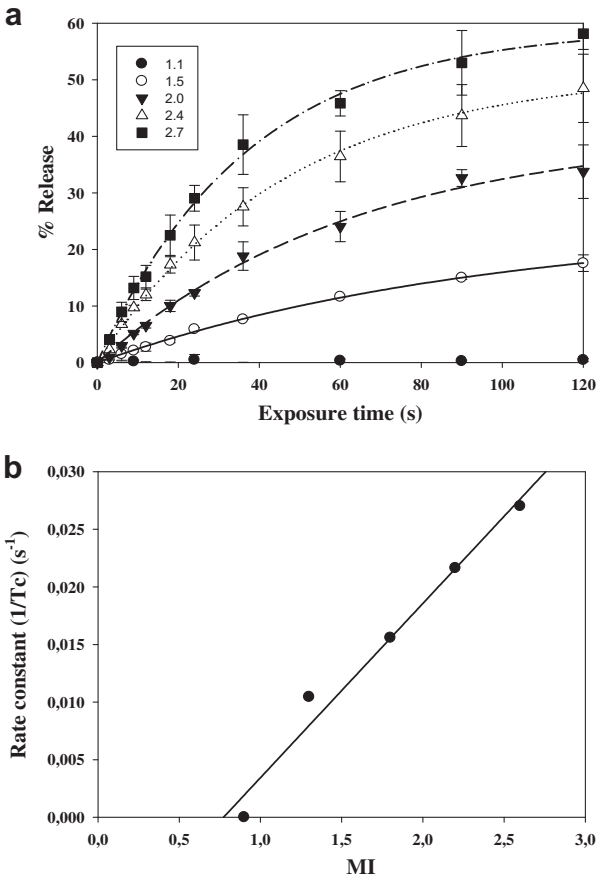

Fig. 3. The effect of the exposure time and MI on the release of calcein from the liposomes. The percentage release is shown as a function of the exposure time for (a) MIs of 1.1 (●); 1.5 (○); 2.0 (▼); 2.4 (△); and 2.7 (■) at constant frequency (300 kHz) and duty cycle (10%). The error bars show the standard deviation (n = 2 to 5) from the mean of the percentage release. The lines represent the fit to the first-order kinetics (Eq. 5). (b) The rate constant, 1/Tc, is shown as a function of the MI. R^2 value > 0.9947; $p < 0.0001$ for all fits.

pressure must be overcome to obtain drug release greater than 5%. The applied pressure needed to overcome the threshold was lower at a transducer frequency of 300 kHz (0.9 MPa) than at 1 MHz (1.9 MPa). However, the respective MI values for the threshold at each frequency were comparable (i.e., 1.6 and 1.9). Above the threshold, the release increased linearly with increasing peak negative pressure, I_{TA}, and MI. For the 1-MHz transducer, a maximal release of approximately 35% was obtained at an acoustic pressure of 2.3 MPa. The amount of drug released decreased at higher pressures. Linear functions of 2 segments for the 300-kHz transducer and 3 segments for the 1-MHz transducer were fitted to the drug-release data and R^2 values greater than 0.9886 and p values less than 0.0001 were found for all fits.

The drug release increased with increasing exposure time (Fig. 3a), and this increase followed first-order kinetics, as shown by fitting Equation 5 to the experimental data:

$$\%R(t) = R_c[1-e^{(-t/T_c)}] \quad (5)$$

where *% R(t)* is the percentage of calcein released at time t, R_c is the total percentage of calcein released at a particular MI, and T_c is the time constant.

To investigate the effect of the MI and exposure time on drug release at a constant frequency (300 kHz), 5 MI values (1.1, 1.5, 2.0, 2.4, and 2.7) were used with increasing exposure times. The amount of calcein release was found to increase with increasing exposure time up to a maximal release. In order to increase the release further, the MI had to increase (Fig. 3a). Thus, the maximum release is dependent on the MI. The experimental data were fitted to Equation 5 for MI values of 1.5 and greater. The percentage maximum release (Rc) obtained for the 4 MI values (i.e., 1.5, 2.0, 2.4, and 2.7) was 17.6%, 33.8%, 48.5%, and 58.2%, respectively. The corresponding time constants (1/Tc) were: 0.011 s^{-1}, 0.016 s^{-1}, 0.022 s^{-1}, and 0.027 s^{-1}. R^2 values greater than or equal to 0.9947 and p values less than 0.0001 were found for all fits. The fit obtained for MI of 1.1 (below the threshold) was poor because of very low drug release. The rate constants increased linearly with increasing MI (Fig. 3b). Thus, the release of calcein from the liposomes was faster at higher MI. Using the 1-MHz transducer at the same duty cycle (10%) and exposure times (1 to 120 s) as for the 300-kHz transducer, less calcein was released and the release rate was slower (data not shown); that is, the rate constants for the 300-kHz (MI = 2.4) and 1-MHz probe (MI = 2.2) were 0.022 s^{-1} and 0.016 s^{-1}, respectively.

Effect of the duty cycle on drug release at a constant frequency

The effect of the duty cycle on drug release was investigated by varying both the PRF and the pulse length at a constant frequency (300 kHz). The lower frequency (300 kHz) was chosen because it induced more release than did the higher frequency transducer. PRF or pulse length was varied at a constant peak negative pressure above the threshold (1.3 MPa, i.e., MI of 2.4), and an insonication time of 3 minutes was used. Drug release increased linearly with pulse length (Fig. 4a) and PRF (Fig. 4b). The same amount of drug release was achieved using the same duty cycle (PRF × pulse length) obtained with various combinations of pulse length and PRF (Fig. 4c). The duty cycles used in Figure 4c corresponded to a certain exposure time (PRF × pulse length × insonication time), and the drug release as a function of exposure time was plotted for increasing pulse length, PRF, and insonication time (Fig. 4d). The drug release

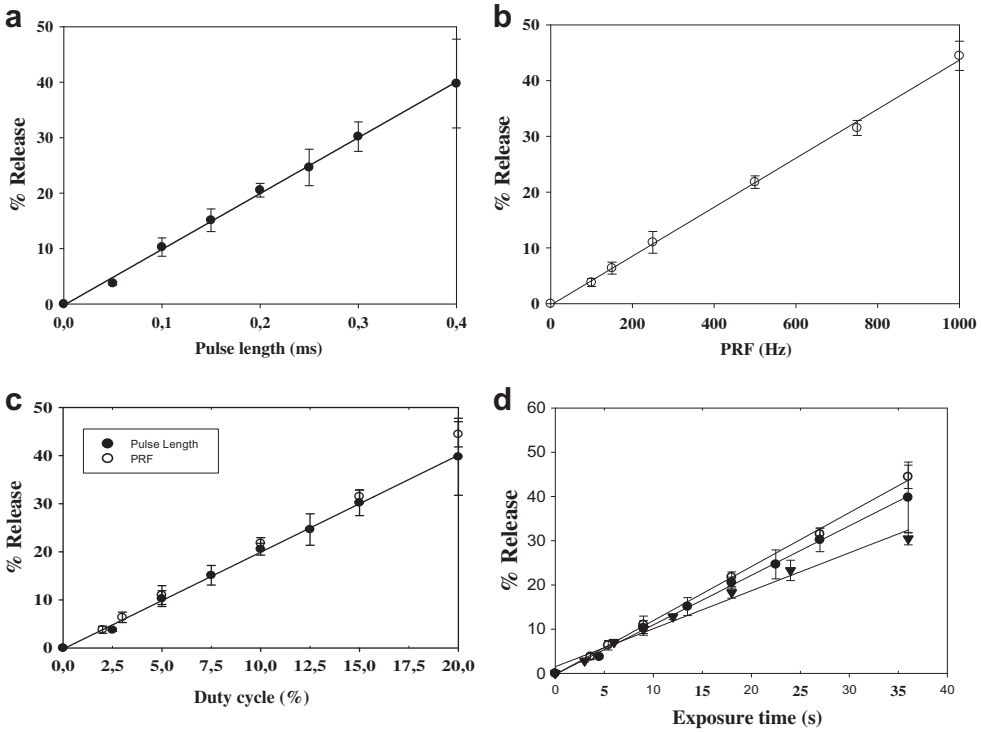

Fig. 4. The effect of the duty cycle (pulse length [•] and PRF [○]) on the release of calcein from liposomes at a constant frequency (300 kHz); peak negative pressure (1.3 MPa); and insonication time (180 s). The error bars show the standard deviation (n = 2) from the mean of the percentage release. The percentage release is shown as a function of the pulse length (a), PRF (b), and duty cycle (c). Release as a function of exposure time with variation in pulse length (d) (constant insonication time and PRF); PRF (constant insonication time and pulse length); and insonication (▼) (pulse length and PRF constant). R^2 value >0.9834; $p < 0.0001$ for all fits.

increased linearly with exposure time, and this corresponds to the first part (exposure time below 40 s) of the first-order kinetics curve in Figure 3a at 2.4 MI.

Thermal effects

The temperature in the sample was measured before and immediately after ultrasound exposure and also continuously during ultrasound exposure of the sucrose/HEPES buffer solution. The increase in temperature was 1 to 9°C, and the increase correlated positively with the MI. The temperature increased within the first 3 min (i.e., 18 s of exposure time), and then the temperature was constant for the remaining 17 min of insonication time. Separate temperature studies showed 1% or less of calcein leakage from the liposomes after 4 hours of incubation at 37°C in sucrose/HEPES solution.

Validation of inertial cavitation

A linear relationship was obtained between the fluorescence intensity and the concentration of HTA measured at concentrations up to 0.5 μM (data not shown). The fluorescence of the ultrasound-exposed TA solution had intensity within the same range as the HTA standard curve (0 to 70 absorbance units a.u.). Minimal fluorescence was detected in samples exposed to ultrasound using peak negative pressures below the threshold for drug release. The thresholds were found to be higher for the higher frequency transducer (1.9 MPa) than for the lower frequency transducer (0.9 MPa), which correspond to MI values of 1.9 and 1.6, respectively. Above the threshold, the fluorescence intensity increased with increasing peak negative pressure, indicating an increase in the production of OH radicals (Fig. 5a). For the 1-MHz transducer, maximal fluorescence intensity was obtained at a peak negative pressure of 2.3 MPa, followed by a decrease in intensity with further increases in negative pressure. The fluorescence intensity of the generated HTA correlated linearly with the release of calcein from the liposomes (Fig. 5b) for both ultrasound transducers (correlation coefficients R^2 = 0.9602 (300 kHz) and R^2 = 0.8826 (1 MHz).

DISCUSSION

The effects of various ultrasound exposure parameters on the release of liposomal calcein in solution were studied. By varying the peak negative pressure at 2 frequencies, the impact of the MI on drug release was

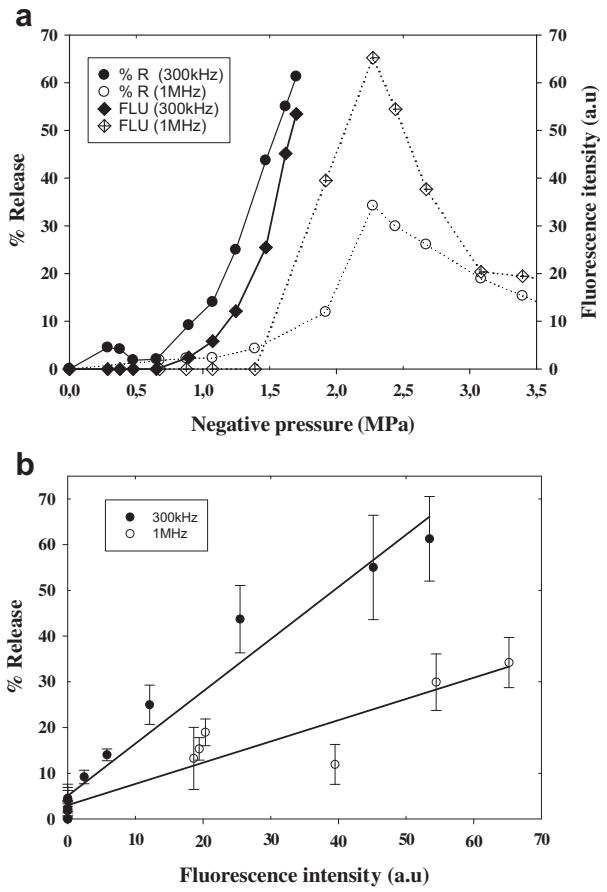

Fig. 5. (a) Fluorescence intensity (in arbitrary units) (FLU, ◇) of HTA produced after ultrasound exposure of a TA solution using the 300-kHz (closed symbol) and 1-MHz (open symbol) transducers as a function of the peak negative pressure. The fluorescence intensity is compared to the percentage release (% R, ○) from liposomes presented in Figure 2(b). (b) The correlation between the percentage release and the fluorescence intensity (in arbitrary units) of HTA for the 300-kHz (closed symbol) and 1-MHz (open symbol) transducers. The error bars show the standard deviation (n = 2) from the mean of the percentage release.

determined. Minimal drug release (less than 5%) occurred until certain threshold values of I_{TA}, peak negative pressure, and MI were reached, at which point a linear increase in the drug release with increase in the 3 parameters followed. The peak negative pressure threshold was lower for the 300-kHz transducer than for the 1-MHz transducer for the same duty cycle (10%). However, the corresponding threshold for the MI was almost the same for the 2 frequencies. The linear dependence between drug release and MI suggests that the drug release is caused by a mechanical mechanism such as stable or inertial cavitation. Inertial cavitation requires the presence of gas bubbles, and the sucrose/HEPES buffer solution used in our work was made of deionized water that might have contained micrometer-sized gas bubbles. Apfel and Holland (1991) found that for 1-MHz transducers, the cavitation threshold was almost independent of initial bubble radius in the micrometer range. Thus, gas bubbles in the sucrose/HEPES buffer can probably cause inertial cavitation. The occurrence of the threshold to obtain drug release also suggests that the drug release was caused by inertial cavitation. Inertial cavitation is reported to occur only above a certain pressure/MI threshold (Daniels et al. 1987; Apfel and Holland 1991; Brennen 1995; Miller et al. 1996; Young 1999). Other studies (Husseini et al. 2000; Schroeder et al. 2007) have also reported the important role of inertial cavitation in drug release and have shown a linear dependence of drug release with the acoustic amplitude (intensity). In our study we extended this relationship and correlated drug release to MI using 2 clinically relevant frequencies and varying the acoustic pressure of the focused ultrasound beam. To verify whether inertial cavitation actually took place, the presence of OH radicals was demonstrated by measuring the fluorescence intensity of an ultrasound-exposed TA solution.

Ultrasound exposure induced only a minor increase in the temperature of the liposome solution. The small increase in temperature did not increase linearly with exposure time (i.e., it was constant after the first 18 s of exposure time), suggesting that this is not a thermal effect but the occurrence of a mechanical effect. Also, 1% or less calcein leakage was found when the liposomes were incubated for 4 h at 37°C in sucrose/HEPES solution, suggesting that these liposomes were not thermally sensitive.

Ultrasound-induced drug release followed a first-order kinetic model that depended on the exposure time and the MI. The maximal drug release was obtained for a certain exposure time, and any further increase in release could occur only if the MI increased. Thus, it is the MI together with overall exposure time that determine the maximal drug release. Additionally, the first-order rate constant was also found to depend linearly on the MI at a constant frequency. Thus, it takes less time for the drug to be released if the MI is higher, and calcein was released faster at a lower frequency than at a higher frequency. These observations also suggest that the release was due to inertial cavitation, and they are consistent with the results reported by other studies (Schroeder et al. 2007; Enden and Schroeder 2009). The experimental validation of the first-order kinetic model demonstrates that it is possible to determine the percentage of drug release at a given MI and exposure time. Whether this will be possible in an *in vivo* setting is, however, the subject of future investigations.

Above the threshold for inertial cavitation, the release increased linearly with the peak negative pressure

for both frequencies used. However, for the 1-MHz transducer, an increase in drug release was followed by a reduction above a certain pressure (2.3 MPa), whereas no reduction in drug release was observed when the 300-kHz transducer was used. The reduction in drug release might be due to attenuation of the ultrasound beam by gas bubbles between the transducer and the sample chamber. Gas bubbles can attenuate the beam through scattering and absorption (Angelsen 2002; Leighton 2007), and the attenuation of the pressure is dependent on the frequency. Thus, higher attenuation is obtained at higher frequencies than at lower frequencies. Also, at higher pressures more energy would be pumped into higher harmonics and because attenuation increases with frequency, the sound wave from the 1 MHz transducer (because of its nonlinearity) would be attenuated more than that of the 300 kHz transducer. When the voltage at the output of the amplifier was monitored, echoes from the front of the sample chamber and the back of the cylindrical PVC tank were observed. The transmit voltage and the echo from the back of the PVC tank showed a stable pulse shape at all voltage levels. At higher voltages (higher pressures), there were drastic oscillations in the echo signal from the front of the sample chamber. They might be echoes from the sample chamber surface or oscillations of gas bubbles attached to the sample chamber's surface that resulted in inertial cavitation and probably movement of bubbles. The reduction of drug release occurred at pressures at which drastic oscillations were also observed. Others have also observed that cavitational activity increases with acoustic intensity, and the resulting bioeffect reached a maximum before declining with further increase in acoustic intensity (Miller et al. 1989, 1996). Furthermore, Miller et al. (1989) showed that at higher acoustic intensities (with a 1-MHz transducer), the number of cells that ruptured decreased with increasing acoustic intensity, whereas the number of visible bubbles (between the insonated test tube and transducer) increased dramatically with acoustic intensity. Thus, the decrease in the bioeffect at higher intensities is likely to be caused by attenuation or absorption of the ultrasound beam by gas bubbles.

The effect of the duty cycle was studied using the 300-kHz transducer by varying the pulse length and PRF. Drug release was found to correlate linearly with duty cycle, as modulated by either PRF or pulse length. The release was also found to be linear at lower exposure times (i.e., 40 s), corresponding with the initial part of the first-order kinetic curve, and this linearity was obtained by increasing PRF, pulse length, or insonication time. These results imply that at constant MI, drug release depends on the overall exposure time, independent of the manner in which the exposure time is obtained. Consistent with our results, Schroeder et al. (2007) found that liposomes released the same amount of drug when exposed to either continuous or pulsed ultrasound applying the same overall exposure time.

The mechanism of cavitation-mediated drug release from the liposomes is thought to involve increased permeability (sonoporation) or total disintegration of the liposome membrane when small oscillating gas bubbles cavitate close to or in the hydrophobic region of the liposomal membrane (Schroeder et al. 2007, 2009; Enden and Schroeder 2009). The dependence of the release on the pulse length may be related to the self-sealing properties of sonoporated liposomes. Earlier reports suggest that lipids reseal rapidly after rupturing (Marin et al. 2001) and that it takes more time for the lipids to reseal when the pulses are longer. Some miscellar formulations have been observed to re-encapsulate during the ultrasound-off phase, yielding greater drug release at shorter pulse intervals (i.e., higher PRF) (Husseini et al. 2000; Marin et al. 2001). Although a mechanism involving lipid pore formation and resealing is consistent with our results, such an interpretation is not supported by reports of collapse of DOPE-based liposomes during low-frequency ultrasound exposure (Evjen et al. 2011). Destabilization of the lipid membrane was here visualized by electron microscopy as larger liposomes or lipid aggregates observed after ultrasound exposure (Evjen et al. 2011). Evjen and coworkers (2011) suggested that the cone-shaped geometry and nonbilayer characteristics of DOPE render the liposome membrane prone to form a so-called reverse hexagonal structure (flip and release) during ultrasound exposure. DEPC, the main phospholipid of the present liposomes, also has a cone-shaped geometry and may release through a similar mechanism. Although our results are limited to DEPC-based liposomes, the first-order drug release kinetics are also reported for other types of liposomes (Schoeder et al. 2007; Enden and Schroeder 2009), suggesting that the results might be generalized to other types of non–thermally sensitive liposomes.

The present work demonstrates that two ultrasound exposure parameters, MI, and overall exposure time, determine the total drug release from liposomes. The optimal value of these two parameters may be obtained in various combinations of the parameters they depend on. Thus, optimal MI may be obtained using either low frequency and low negative pressure or high frequency and high negative pressure. Optimal exposure time may be achieved by using both continuous and pulsed waves. Clinically, this can be of importance because the ultrasound exposure can be tuned to avoid heating of the tissue. However, because of the complexity of the *in vivo* environment, the translation from *in vitro* to

in vivo cavitation is not straightforward. There is evidence that submicrometer gas bodies exist naturally *in vitro* (Blatteau et al. 2006), but bubble nucleation, distribution in terms of nucleus size and local concentration, and the activation of these potential natural nuclei by ultrasound exposure is still relatively poorly understood. The induction of cavitation also depends on viscosity and cell density (Apfel and Holland 1991). An *in vitro* study of inertial cavitation in human blood showed a significant reduction in cavitation threshold when the viscosity was reduced by reducing the hematocrit and by adding polymeric particles to the blood (Deng et al. 1996). Altogether, these factors show the challenges involved in predicting the optimal MI in a clinical situation.

CONCLUSIONS

This study characterized the ultrasound parameters optimal for drug release from DEPC-based liposomes and pointed to MI and overall exposure time as the major parameters that determine the drug release. The first-order kinetic for drug release demonstrated that increasing the exposure time above a certain value does not enhance the release further. The observation that drug release was dependent on the MI was supported by sonochemical experiments indicating free radical formation. Only minor temperature effects were found. Altogether, this demonstrated that the release mechanism involved a mechanical effect or, more specifically, inertial cavitation. The study also suggested that the duty cycle may be used to control the amount of energy deposited and the heat generated in tissue. An optimization of ultrasound exposure is, however, needed to enhance ultrasound-mediated drug release from liposomes and facilitate future clinical applications.

Acknowledgments—The authors thank Sibylla Rögnvaldsson (Epitarget AS, Oslo) for producing and characterizing the liposomes, as well as Kristin G. Sæterbø and Ingerid Arbo for their assistance at the laboratory. This project is supported by the Schlumberger Foundation PhD Fellowship (Faculty for the Future).

REFERENCES

Allen TM. Liposomes: Opportunities in drug delivery. Drugs 1997;54: 8–14.

Angelsen BAJ. Waves, signals, and siginal processing. Trondheim, Norway: Emantec; 2002.

Apfel RE, Holland CK. Gauging the likelihood of cavitation from short-pulse, low-duty-cycle diagnostic ultrasound. Ultrasound Med Biol 1991;17:179–185.

Bae YH. Drug targeting and tumor heterogeneity. J Control Release 2009;133:2–3.

Bednarski MD, Lee JW, Callstrom MR, Li KC. In vivo target-specific delivery of macromolecular agents with MR-guided focused ultrasound. Radiology 1997;204:263–268.

Barenholz Y. In: Liposome Technology. London: Gregoriadis; 2007. p. 1–21.

Barenholz Y. Liposome application: problems and prospects. Curr Opin Colloid Interface Sci 2001;6:66–77.

Blatteau JE, Souraud JB, Gempp E, Boussuges A. Gas nuclei, their origin, and their role in bubble formation. Aviat Space Environ Med 2006;77:1068–1076.

Brennen CE. Cavitation and bubble dynamics. New York: Oxford University Press; 1995.

Daniels S, Blondel D, Crum LA, Haar GR, Dyson M. Ultrasonically induced gas bubbles production in agar-based gels: Part I. Experimental investigation. Ultrasound Med Biol 1987;9:527–539.

Davies CD, Lundsrøm LM, Frengen J, Eikenes L, Bruland ØS, Kaalhus O, Hjelstuen MHB, Brekken C. Radiation improves the distribution and uptake of liposomal doxorubicin (caelyx) in human osteosarcoma xenografts. Cancer Res 2004;64:547–553.

Deng CX, Xu Q, Apfel RE, Holland CK. In vitro measurements of inertial cavitation thresholds in human blood. Ultrasound Med Biol 1996;22:939–948.

Drummond DC, Meyer O, Hong K, Kirpotin DB, Papahadjopoulos D. Optimizing liposomes for delivery of chemotherapeutic agents to solid tumors. Pharmacol Rev 1999;51:691–743.

Duzgunes N, Straubinger RM, Baldwin PA, Friend DS, Papahadjopoulos D. Proton-induced fusion of oleic acid-phosphatidylethanolamine liposomes. Biochemistry 1985;24:3091–3098.

Düzgünes N, Bagatolli LA, Meers P, Oh YK, Straubinger RM. Fluorescence methods in liposome research. In: Torchilin VP, Weissig V, (eds). Liposomes. New York: Oxford University Press; 2003. p. 118–119.

Enden G, Schroeder A. A mathematical model of drug release from liposomes by low-frequency ultrasound. Ann Biomed Eng 2009;37: 2640–2645.

Evjen TJ, Nilssen EA, Rögnvaldsson S, Brandl M, Fossheim SL. Distearoylphosphatidylethanolamine-based liposomes for ultrasound-mediated drug delivery. Eur J Pharm Biopharm 2010;75:327–333.

Evjen TJ, Nilssen EA, Barnert S, Schubert R, Brandl M, Fossheim SL. Ultrasound-mediated destabilization and drug release from liposomes comprising dioleoylphosphatidylethanolamine. Eur J Pharm Sci 2011;42:380–386.

Guaman H, Nguyen D, Khan S, Prausnitz M. Ultrasound-mediated disruption of cell membranes.I. Quantification of molecular uptake and cell viability. J Acous Soc Am 2001;110:588–596.

Hagtvet E, Evjen TJ, Olsen DR, Fossheim SL, Nilssen EA. Ultrasound-enhanced antitumor activity of liposomal doxorubicin in mice. J Drug Target 2011;1:1–8.

Huang SL, MacDonald C. Acoustically active liposomes for drug encapsulation and ultrasound-triggered release. Biochim Biopys Acta 2004;1665:134–141.

Humphrey VF. Ultrasound and matter: Physical interactions. Prog Biophys Mol Biol 2007;93:195–211.

Husseini GA, Myrup GD, Pitt WG, Christensen DA, Rapoport NY. Factors affecting acoustically triggered release of drugs from polymeric micelles. J Control Release 2000;69:43–52.

Kost J, Langer R. Responsive polymeric delivery systems. Adv Drug Deliv Rev 2001;46:125–148.

Lasic DD. Liposomes: From Physics to Applications. Amsterdam, London, New York, Tokyo: Elsevier; 1993.

Leighton TG. The acoustic bubble. London: Academic Press; 1994.

Leighton TG, Phelps AD, Cox BT, Ho WL. Theory and preliminary measurements of the Rayleigh-like collapse of a conical bubble. Acta Acoust 1998;84:801–814.

Leighton TG. What is ultrasound? Prog Biophs Mol Biol 2007;93:3–83.

Lin HY, Thomas JL. PEG-lipids and oligo (ethylene glycol) surfactants enhance the ultrasonic permeabilizability of liposomes. Langmuir 2003;19:1098–1105.

Lin HY, Thomas JL. Factors affecting responsivity of unilamellar lipsomes to 20 kHz ultrasound. Langmuir 2004;20:6100–6106.

Liu J, Lewis TN, Prausnitz MR. Non-invasive assessment and control of ultrasound-mediated membrane permeabilzation. Pharm Res 1988; 15:918–924.

Liu Y, Miyoshi H, Nakamura M. Encapsulated ultrasound microbubbles: Therapeutic application in drug/gene delivery. J Control Release 2006;114:89–99.

Marin A, Muniruzzaman MD, Rapoport N. Acoustic activation of drug delivery from polymeric micelles: Effect of pulsed ultrasound. J Control Release 2001b;71:239–249.

Mason TJ, Lorimer JP, Bates DM, Zhao Yl. Dosimetry in sonochemistry: The use of aqueous terephthalate ion as a fluorescence monitor. Ultrason Sonochem 1994;1:91–95.

Miller MW, Church CC, Brayman AA, Malcuit MS, Boyd RW. An explanation for the decrease in cell lysis in a rotating tube with increasing ultrasound intensity. Ultrasound Med Biol 1989;15:67–72.

Miller MW, Miller DL, Brayman AA. A review of in vitro bioeffect of inertial ultrasonic cavitation from a mechanistic perspective. Ultrasound Med Biol 1996;22:1131–1154.

Miller DL. Overview of experimental studies of biological effects of medical ultrasound caused by gas activation and inertial cavitation. Prog Biophys Mol Biol 2007;93:314–330.

Myhr G, Moan J. Synergistic and tumour selective effects of chemotherapy and ultrasound. Cancer Lett 2006;232:206–213.

Pangu GD, Davies KP, Bates FS, Hammer DA. Ultrasonically induced release from nanosized polymer vesicles. Macromol Biosci 2010; 10:546–554.

Pitt WG, Husseini GA, Staples BJ. Ultrasonic drug delivery: A general review. Expert Opin Drug Deliv 2004;1:37–56.

Pitt WG, Husseini GA, Roeder BL, Dickinson DJ, Warden DR, Hartley JM, Jones PW. Preliminary results of combining low-frequency low-intensity ultrasound and liposomal drug delivery to treat tumors in rats. J Nanosci Nanotechnol 2011;11:1866–1870.

Price RJ, Skyba DM, Kaul S, Skalak TC. Delivery of colloidal particles and red blood cells to tissue through microvessel ruptures created by targeted microbubble destruction with ultrasound. Circulation 1998; 98:1264–1267.

Rapoport N. Physical stimuli-responsive polymeric micelles for anticancer drug delivery. Prog Polym Sci 2007;32:962–990.

Schroeder A, Avnir Y, Weisman S, Najajreh Y, Gabizon A, Talmon Y, Kost J, Barenholz Y. Controlling liposomal drug release with low-frequency ultrasound mechanism and feasibility. Langmuir 2007; 23:4019–4025.

Schroeder A, Kost J, Barenholz Y. Ultrasound, liposomes, and drug delivery: Principles for ultrasound to control the release of drugs from liposomes. Chem Phys Lipids 2009;162:1–16.

Somaglino L, Bouchoux G, Mestas JL, Lafon C. Validation of an acoustic cavitation dose with hydroxyl radical production generated by inertial cavitation in pulsed mode: Application to in vitro drug release from liposomes. Ultrason Sonochem 2010;18:577–588.

Steinberg Y, Schroeder A, Talmon Y, Schmidt J, Khalfin RL, Cohen Y, Dvoissele JM, Begu S, Avnir D. Synergistic and tumour selective effects of chemotherapy and ultrasound. Langmuir 2007;23: 12024–12031.

Torchilin VP. Recent advances with liposomes as pharmaceutical carriers. Nat Review Drug Discov 2005;4:145–160.

Vaage J, Donovan D, Uster P, Working P. Tumour uptake of doxorubicin in polyethylene glycol-coated liposomes and therapeutic effect against a xenografted human pancreatic carcinoma. Br J Cancer 1997;75:482–486.

Villeneuve L, Alberti L, Steghens JP, Lancelin JM, Mestas JL. Assay of hydroxyl radicals generated by focused ultrasound. Ultrason Sonochem 2009;16:339–344.

Yuan F, Leunig M, Huang SK, Berk DA, Papahadjopoulos D, Jain K. Microvascular permeability and interstitial penetration of sterically-stabilized (Stealth) liposomes in a human tumor xenograft. Cancer Res 1994;54:3352–3356.

Young FR. Cavitation. London: Imperial College Press; 1999.

Paper II

MECHANISMS OF THE ULTRASOUND-MEDIATED INTRACELLULAR DELIVERY OF LIPOSOMES AND DEXTRANS

t04938

Mechanisms of the Ultrasound-Mediated Intracellular Delivery of Liposomes and Dextrans

Mercy Afadzi, Sabina P. Strand, Esben A. Nilssen, Svein-Erik Måsøy, Tonni F. Johansen, Rune Hansen, Bjørn A. Angelsen, and Catharina de L. Davies

***Abstract*—The mechanism involved in the ultrasound-enhanced intracellular delivery of fluorescein-isothiocyanate (FITC)-dextran (molecular weight 4 to 2000 kDa) and liposomes containing doxorubicin (Dox) was studied using HeLa cells and an ultrasound transducer at 300 kHz, varying the acoustic power. The cellular uptake and cell viability were measured using flow cytometry and confocal microscopy. The role of endocytosis was investigated by inhibiting clathrin- and caveolae-mediated endocytosis, as well as macropinocytosis. Microbubbles were found to be required during ultrasound treatment to obtain enhanced cellular uptake. The percentage of cells internalizing Dox and dextran increased with increasing mechanical index. Confocal images and flow cytometric analysis indicated that the liposomes were disrupted extracellularly and that released Dox was taken up by the cells. The percentage of cells internalizing dextran was independent of the molecular weight of dextrans, but the amount of the small 4-kDa dextran molecules internalized per cell was higher than for the other dextrans. The inhibition of endocytosis during ultrasound exposure resulted in a significant decrease in cellular uptake of dextrans. Therefore, the improved uptake of Dox and dextrans may be a result of both sonoporation and endocytosis.**

I. Introduction

The encapsulation of cytotoxic drugs into nanoparticles is known to enhance their accumulation in tumor tissue and to reduce the toxicity to normal tissue when compared with the administration of free cytotoxic drugs [1]–[3]. This difference is mainly due to the hyperpermeable tumor vessels, which allow for extravasation of the nanoparticles [4], [5]. Although drug delivery by nanoparticles improves the drug uptake by tumor tissues compared with that of free drugs, the distribution of both the nanoparticles and the released drugs within the tumor tissue is heterogeneous [4], [6], [7]. Consequently, large areas of the tumor are not reached by the drugs. A prerequisite for successful cancer therapy is that the therapeutic agents reach all of the cancer cells in sufficient concentrations to inactivate them. It is therefore important to improve both the distribution of the drug within tumor tissue and the cellular uptake of the cancer drug. These improvements may be achieved by treating the tumor chemically using enzymes [8], [9] or physically by radiation [6] or ultrasound [10]–[12].

The use of ultrasound may improve the delivery of nanoparticles in various ways depending on the frequency and the acoustic intensity applied. In particular, high-intensity focused ultrasound (HIFU) has been reported to improve the therapeutic efficacy of liposomes [13], [14]. The interaction of ultrasound with tissues generally produces two main effects, one thermal and one non-thermal. The thermal effect is a result of the absorption of ultrasound energy, which leads to heating, whereas the non-thermal effect is associated with cavitation and radiation force [14], [15]. Radiation force (using megahertz-frequency ultrasound) may generate acoustic streaming, which improves the convection of the nanoparticles in the extracellular matrix, enhances the penetration and distribution of the nanoparticles, and augments the release of the drug from the particles. Furthermore, studies [14], [16], [17] have shown that radiation force can generate shear stress that increases vascular permeability and produces pores in cell membranes, a process called sonoporation. Cavitation is the most commonly observed process at low frequency (kilohertz-frequency ultrasound) and can be stable or transient depending on the acoustic pressures. At lower acoustic pressures, the oscillations of gas nuclei can be stable and can lead to micro-streaming and shear stresses. When the acoustic pressure increases, these gas nuclei will grow and finally collapse, producing shock waves and micro-jet streams, which may cause transient perforations (sonoporation) of cell membranes, improving the cellular uptake of nanoparticles and drugs [14], [15].

Because the cellular uptake of chemotherapeutic drugs is restricted by the cell membrane [18]–[20], sonoporation may be of importance for improving therapeutic efficacy. The efficiency of sonoporation has been reported to improve in the presence of ultrasound contrast agents (microbubbles) [18]–[20]. Although microbubbles have been used clinically to enhance ultrasound imaging for more than two decades, a full understanding of how ultrasound and microbubbles improve cellular uptake is lacking. To develop safe and effective protocols for successful cancer

Manuscript received January 31, 2012; accepted May 14, 2012. This project is supported by the Schlumberger Foundation Ph.D. Fellowship (Faculty for the Future).

M. Afadzi and C. de L. Davies are with the Department of Physics, The Norwegian University of Science and Technology, Trondheim, Norway (e-mail: mercy.afadzi@ntnu.no).

S. P. Strand is with the Department of Biotechnology, The Norwegian University of Science and Technology, Trondheim, Norway.

E. A. Nilssen is with Epitarget AS, Oslo, Norway.

S.-E. Måsøy, T. F. Johansen, R. Hansen, and B. A. Angelsen are with the Department of Circulation and Medical Imaging, The Norwegian University of Science and Technology, Trondheim, Norway.

R. Hansen is with the Department of Medical Technology, SINTEF Technology and Society, Trondheim, Norway.

DOI http://dx.doi.org/TBC

therapy, the mechanism of sonoporation must be elucidated.

Endocytosis, the most common mechanism for the internalization of nanoparticles and macromolecules, can be categorized as clathrin-mediated or clathrin-independent endocytosis. Clathrin is the main scaffold protein in clathrin-coated pits and occupies the plasma membrane along with the protein complex AP2 and dynamin. Clathrin-independent endocytosis includes several cholesterol-rich pathways; the best characterized is the caveolae-mediated pathway. Caveolae are subdomains of glycolipid rafts that use the membrane protein caveolin to form stable cell-associated structures [21]–[23]. Another clathrin-independent pathway is macropinocytosis. During macropinocytosis, bulk and non-selective uptake of extracellular fluid occurs via the actin-dependent reorganization of the plasma membrane to form macropinosomes. Macropinosomes are heterogeneous phase-bright organelles that emanate from ruffles [24]. Selective inhibition of the various endocytic pathways by chemical inhibitors is a useful approach for investigating the cellular uptake mechanism of nanoparticles, although the results should be interpreted with caution because of the lack of complete specificity of the inhibitors [25]. Commonly used endocytosis inhibitors include chlorpromazine, which inhibits mainly clathrin-mediated endocytosis by reversibly translocating clathrin and its adapter proteins from the plasma membrane to intracellular vesicles [26]; genistein, a tyrosine kinase inhibitor, which inhibits mainly caveolae-mediated uptake [27], [28]; and wortmannin, an inhibitor of phosphoinositide 3-kinases (PI3Ks), which plays a role in the enclosure of ruffles to form macropinosomes [24], [29].

The purpose of the present study was to determine the effect of ultrasound on the cellular uptake of liposomes and dextran and to investigate whether the mechanism responsible for cellular uptake is related to pore formation or endocytosis. Furthermore, we studied the impact of microbubbles on cellular uptake and whether the encapsulated drug was released extracellularly before being taken up by the cells. HeLa cells were incubated with either sonosensitive dierucoyl-phosphatidylcholine (DEPC)-based liposomes [30] containing doxorubicin (Dox) or with fluorescein-isothiocyanate (FITC)-dextran of various sizes in the presence or absence of microbubbles and ultrasound. A lower frequency (300 kHz) was applied; in a previous study [30] we found this frequency to be more efficient for inducing drug release than 1 MHz . Endocytic inhibitors were used to investigate whether endocytosis was affected by ultrasound exposure. The cellular uptake was measured by flow cytometry, and the intracellular location of liposomes/Dox and dextrans was imaged by confocal laser scanning microscopy.

II. Materials and Methods

A. Cell Culture

The HeLa cell line (human cervical carcinoma cells) was grown in Dulbecco's modified Eagle's medium (DMEM) supplemented with 10% fetal bovine serum (FBS; Sigma-Aldrich, Oslo, Norway), 2 mM of nonessential amino acids and 1 mM of L-glutamine (Sigma-Aldrich). The cell cultures were grown at 37°C and in 5% CO_2. Exponentially growing cells were harvested with 3 mL of trypsin (0.25%) and resuspended in growth medium.

B. Liposome Production

Dierucoyl-phosphatidylcholine (DEPC) was supplied by Avanti Polar Lipids (Alabaster, AL). Distearoylphosphatidylcholine (DSPC) and distearoylphosphatidylethanolamine-(methoxy(polyethyleneglycol)2000) (DSPE-PEG) were purchased from Genzyme Pharmaceuticals (Liestal, Switzerland). Dox, cholesterol, 4-(2-hydroxyethyl)-1-piperazineethanesulfonic acid (HEPES), and sucrose were obtained from Sigma Aldrich. The liposomes consisted of DEPC: DSPC: DSPE-PEG 2000: Cholesterol (52:5:8:35 mol %) and were prepared by the thin-film hydration and sequential extrusion method [31]. Briefly, lipids were dissolved in a choloroform/methanol mixture (9/1, v/v) at 60°C, and rotary evaporated to dryness under vacuum for 6 to 8 h. The dry lipid film was hydrated with 300 mM ammonium sulfate solution, giving a nominal lipid concentration of 20 mg/mL. After three freeze–thaw cycles in a dry-ice/acetone/methanol mixture and water, respectively, the liposomes were downsized by step-wise extrusion (Lipex extruder, Biomembrane Inc., Vancouver, BC, Canada) through polycarbonate filters with decreasing pore size from 800 to 80 nm (Nuclepore, West Chester, PA). The lipid hydration, liposome extrusion, and thawing process were performed at 25°C, above the gel-to-liquid crystalline phase transition temperature of the liposome membrane.

Dox was remote loaded according to the ammonium sulfate transmembrane gradient method [32]. An ammonium sulfate transmembrane gradient was obtained by extensive dialysis of the liposomes against unbuffered isotonic 255 mM sucrose solution. The dialysis was performed by placing disposable dialysis bags (molecular weight cut-off 100 kD; Float-A-Lyzer, Spectra/Por, Spectrum Laboratories Inc., Rancho Dominguez, CA) containing the liposome dispersions in a magnetically stirred dialysis solution for approximately 2 to 3 d (volume ratio liposome dispersion:dialysis solution, 1:100) with intermediate exchanges of the dialysis solution. Dox hydrochloride solution was added to the liposome dispersion to give a final ratio of drug-to-lipid of 1:8 (w/w). The resulting lipid and Dox concentrations were 16 and 2 mg/mL, respectively. To provide optimal loading efficiency, the liposome dispersions were, after Dox addition, further incubated under stirring for 60 min at 48°C. Any remaining non-encapsulated Dox was removed by liposome dialysis against sucrose/HEPES buffer (pH 7.4). Free Dox is a substance with fluorescent properties (maximum absorption/emission respectively 480/595 nm). The self-quenching of Dox at the current high intraliposomal concentrations is exploited to distinguish between free and liposomal Dox.

C. Liposome Characterization and the Labeling of Liposomes

The mean intensity-weighted hydrodynamic liposome diameter and polydispersity index (pdi) were determined by photon correlation spectroscopy (Nanosizer, Malvern Instruments, Malvern, UK). The diameter was 88 to 90 nm (pdi 0.06 to 0.07) for all liposomes used. A liposome stability in serum was conducted as described in [33]. After 6 h incubation in 20% serum, less than 1% Dox leakage was detected.

The membranes of the liposomes were labeled with a hydrophobic dye (1,1'-dioctadecyl-3,3,3′,3- tetramethylindodicarbocyanine) (DiD; Molecular Probes, Invitrogen, Grand Island, NY). 3 μL of DiD (2.5 mg/mL in ethanol) were added to 497 μL of liposomes to a final concentration of 15 μg/mL. The labeling solution was mixed by aspiration and allowed to incubate for 2 h at room temperature. Free DiD that did not bind to the liposomes was removed by dialysis (Float-A-lyzer G2, Spectrum Laboratories Inc.). The size of the liposomes before and after labeling (24 h, 48 h, and 7 d) was measured using dynamic light scattering (Nanosizer, Malvern Instruments). No significant change in the liposome mean size or pdi was observed after labeling.

D. Ultrasound Exposure Set-Up and Treatment

The ultrasound exposure set-up consisted of a signal generator (33120A, Hewlett-Packard, San Jose, CA), an oscilloscope (Waverunner, LT262, Lecroy Corp., Long Branch, NJ), a power amplifier (ENI 2100L, Electronic Navigation Industries, Rochester, NY), custom-made single-element ultrasound transducers (Imasonic, Besancon, France) with a frequency of 300 kHz and an insonication chamber containing a sample chamber (Fig. 1). The transducer has a geometric focus of 90 mm, an active diameter of 55 mm and a maximum intensity of 69 mm. The −3-dB beam width in the lateral direction at the maximum intensity was 6.6 mm. The acoustic field was characterized using a hydrophone (Onda HGL-0200, Onda Corp., Sunnyvale, CA) with a tip diameter of 200 μm connected to a 20-dB pre-amplifier (Onda AH-2020). The insonication chamber was a rectangular (150 × 350 mm) Plexiglas (Evonik Industries AG, Essen, Germany) water tank. To prevent reflections of the sound wave, a regular sponge with a thickness of 10 mm was used to coat the inside of the insonication chamber. The Plexiglas tank was filled with deionized and partially degassed water and was kept at room temperature. The sample chamber was made from the bulb of a disposable (polyethylene) 1-mL transfer pipette. The pipette was attached to a rotating motor (20 to 22 rotations per 10 s) at a position equivalent to the maximum intensity of the ultrasound beam. The rotating motor was used to maintain a uniform exposure of the sample to the ultrasound.

When no microbubbles were added, the samples were exposed to ultrasound for 180 s using mechanical index (MI) of 0 to 2.7 (corresponding to peak negative pressures of 0 to 1.5 MPa) and a duty cycle of 20% [i.e., a 100-μs pulse length and pulse repetition frequency (PRF) of 2 kHz]. In the presence of microbubbles, the ultrasound exposure had to be reduced to avoid massive cell death. The cells were exposed to ultrasound for 120 s using MI of 0 to 1.05 (corresponding to peak negative pressures of 0 to 0.58 MPa) and a duty cycle of 10% (i.e., a 33-μs pulse length and a PRF of 3 kHz). The stated levels of pressure were measured in free space (inside the water tank), not inside the sample chamber.

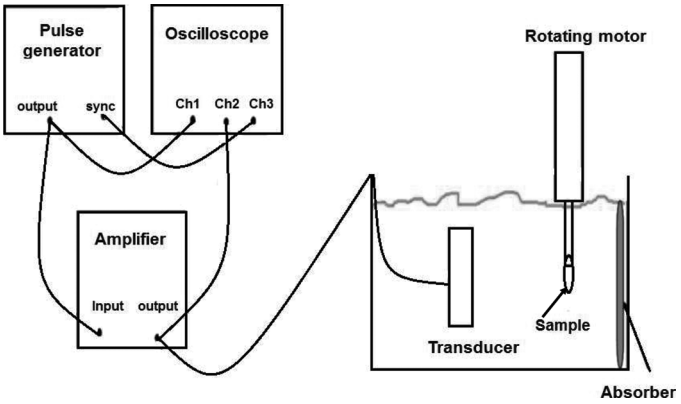

Fig. 1. A schematic diagram of the ultrasound exposure setup.

E. The Cellular Uptake of Liposomes and Dextran

Prior to ultrasound exposure, the sample chamber was filled with 2.5 mL of cell suspension in growth medium (10^6 cells/mL), 5 μL of DiD-labeled liposomes, and microbubbles (Definity, 1.1 to 2.5 μm). The microbubbles were activated with a Vial-Mix (Penn Pharmaceutical Services Ltd., Wales, UK) for 45 s, the vial was vented and a volume of 86 μL was added to 2.5 mL of the cell suspension, which corresponds to a volume concentration of 3.4%. This concentration was chosen based on a previous report by Karshafian *et al.* [19]. The samples were placed on ice immediately after ultrasound exposure.

To investigate the effect of the size of the nanoparticles on cellular uptake, FITC-dextran (Sigma-Aldrich) with various molecular weights (4, 40, 150, 500, and 2000 kDa) were used. FITC-dextran was chosen because it is readily available in different sizes. 50 mL of 7.7 mg/mL dextran and 86 μL of microbubbles were added to 2.5 mL of cell suspension (10^6 cells/mL) immediately before ultrasound exposure. Immediately after ultrasound exposure, 2 mL of the sample was placed on ice, and the remaining 500 μL was kept at room temperature for 1 to 2 h for a viability test. To remove FITC-dextran bound to the cell surface, the samples were centrifuged 3 times for 5 min at 4°C with a speed of 1500 rpm and resuspended in cold PBS. The samples containing DiD-labeled liposomes were not washed because washing had no effect on the fluorescence signal of these samples.

F. The Inhibition of Endocytosis

To investigate whether ultrasound in the presence of microbubbles affected endocytosis, the cells were incubated with the endocytic inhibitors genistein (70 μg/mL, Sigma-Aldrich), wortmannin (0.1 μmol/L, Sigma-Aldrich) and chlorpromazine (10 μg/mL, Sigma-Aldrich) for 30 min before and during ultrasound exposure in the presence of 500-kDa FITC-dextran. The optimal concentrations of the inhibitors that resulted in low cellular toxicity and considerable inhibition have previously been determined [34]. Immediately after ultrasound exposure, the cells were placed on ice and then washed 3 times at 4°C and resuspended in PBS.

To investigate whether endocytosis triggered by ultrasound was transient, 500-kDa FITC-dextran was added after the cells had been exposed to ultrasound and microbubbles for 120 s. The cells were then incubated with FITC-dextran at room temperature for 30 min. Endocytosis is a temperature-dependent process [35], [36], and to completely inhibit the endocytosis of FITC-dextran, the cells were exposed to ultrasound in the presence of microbubbles followed by incubation with 500-kDa FITC-dextran on ice for at least 30 min. After the 30-min incubation on ice or at room temperature, the cells were washed 3 times at 4°C and then resuspended in PBS.

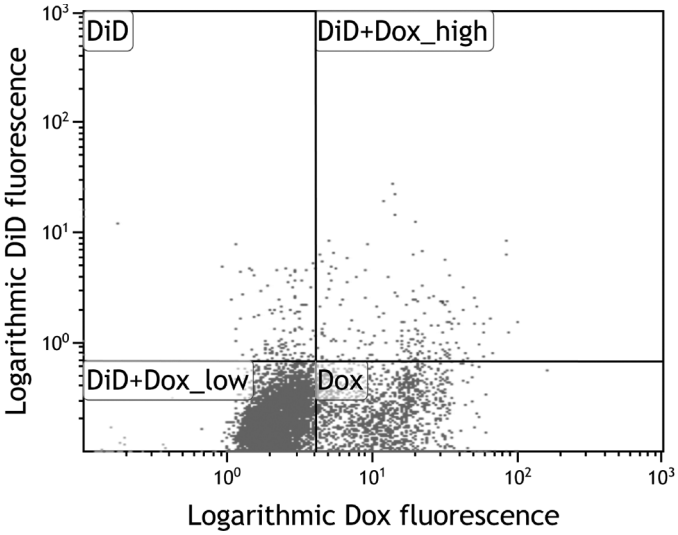

Fig. 2. The flow cytometric fluorescence intensity (2-parameter dot plot) of (1,1′-dioctadecyl-3,3,3′,3- tetramethylindodicarbocyanine) (DiD) versus doxorubicin (Dox). The upper-left quadrant represents cells that are positive for only DiD; the lower-left quadrant represents cells that are neither positive for DiD nor Dox. The upper-right quadrant signifies cells positive for both DiD and Dox, whereas the lower-right quadrant represents cells positive for only Dox. The cells were exposed to ultrasound and microbubbles with a 33 μs pulse length, 3 kHz pulse repetition frequency (PRF), 0.53 mechanical index (MI), and 120 s insonication time.

G. Flow Cytometric Measurements

The cellular uptake of liposomes and dextran was measured by flow cytometry (Gallios, Beckman Coulter Inc., Indianapolis, IN). In the case of DiD-labeled liposomes containing Dox, live and dead cells were distinguished using PicoGreen (Molecular Probes, Invitrogen, Grand Island, NY). 4 mL of PicoGreen (1:200) was added to 1 mL of sample just before flow cytometric measurements. The 488-nm laser line was used to excite Dox and PicoGreen, and the 633-nm laser line was used to excite DiD. The fluorescence was detected in the spectral intervals of 620 ± 30 nm, 530 ± 30 nm, and 660 ± 20 nm. To eliminate any spectral cross talk between the 3 dyes, the cells were incubated with liposomes not stained with DiD, liposomes stained with DiD but not containing Dox, or PicoGreen only. Based on these three single-labeled samples, the necessary percentage of electronic spectral compensation was determined. To distinguish the cellular uptake of free Dox from that of intact liposomes or fragments of liposomes, a two-dimensional scatter plot of Dox intensity versus DiD intensity was used (Fig. 2). The cells that exhibited a fluorescent intensity of Dox or DiD higher than those of the unlabeled control (negative cells) were classified as positive cells.

When the cellular uptake of FITC-dextran was studied, propidium iodide (PI) was used to detect dead cells, and 100 μL of PI (50 μg/mL) was added to 1 mL of sample before measurements. The 488-nm laser line was used to excite both FITC and PI, and the fluorescence was detected in the spectral intervals of 530 ± 30 nm and 620 ± 30 nm, respectively. The percentage of electronic spectral compensation was determined based on single-labeled samples (cells labeled with only PI or FITC-dextran). The cells that had taken up FITC-dextran but not PI were considered to be transiently permeabilized by ultrasound and viable. Only these cells were included in the analysis of the percentage of cells internalizing dextran. Cell viability was also measured 1 to 2 h after ultrasound exposure.

The cellular uptake was calculated both as the percentage of fluorescent cells (positive cells) and as the amount of internalized fluorochrome, which was estimated based on the median fluorescence intensity (MFI) of the positive cell population. Relative MFI was then calculated as the ratio of MFI of ultrasound treated and untreated cells incubated with liposomal Dox or dextrans. The forward-angle light-scatter signal was used to identify cell fragments and debris. The lowest size possible to detect was approximately 400 nm according to the producer. Data analysis was performed using Kaluza flow cytometry analysis software and SigmaPlot (Systat Software, Chicago, IL).

H. Confocal Laser Scanning Microscopy

The cells were placed in 8-well microscopic slides (ibidi GmBH, München, Germany) and imaged with confocal laser scanning microscopy (SP5, Leica Microsytems CMS GMH, Wetzlar, Germany) using an X63/1.2 water objective. The frame size was 512 × 512 pixels. Dox and FITC-dextran were excited with the 488-nm laser line, and the fluorescence was detected in the spectral intervals

of 500 to 600 nm and 500 to 550 nm, respectively. The fluorescence of DiD was detected with the 600 to 700 nm band-pass filter and excited by the 633-nm laser. A z-stack of images through the cells was obtained to verify whether the nanoparticles were intracellular or on the cell surface.

I. Statistical Analyses

All of the measurements were repeated 2 to 5 independent times, and the mean and standard deviations were calculated. All of the statistical analyses were conducted with Minitab software (Minitab Inc., Coventry, UK) using a one-way analysis of variance (ANOVA). A p value ≤ 0.05 was considered statistically significant.

III. Results

A. The Cellular Uptake of Liposomes and Dox

Ultrasound exposure did not enhance the cellular uptake of liposomes or Dox in the absence of microbubbles, whereas an increased uptake of Dox was observed after ultrasound exposure in the presence of microbubbles. Fig. 3 shows the flow cytometry analysis of HeLa cells exposed to DiD-labeled liposomes containing Dox and ultrasound at varying MIs. Without any ultrasound exposure, approximately 2 to 3% of the cells contained a very low amount of DiD and Dox. At the highest MI used, the percentage of cells containing Dox increased to 5%; however, the increase was not statistically significant compared with untreated cells [Fig. 3(a)]. Hence, ultrasound exposure alone did not enhance the cellular uptake of DiD or Dox. These observations were confirmed by the confocal images, in which no DiD or Dox signal could be detected (data not shown).

Cell damage after ultrasound exposure was categorized both as cells with leaky plasma membrane, which was detected by their uptake of PicoGreen, and as cells that had degraded into fragments and debris. The number of dead cells, indicated by the uptake of PicoGreen, did not increase after ultrasound exposure, but the number of cell fragments measured by the forward-angle light-scatter signal increased to approximately 15% [Fig. 3(b)]. The percentage indicating cell death may be a combination of cell fragments and aggregates of liposomes larger than 400 nm. However, any contribution of aggregates of liposomes is likely to be negligible because the uptake of such DiD-labeled liposomes is small.

Treating the cells with ultrasound in the presence of microbubbles increased the cellular uptake of both Dox and DiD (Fig. 4). The percentage of cells with Dox increased with increasing MI to 8% of the live cells (PicoGreen-negative cells) and 45% of the total cell population (live + dead cells) [Figs. 4(a) and 4(c)]. However, the amount of intracellular Dox in positive cells was rather low and was not significantly different from that in untreated cells [Figs. 4(b) and 4(d)], indicating that little Dox was internalized although the cells were categorized as Dox-positive. Ultrasound slightly increased the percentage of cells internalizing DiD (i.e., DiD bound to liposomes or fragments of liposomes or free DiD) in the population of live cells [Fig. 4(a)]. However, no significant increase of DiD-fluorescence could be detected in the cell population as a whole [Fig. 4(c)]. The percentage of cells containing fluorescence of both free Dox and DiD (i.e., cells with Dox+DiD) was not significantly different from that of untreated cells. These findings suggest that in the presence of microbubbles, Dox is released from the liposomes extracellularly before being internalized by the cells. It is not likely that the observed Dox fluorescence is from intact liposomes because Dox flu-

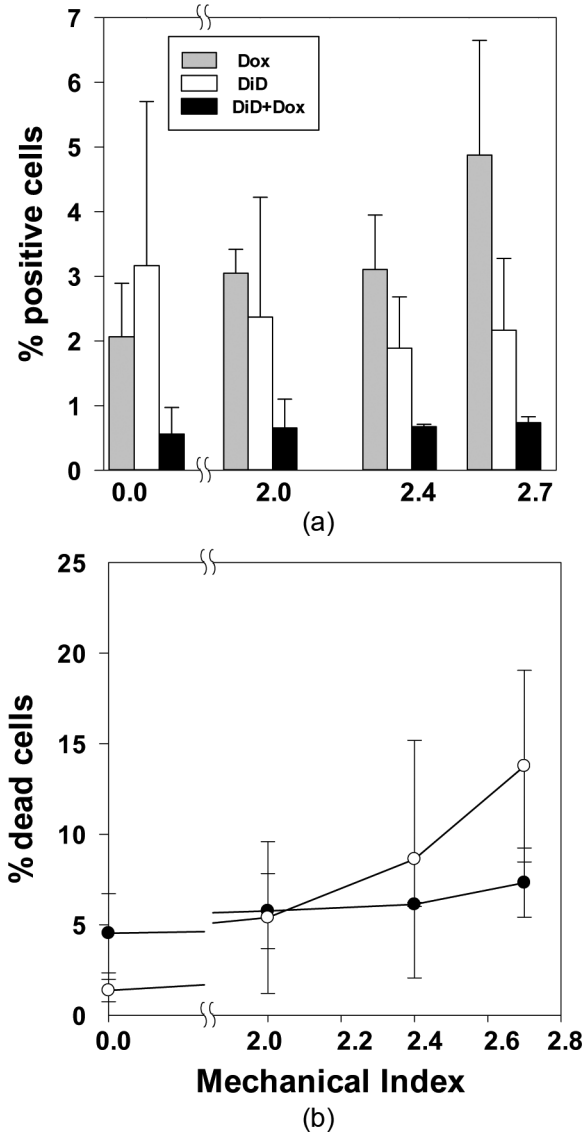

Fig. 3. The flow cytometric analysis of (a) the percentage of positive cells (gray) with doxorubicin (Dox), (white) (1,1′-dioctadecyl-3,3,3′,3- tetramethylindodicarbocyanine) (DiD), and (black) DiD+Dox as a function of the mechanical index (MI); (b) the percentage of dead cells as a function of the MI, (open circles) cell fragments and (closed circles) PicoGreen-positive cells. The cells were exposed to ultrasound with a pulse duration of 100 μs, 2-kHz pulse repetition frequency, and an insonication time of 180 s, all without microbubbles. The data points are the mean of 2 measurements with standard deviation.

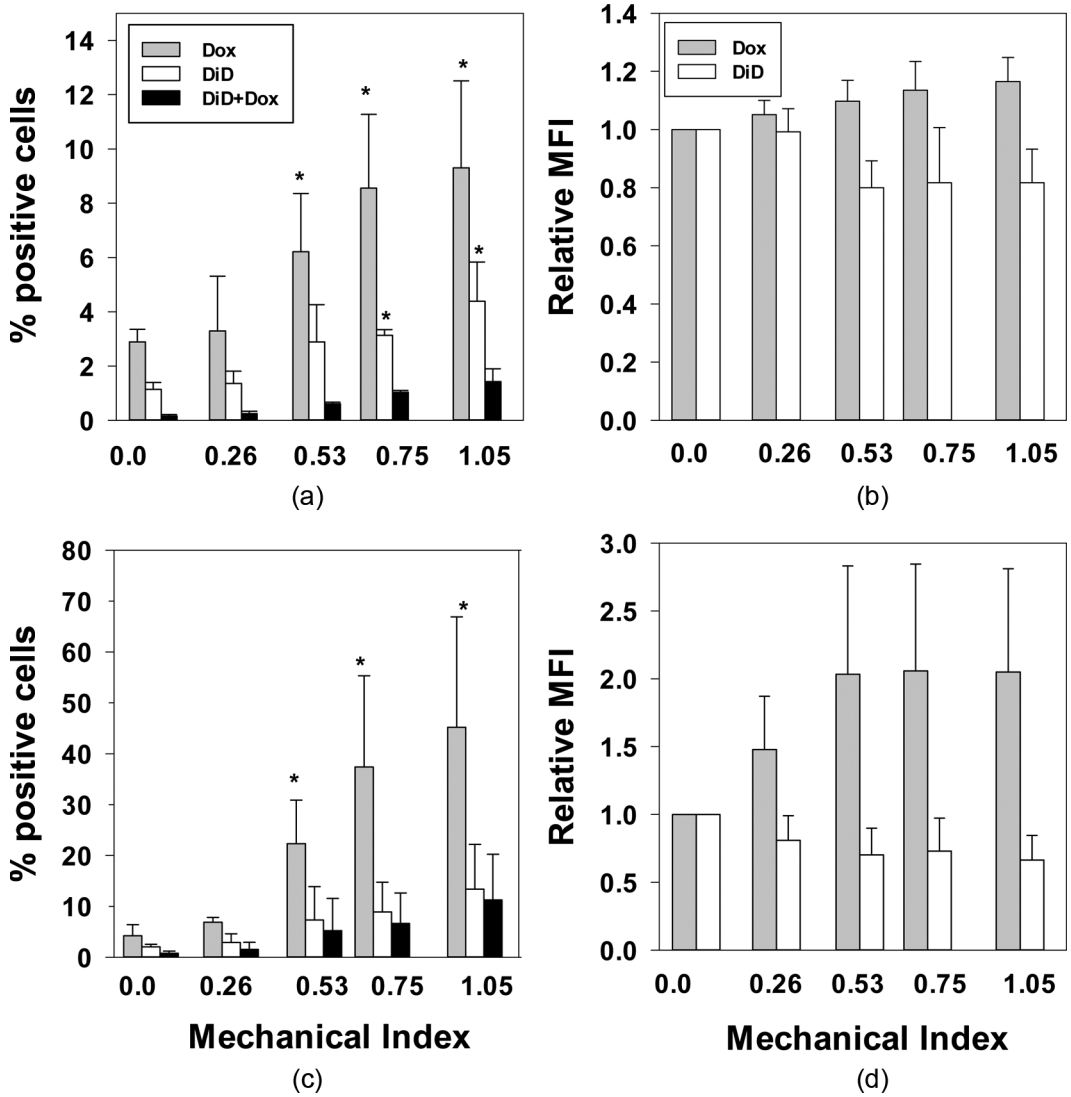

Fig. 4. The flow cytometric analysis of the cellular content of (gray) doxorubicin (Dox), (white) (1,1′-dioctadecyl-3,3,3′,3- tetramethylindodicarbocyanine) (DiD), and (black) DiD+Dox. The percentage of fluorescent cells (a) that are live (PicoGreen-negative) and (c) of the total population (live and dead) as a function of the mechanical index (MI). The relative median fluorescence intensity (MFI) of the positive cells (b) that are viable and (d) including both viable and dead, as a function of the MI. The cells were exposed to ultrasound and microbubbles with a pulse duration of 33 μs, 3-kHz pulse repetition frequency, and an insonication time of 120 s. The data points are the mean of 3 measurements with standard deviation; asterisk indicates a significant increase ($p < 0.019$).

orescence is quenched at intraliposomal Dox concentration [37]. This finding was also confirmed by confocal images in which Dox was observed in the cytoplasm and nucleus of the cells, whereas DiD was located in the periphery of the cells and in the cell membrane (Fig. 5). The confocal image in Fig. 5 shows an area of the cell population with cells internalizing both Dox and DiD, but it should be emphasized that the majority of the cells in other areas of the slide showed no Dox or DiD fluorescence.

Ultrasound exposure combined with microbubbles destroyed a considerable number of the cells incubated with the liposomes. The number of PicoGreen-positive cells and cell fragments increased with an increasing MI up to 18% and 57%, respectively, leaving only approximately 25% of the cells intact (Fig. 6). The number of dead cells (cell fragments + PicoGreen positive cells) after ultrasound exposure in the presence of microbubbles, was considerably higher than what was observed in preliminary experiments using the same MI without microbubbles (data not shown). In that case, hardly any cell death was observed.

B. The Effect of Dextran Size on Cellular Uptake

To investigate the potential effects of molecular weight on ultrasound-mediated cellular uptake, dextrans of different sizes were tested in combination with microbubbles. Generally, cellular uptake increased with an increasing MI for all dextran sizes (4 to 2000 kDa), reaching 65% dextran-positive cells at an MI of 1.05 [Fig. 7(a)]. Fig. 7 shows the cellular uptake in live cells (i.e., PI-negative cells). At the lowest MI applied (MI = 0.2), no significant increase in the uptake of dextran was observed, indicating

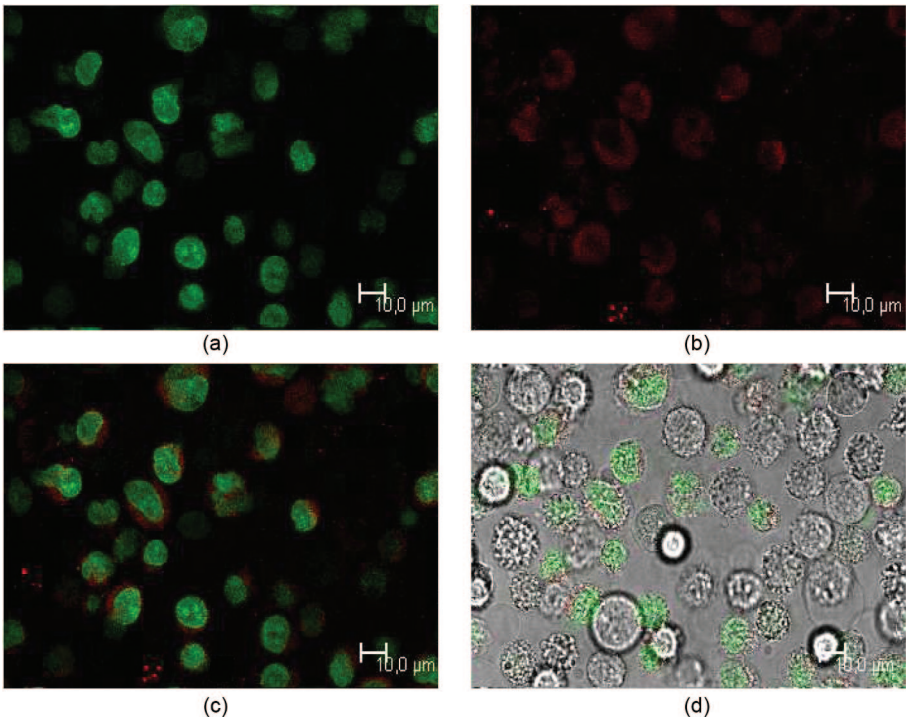

Fig. 5. Confocal images of HeLa cells exposed to (1,1′-dioctadecyl-3,3,3′,3- tetramethylindodicarbocyanine) (DiD)-labeled liposomes containg doxorubicin (Dox), microbubbles and ultrasound with a mechanical index (MI) of 0.53, a pulse duration of 33 µs, 3-kHz pulse repetition frequency, and an insonication time of 120 s. The cellular uptake of (a) Dox (green) and (b) DiD (red). (c) The overlaid images of (a) and (b). (d) The overlay of the light transmission image and images of (a) and (b). The images show an example of cells with Dox and DiD fluorescence, but the majority of the cells had no such fluorescence.

a threshold level for enhanced cellular uptake. The percentage of cells internalizing dextran was independent of the size of the dextran molecules up to 2 MDa; no significant difference was found between the percentages of cells that had taken up dextran among the five sizes tested. However, the amount of internalized FITC-dextran, which was estimated from the median fluorescence intensity of FITC-dextran positive cells, was found to be approximately five times higher for the 4-kDa dextran than for the other dextran sizes [Fig. 7(b)], even though the larger dextrans had more FITC label than the smaller dextrans. Thus, the amount of the smaller dextrans internalized is probably larger than indicated in Fig. 7(b). In the absence of microbubbles, cells treated with the same exposure parameters [MI (0.26 to 1.05), duty cycle (10%), and insonication time (120 s)] as those with microbubbles, showed negligible cellular uptake of dextrans (data not shown).

Cell viability was high immediately after ultrasound exposure, with a maximum cell death of approximately 9% at the maximum MI used (i.e., 1.05; data not shown). To study the long-term effect of ultrasound on cell viability, PI was added 2 h after insonication with 2000-kDa dextran. A cell death of 20% was measured at the highest MI (1.05), see Fig. 8. Notably, cells incubated with DiD-labeled liposomal Dox showed a higher cell death compared with cells incubated with dextran, although the exposure conditions were the same.

C. The Role of Endocytosis in Cellular Uptake

The effect of ultrasound on endocytosis in the presence of microbubbles was studied by incubating the cells with endocytic inhibitors before and during ultrasound exposure. The three inhibitors (genistein, wortmannin, and chlorpromazine) inhibited caveolae-mediated endocyto-

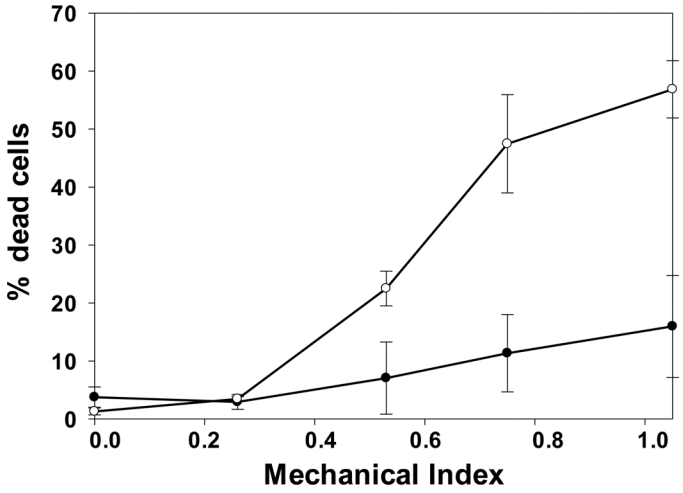

Fig. 6. The percentage of dead cells as a function of the mechanical index, measured by flow cytometry: (open circles) cell fragments and (closed circles) PicoGreen-positive cells. The cells were exposed to ultrasound and microbubbles with a pulse duration of 33 µs, 3-kHz pulse repetition frequency, and an insonication time of 120 s. The data points are the mean of 3 measurements with standard deviation.

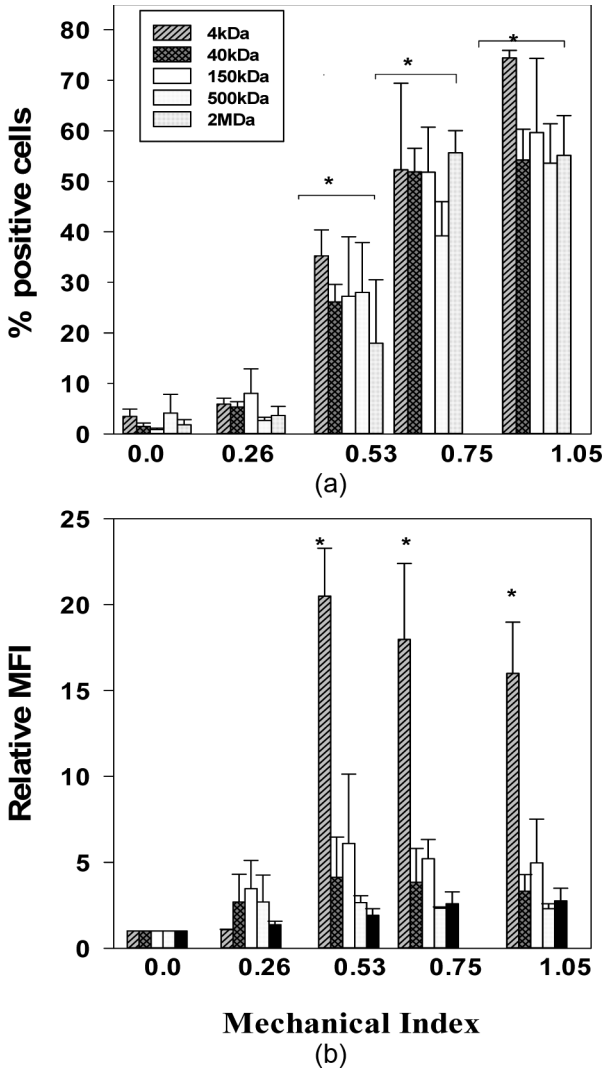

Fig. 7. The cellular uptake of different sizes of dextran (4 to 2000 kDa) in live cells as a function of the mechanical index (MI). (a) The percentage of FITC-dextran-positive cells for all dextran sizes, (b) the relative median fluorescence intensity (MFI) of FITC-dextran internalized estimated from the positive cell population. The cells were exposed to ultrasound and microbubbles with pulse duration of 33 μs, 3-kHz pulse repetition frequency, and an insonication time of 120 s. The data points are the means of 2 to 5 measurements with standard deviation. Asterisk indicates a significant increase ($p < 0.003$).

sis, macropinocytosis, and clathrin-mediated endocytosis, respectively. The cells treated with endocytic inhibitors exhibited a significant reduction in cellular uptake of 500-kDa dextran compared with cells without any inhibitors (Fig. 9). Using an MI of 1.05 and a 10% duty cycle, the cellular uptake in the live cell population (i.e., PI-negative cells) decreased from approximately 60% when no inhibitors were added to approximately 30%, 22%, and 14% in combination with genistein, wortmannin, and chlorpromazine, respectively [Fig. 9(a)].

To investigate whether ultrasound also had any lasting effect on endocytosis after ultrasound exposure, the cells were incubated with 500-kDa dextran at room temperature after ultrasound treatment, i.e., cells were treated with ultrasound in the presence of microbubbles and then 500-kDa dextrans were added to the cells and incubated for 30 min at room temperature or at 4°C. Thus, the cellular uptake was compared with the complete inhibition of endocytosis (i.e., incubating cells with dextran on ice after treatment with ultrasound in the presence of microbubbles) as well as the uptake of dextran incubated during ultrasound treatment. The cells incubated with dextran at room temperature after ultrasound exposure in the presence of microbubbles showed a significant reduction in the cellular uptake (in terms of both the percentage of positive cells and the fluorescent median intensity) of dextran compared with the cellular uptake of dextran incubated during ultrasound (Fig. 10). However, the uptake was higher than for dextran incubated on ice without ultrasound exposure. Comparing the uptake of dextrans incubated on ice without or after insonication, demonstrated a higher dextran uptake in the insonicated cells, indicating that sonoporation occurred.

IV. Discussion

The main findings of the present study are that 1) ultrasound enhanced the cellular uptake of Dox and dextran only in the presence of microbubbles; 2) DEPC-based liposomes released their contents extracellularly during ultrasound exposure; 3) cell death was more prominent when incubating cells with liposomal Dox compared with cell death with dextran during insonication in the presence of microbubbles; 4) ultrasound-mediated intracellular uptake was more efficient with low-molecular-weight entities; 5) enhanced cellular uptake was observed after the termination of sonication; and 6) both sonoporation

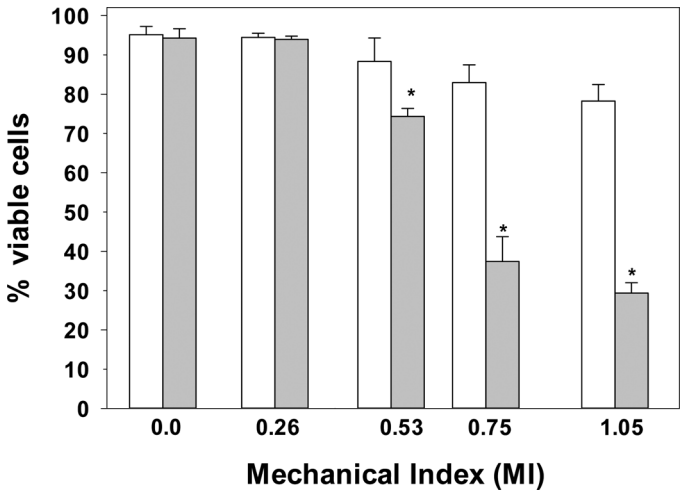

Fig. 8. The percentage of viable cells as a function of the mechanical index measured by flow cytometry. The cells were incubated with (white) 2000-kDa FITC-dextran or (gray) (1,1′-dioctadecyl-3,3,3′,3- tetramethylindodicarbocyanine) (DiD)-labeled liposomes with doxorubicin (Dox) and microbubbles, and exposed to ultrasound with a pulse duration of 33 μs, 3-kHz pulse repetition frequency, and an insonication time of 120 s. The data points are the mean of 2 to 3 measurements with standard deviation. Asterisk indicates a significant increase ($p < 0.03$).

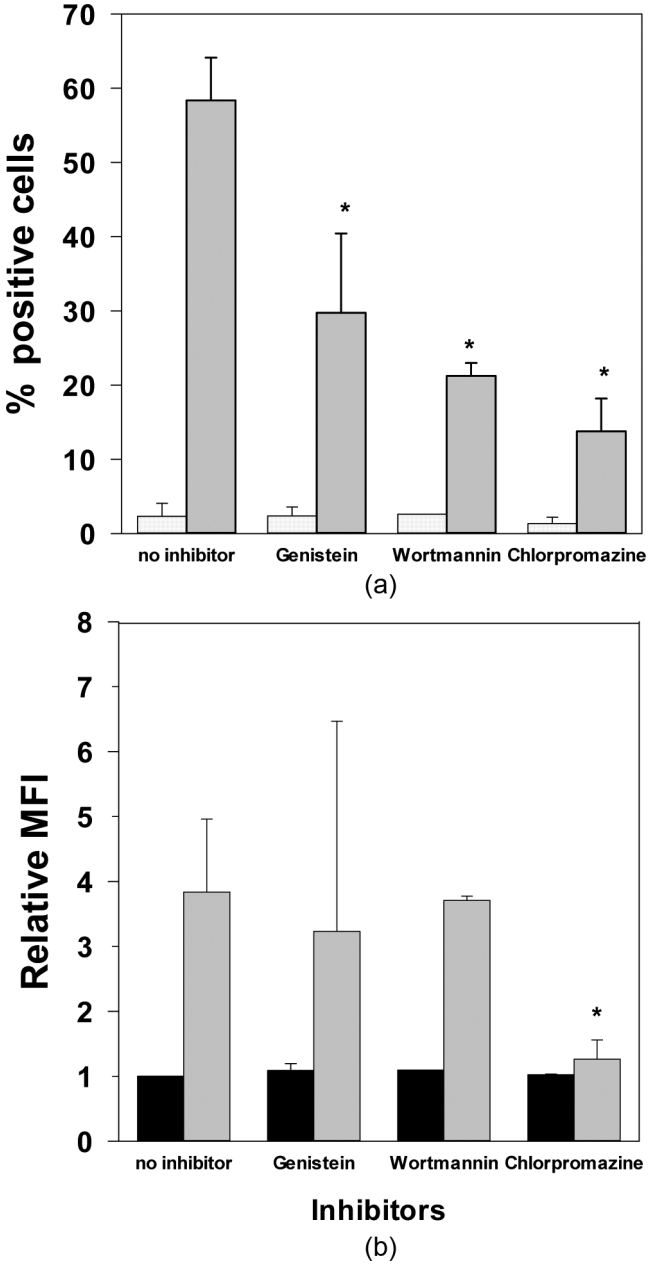

Fig. 9. The flow cytometric analysis of the cellular uptake of 500-kDa dextran treated (gray) with or (black) without ultrasound [mechanical index (MI) of 1.05, pulse duration of 33 μs, 3-kHz pulse repetition frequency, and an insonication time of 120 s] in the presence of microbubbles and one or none of the endocytic inhibitors genistein, wortmannin, or chlorpromazine. (a) The percentage of dextran-positive cells; (b) the relative median fluorescence intensity (MFI, the ratio between treated cells and cells not treated with inhibitors or ultrasound) of FITC-dextran internalized, estimated from the positive cell population. The data points are the mean of 2 to 5 measurements with standard deviation. Asterisk indicates a significant reduction ($p < 0.001$).

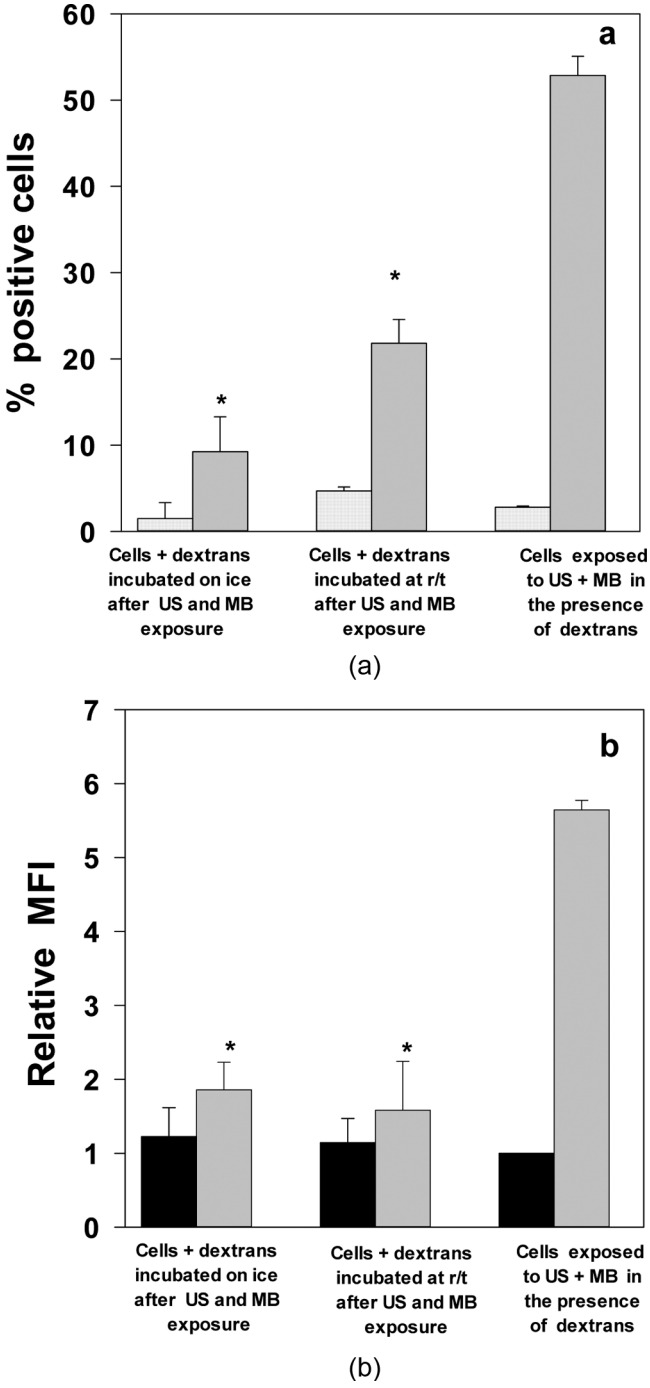

Fig. 10. The flow cytometric analysis of the cellular uptake of 500-kDa dextran incubated after treatment (gray) with or (black) without ultrasound (US) in the presence of microbubbles (MB). The cells were exposed to ultrasound [mechanical index (MI) of 1.05, pulse duration of 33 μs, 3-kHz pulse repetition frequency, and an insonication time of 120 s] and microbubbles before FITC-dextran was added and then incubated on ice or at room temperature (r/t) and compared with cells exposed to ultrasound and microbubbles in the presence of dextran. (a) The percentage of dextran-positive cells; (b) the relative median fluorescence intensity (MFI, normalized to cells incubated with dextrans without US treatment) of FITC-dextran internalized estimated from the positive population. The data points are the mean of 2 to 4 measurements with standard deviation. Asterisk indicates a significant reduction ($p < 0.001$).

and endocytosis played a role in the ultrasound-enhanced cellular uptake.

The dependency of microbubbles to obtain efficient intracellular uptake indicates that cavitation plays a central role in the uptake, likely by causing sonoporation of the plasma membrane [14], [15], [19]. Depending on the ultrasound exposure conditions, these bubbles can undergo sta-

ble oscillation or total collapse (causing micro-jet streams, shear stress, high temperature, etc.) or a combination of the two effects, which may lead to the sonoporation of membranes [14], [15], [19]. The contribution of stable and inertial cavitation to sonoporation and cell death was not measured in this study. However, in a previous study [30], we observed inertial cavitation and drug release from the same type of liposomes as used in this study, with a frequency of 300 kHz and MI above 1.6 without adding microbubbles. Furthermore, Schroeder *et al.* [38] has demonstrated release of liposomes with low-frequency ultrasound without the introduction of microbubbles. It should be emphasized that the presence of cells and proteins as in the present work, as well as the amount of cavitation nuclei, may cause different effects on the ultrasound-induced drug release compared with the studies of drug release from liposomes in solution. The threshold for inducing cavitation will increase with fewer cavitation nuclei present in the medium, and with increasing viscosity of the medium and cell density [39]. During ultrasound exposure, the cells were suspended in growth medium, and the amount and sizes of the gas nuclei in the medium did not appear to be sufficient to cause sonoporation using 300 kHz and MI up to 2.7. The observed need for microbubbles to obtain enhanced cellular uptake may be a challenge when treating tumors *in vivo* because only the vasculature and adjacent cells can be exposed to microbubbles, whereas the tumor cells embedded in the extracellular matrix will not be exposed to microbbubles.

The liposomes used in this study are DEPC-based liposomes comprising phospholipids with small head groups and long unsaturated acyl chains, which makes them more sonosensitive than the liposomes currently in clinical use [30], [40]. The cellular uptake of these liposomes caused by ultrasound and microbubbles treatment (judged by DiD fluorescence) was small; only approximately 5% of the cells showed DiD fluorescence, indicating either internalized liposomes or fragments of liposomes. This low uptake of liposomes may be due to the degradation of the liposomes extracellularly by ultrasound and microbubbles before the cellular uptake of the released Dox. Such degradation was supported by confocal images in which Dox was found in the cytoplasm and nucleus of the cells, whereas DiD was located in the periphery of the cells and in the cell membrane. Thus, our data suggest that ultrasound-induced cavitation causes the extracellular degradation of the liposomes and Dox release followed by intracellular Dox uptake. Also, the ultrasound-induced degradation of DEPC-based liposomes is supported by electron microscopic characterization of DOPE-based liposomes, the latter liposomes having an ultrasound-sensitive mechanism similar to the current liposomes. Extracellular degradation of liposomes after ultrasound exposure has also been found by Lentaker *et al.* [41]. The uptake of Dox in live cells was different from the uptake of Dox in the total cell population. Whereas only a small number of live cells had internalized Dox, almost half of the total cell population expressed Dox fluorescence. This result shows that Dox was primarily associated with membrane-damaged cells. The ultrasound exposure in the presence of microbubbles and liposomal Dox killed more cells than liposomal Dox and ultrasound alone. Two groups of dead cells were identified by flow cytometry: membrane-damaged, leaky cells and cell fragments. The fraction of cell fragments was larger in the presence of microbubbles, indicating cell degradation caused by the collapse of the microbubbles [14], [15], [19]. However, Karshafian *et al.* [19] reported that bubble disruption is a necessary but not a sufficient condition to cause sonoporation and cell death. The higher rate of cell death after incubation with liposomal Dox compared with dextran during ultrasound exposure suggests a cytotoxic effect of Dox, which has also been reported by others [41].

The percentage of live cells internalizing dextran increased with an increase in MI. An MI of 0.53 was required before the uptake of dextran was enhanced, indicating a threshold effect. Such a threshold is known to occur before the onset of inertial cavitation [14], [15]. The presence of a threshold during sonoporation has been previously reported [19]. The uptake of dextran of sizes from 4 kDa to 2 MDa was compared, and no significant differences were found in the percentage of internalizing cells at constant acoustic parameters, consistent with [18]. However, a higher amount of the smallest dextran (4 kDa) was internalized per cell. This implies that the use of drugs with a lower molecular weight (e.g., Dox) would be more desirable in ultrasound-mediated cancer therapy than drugs with a higher molecular weight.

The use of ultrasound in the presence of microbubbles is known to cause the sonoporation of the plasma membrane. The most common mechanism of cells for internalizing macromolecules without any external exposure, is endocytosis. The macromolecules are internalized through invaginations of the plasma membrane in a clathrin-dependent or clathrin-independent pathway, forming vesicles, which most likely fuse with early endosomes [42]. To investigate whether the ultrasound-enhanced uptake was caused by sonoporation alone or whether endocytosis also played a role, the effect of inhibiting three common endocytic pathways was studied. Inhibition of endocytosis caused a significant reduction in the ultrasound-mediated cellular uptake of dextran, with the clathrin-mediated pathway playing the most prominent role. This finding indicates that the ultrasound-mediated enhanced uptake of dextran is a result of both sonoporation and endocytosis. Ultrasound-enhanced endocytosis has been previously reported [43]. Consistent with our results, this study also found that endocytic inhibitors reduced ultrasound-mediated cellular uptake of 500-kDa dextrans. Furthermore, an increased number of endocytic vesicles have been observed in insonicated cells [44], which also support the hypothesis of ultrasound-enhanced endocytosis. However, the mechanism involved in this enhancement has not yet been elucidated. One explanation for this phenomenon may be that ultrasound triggers stable or transient cavitation, which causes shear stress on the cell membrane. Shear stress has

been suggested to stimulate endocytosis through a deformation of the plasma membrane, causing a reorganization of the cytoskeleton, which affects endocytosis [45]. Shear stress has also been suggested to stimulate endocytosis by inducing the activation, translocation, and clustering of integrins to counteract stress, which triggers endocytosis [35].

Endocytosis is a slow process compared with the duration of ultrasound exposure used in the present experiments. We therefore investigated the cellular uptake of dextran after ultrasound treatment. Endocytosis is energy dependent and is therefore strongly inhibited at low temperatures [35], [36]. Consistent with this temperature dependence, the uptake of dextran was reduced when the cells were incubated with dextran on ice following insonication in the presence of microbubbles, but the uptake was higher than for untreated cells (cells not treated with ultrasound) incubated with dextran on ice. This difference indicates that a mechanism other than endocytosis, likely sonoporation, also occurred. Studies have shown that pores formed in the membranes of cells exposed to ultrasound last from milliseconds to minutes [46], [47]. Therefore, pores were likely still open when dextran was added. Indeed, incubation with dextran at room temperature after 120 s of exposure to ultrasound and microbubbles enhanced the cellular uptake of dextran compared with the cellular uptake of dextran incubated on ice, but the uptake was lower than in cells incubated with dextran during ultrasound treatment. The difference in cellular uptake may be due to a more efficient pore formation during ultrasound treatment and ultrasound-triggered endocytosis. These observations also suggest that sonoporation is transient and that pore formation is part of the internalization process because the total inhibition of endocytosis did not result in the total blockage of cellular uptake. However, Meijering *et al.* [43] reported that larger dextrans (500 kDa) are taken up mainly through endocytosis and not through pore formation, whereas the smaller dextrans (4 kDa) are taken up through both endocytosis and pores. Additional studies are needed to understand the dependence of ultrasound-enhanced endocytosis on the molecular weight of nanoparticles. In summary, the effect of ultrasound on cellular uptake is transient, and the post-exposure effect is small both for sonoporation and endocytosis induced by ultrasound.

V. Conclusion

Ultrasound combined with microbubbles was found to be more effective in enhancing the cellular uptake of liposomes and dextran than ultrasound alone; the uptake increased with increasing MI. In the presence of microbubbles, the data suggest extracellular disruption of the liposomes followed by intracellular Dox uptake. Higher cell death was observed when cells were exposed to liposomes, ultrasound, and microbubbles than only ultrasound, and cells incubated with liposomal Dox demonstrated higher cell death than cells incubated with dextran during ultrasound treatment. The percentage of cells internalizing dextran was size-independent (up to 2 MDa); however, 4-kDa dextran was internalized in higher quantities than larger dextrans. The ultrasound and microbubble-enhanced uptake of 500-kDa dextran was significantly reduced by endocytic inhibitors, suggesting that endocytosis plays an important role in the enhanced cellular uptake caused by ultrasound. However, complete inhibition of endocytosis did not result in the complete blockage of cellular uptake, suggesting that pore formation is a part of the mechanism. Therefore, the improved cellular uptake might be due to both sonoporation and endocytosis. The results show that ultrasound enhances the cellular uptake of therapeutic molecules and has potential to improve cancer therapy.

Acknowledgments

The authors wish to thank K. G. Sæterbø, Department of Physics, NTNU, for her assistance in the laboratory and S. Røgnvaldsson at Epitarget AS for producing the liposomes.

References

[1] T. M. Allen, "Liposomes. Opportunities in drug delivery," *Drugs*, vol. 54, suppl. 4, pp. 8–14, 1997.

[2] Y. Barenholz, "Liposome application: Problems and prospects," *Curr. Opin. Colloid Interface Sci.*, vol. 6, no. 1, pp. 66–77, 2001.

[3] D. C. Drummond, O. Meyer, K. Hong, D. B. Kirpotin, and D. Papahadjopoulos, "Optimizing liposomes for delivery of chemotherapeutic agents to solid tumors," *Pharmacol. Rev.*, vol. 51, no. 4, pp. 691–743, 1999.

[4] Y. H. Bae, "Drug targeting and tumor heterogeneity," *J. Control. Release*, vol. 133, no. 1, pp. 2–3, 2009.

[5] F. Yuan, M. Leunig, S. K. Huang, D. A. Berk, D. Papahadjopoulos, and R. K. Jain, "Microvascular permeability and interstitial penetration of sterically stabilized (stealth) liposomes in a human tumor xenograft," *Cancer Res.*, vol. 54, pp. 3352–3356, Jul. 1, 1994.

[6] C. de L. Davies, L. M. Lundstrøm, J. Frengen, L Eikenes, Ø. S. Bruland, O. Kaalhus, M. H. Hjelstuen, and C. Brekken, "Radiation improves the distribution and uptake of liposomal doxorubicin (caelyx) in human osteosarcoma xenografts," *Cancer Res.*, vol. 64, pp. 547–553, Jan. 15, 2004.

[7] J. Vaage, D. Donovan, P. Uster, and P. Working, "Tumour uptake of doxorubicin in polyethylene glycol-coated liposomes and therapeutic effect against a xenografted human pancreatic carcinoma," *Br. J. Cancer*, vol. 75, no. 4, pp. 482–486, 1997.

[8] L. Eikenes, Ø. S. Bruland, C. Brekken, and C. de L. Davies, "Collagenase increases the transcapillary pressure gradient and improves the uptake and distribution of monoclonal antibodies in human osteosarcoma xenografts," *Cancer Res.*, vol. 64, pp. 4768–4773, Jul. 15, 2004.

[9] L. Eikenes, M. Tari, I. Tufto, O. S. Bruland, and C. de L. Davies, "Hyaluronidase induces a transcapillary pressure gradient and improves the distribution and uptake of liposomal doxorubicin (Caelyx) in human osteosarcoma xenografts," *Br. J. Cancer*, vol. 93, pp. 81–88, Jul. 11, 2005.

[10] A. Schroeder, J. Kost, and Y. Barenholz, "Ultrasound, liposomes, and drug delivery: Principles for using ultrasound to control the release of drugs from liposomes," *Chem. Phys. Lipids*, vol. 162, pp. 1–16, Nov. 2009.

[11] E. Hagtvet, T. J. Evjen, D. R. Olsen, S. L. Fossheim, and E. A. Nilssen, "Ultrasound enhanced antitumor activity of liposomal doxorubicin in mice," *J. Drug Target.*, vol. 19, pp. 701–708, Sep. 2011.

[12] W. G. Pitt, G. A. Husseini, B. L. Roeder, D. J. Dickinson, D. R. Warden, J. M. Hartley, and P. W. Jones, "Preliminary results of

combining low frequency low intensity ultrasound and liposomal drug delivery to treat tumors in rats," *J. Nanosci. Nanotechnol.*, vol. 11, pp. 1866–1870, Mar. 2011.

[13] S. Dromi, V. Frenkel, A. Luk, B. Traughber, M. Angstadt, M. Bur, J. Poff, J. Xie, S. K. Libutti, K. C. Li, and B. J. Wood, "Pulsed-high intensity focused ultrasound and low temperature-sensitive liposomes for enhanced targeted drug delivery and antitumor effect," *Clin. Cancer Res.*, vol. 13, no. 9, pp. 2722–2727, 2007.

[14] V. Frenkel, "Ultrasound mediated delivery of drugs and genes to solid tumors," *Adv. Drug Deliv. Rev.*, vol. 60, pp. 1193–1208, Jun. 30, 2008.

[15] W. G. Pitt, G. A. Husseini, and B. J. Staples, "Ultrasonic drug delivery—A general review," *Expert Opin. Drug Deliv.*, vol. 1, no. 1, pp. 37–56, 2004.

[16] P. A. Dayton, J. S. Allen, and K. W. Ferrara, "The magnitude of radiation force on ultrasound contrast agents," *J. Acoust. Soc. Am.*, vol. 112, no. 5, pt. 1, pp. 2183–2192, 2002.

[17] A. F. Lum, M. A. Borden, P. A. Dayton, D. E. Kruse, S. I. Simon, and K. W. Ferrara, "Ultrasound radiation force enables targeted deposition of model drug carriers loaded on microbubbles," *J. Control. Release*, vol. 111, no. 1–2, pp. 128–134, 2006.

[18] H. R. Guzman, D. X. Nguyen, A. J. McNamara, and M. R. Prausnitz, "Equilibrium loading of cells with macromolecules by ultrasound: Effects of molecular size and acoustic energy," *J. Pharm. Sci.*, vol. 91, no. 7, pp. 1693–1701, 2002.

[19] R. Karshafian, P. D. Bevan, R. Williams, S. Samac, and P. N. Burns, "Sonoporation by ultrasound-activated microbubble contrast agents: Effect of acoustic exposure parameters on cell membrane permeability and cell viability," *Ultrasound Med. Biol.*, vol. 35, no. 5, pp. 847–860, 2009.

[20] A. Marin, H. Sun, G. A. Husseini, W. G. Pitt, D. A. Christensen, and N. Y. Rapoport, "Drug delivery in pluronic micelles: Effect of high-frequency ultrasound on drug release from micelles and intracellular uptake," *J. Control. Release*, vol. 84, no. 1–2, pp. 39–47, 2002.

[21] A. Hayer, M. Stoeber, D. Ritz, S. Engel, H. H. Meyer, and A. Helenius, "Caveolin-1 is ubiquitinated and targeted to intralumenal vesicles in endolysosomes for degradation," *J. Cell Biol.*, vol. 191, no. 3, pp. 615–629, 2010.

[22] S. Mayor and R. E. Pagano, "Pathways of clathrin-independent endocytosis," *Nat. Rev. Mol. Cell Biol.*, vol. 8, no. 8, pp. 603–612, 2007.

[23] P. Midoux, G. Breuzard, J. P. Gomez, and C. Pichon, "Polymer-based gene delivery: A current review on the uptake and intracellular trafficking of polyplexes," *Curr. Gene Ther.*, vol. 8, no. 5, pp. 335–352, 2008.

[24] M. C. Kerr and R. D. Teasdale, "Defining macropinocytosis," *Traffic*, vol. 10, no. 4, pp. 364–371, 2009.

[25] T.-G. Iversen, T. Skotland, and K. Sandvig, "Endocytosis and intracellular transport of nanoparticles: Present knowledge and need for future studies," *Nano Today*, vol. 6, no. 2, pp. 176–185, 2011.

[26] L. H. Wang, K. G. Rothberg, and R. G. Anderson, "Mis-assembly of clathrin lattices on endosomes reveals a regulatory switch for coated pit formation," *J. Cell Biol.*, vol. 123, no. 5, pp. 1107–1117, 1993.

[27] I. R. Nabi and P. U. Le, "Caveolae/raft-dependent endocytosis," *J. Cell Biol.*, vol. 161, no. 4, pp. 673–677, 2003.

[28] R. G. Parton, B. Joggerst, and K. Simons, "Regulated internalization of caveolae," *J. Cell Biol.*, vol. 127, no. 5, pp. 1199–1215, 1994.

[29] H. S. Kruth, N. L. Jones, W. Huang, B. Zhao, I. Ishii, J. Chang, C. A. Combs, D. Malide, and WY. Zhang, "Macropinocytosis is the endocytic pathway that mediates macrophage foam cell formation with native low density lipoprotein," *J. Biol. Chem.*, vol. 280, no. 3, pp. 2352–2360, Jan. 21, 2005.

[30] M. Afadzi, C. de L. Davies, Y. H. Hansen, T. Johansen, O. K. Standal, R. Hansen, S. E. Måsøy, E. A. Nilssen, and B. Angelsen, "Effect of ultrasound parameters on the release of liposomal calcein," *Ultrasound Med. Biol.*, vol. 38, pp. 476–486, Mar. 2012.

[31] D. Lasic, *Liposomes: From Physics to Applications*. Amsterdam, The Netherlands: Elsevier, 1993.

[32] G. Haran, R. Cohen, L. K. Bar, and Y. Barenholz, "Transmembrane ammonium sulfate gradients in liposomes produce efficient and stable entrapment of amphipathic weak bases," *Biochim. Biophys. Acta*, vol. 1151, pp. 201–215, Sep. 19, 1993.

[33] T. J. Evjen, E. A. Nilssen, S. Rögnvaldsson, M. Brandl, and S. L. Fossheim, "Distearoylphosphatidylethanolamine-based liposomes for ultrasound-mediated drug delivery," *Eur. J. Pharm. Biopharm.*, vol. 75, pp. 327–333, Aug. 2010.

[34] Z. Garaiova, S. P. Strand, N. K. Reitan, S. Lelu, S. Ø. Størset, K. Berg, J. Malmo, O. Folasire, A. Bjorkøy, and C. deL. Davies, "Cellular uptake of DNA-chitosan nanoparticles: The role of clatrin-and caveolae-mediated pathways," *Int. J. Biol. Macromol.*, 2012, to be published.

[35] K. Lawler, G. O'Sullivan, A. Long, and D. Kenny, "Shear stress induces internalization of E-cadherin and invasiveness in metastatic oesophageal cancer cells by a Src-dependent pathway," *Cancer Sci.*, vol. 100, pp. 1082–1087, Jun. 2009.

[36] M. Rimann, T. Lühmann, M. Textor, B. Guerino, J. Ogier, and H. Hall, "Characterization of PLL-g-PEG-DNA nanoparticles for the delivery of therapeutic DNA," *Bioconjug. Chem.*, vol. 19, pp. 548–557, Feb. 2008.

[37] I. V. Zhigaltsev, N. Maurer, K. F. Wong, and P. R. Cullis, "Triggered release of doxorubicin following mixing of cationic and anionic liposomes," *Biochim. Biophys. Acta*, vol. 1565, no. 1, pp. 129–135, 2002.

[38] A. Schroeder, Y. Avnir, S. Weisman, Y. Najajreh, A. Gabizon, Y. Talmon, J. Kost, and Y. Barenholz, "Controlling liposomal drug release with low frequency ultrasound: Mechanism and feasibility," *Langmuir*, vol. 23, no. 7, pp. 4019–4025, 2007.

[39] R. E. Apfel and C. K. Holland, "Gauging the likelihood of cavitation from short-pulse, low-duty cycle diagnostic ultrasound," *Ultrasound Med. Biol.*, vol. 17, no. 2, pp. 179–185, 1991.

[40] T. J. Evjen, E. A. Nilssen, S. Barnert, R. Schubert, M. Brandl, and S. L. Fossheim, "Ultrasound-mediated destabilization and drug release from liposomes comprising dioleoylphosphatidylethanolamine," *Eur. J. Pharm. Sci.*, vol. 42, pp. 380–386, Mar. 18, 2011.

[41] I. Lentacker, B. Geers, J. Demeester, S. C. De Smedt, and N. N. Sanders, "Design and evaluation of doxorubicin-containing microbubbles for ultrasound-triggered doxorubicin delivery: Cytotoxicity and mechanisms involved," *Mol. Ther.*, vol. 18, pp. 101–108, Jan. 2010.

[42] A. Diaz-Moscoso, D. Vercauteren, J. Rejman, J. M. Benito, C. Ortiz Mellet, S. C. De Smedt, and J. M. Fernández, "Insights in cellular uptake mechanisms of pDNA-polycationic amphiphilic cyclodextrin nanoparticles (CDplexes)," *J. Control. Release*, vol. 143, pp. 318–325, May 10, 2010.

[43] B. D. Meijering, L. J. Juffermans, A. van Wamel, R. H. Henning, I. S. Zuhorn, M. Emmer, A. M. Versteilen, W. J. Paulus, W. H. van Gilst, K. Kooiman, N. de Jong, R. J. Musters, L. E. Deelman, and O. Kamp, "Ultrasound and microbubble-targeted delivery of macromolecules is regulated by induction of endocytosis and pore formation," *Circ. Res.*, vol. 104, pp. 679–687, Mar. 13, 2009.

[44] J. Hauser, M. Ellisman, H. U. Steinau, E. Stefan, M. Dudda, and M. Hauser, "Ultrasound enhanced endocytotic activity of human fibroblasts," *Ultrasound Med. Biol.*, vol. 35, pp. 2084–2092, Dec. 2009.

[45] G. Apodaca, "Modulation of membrane traffic by mechanical stimuli," *Am. J. Physiol. Renal Physiol.*, vol. 282, pp. F179–F190, Feb. 2002.

[46] S. Gambihler, M. Delius, and J. W. Ellwart, "Permeabilization of the plasma membrane of L1210 mouse leukemia cells using lithotripter shock waves," *J. Membr. Biol.*, vol. 141, pp. 267–275, Sep. 1994.

[47] Y. Qiu, Y. Luo, Y. Zhang, W. Cui, D. Zhang, J. Wu, J. Zhang, and J. Tu, "The correlation between acoustic cavitation and sonoporation involved in ultrasound-mediated DNA transfection with polyethylenimine (PEI) in vitro," *J. Control. Release*, vol. 145, pp. 40–48, Jul. 1, 2010.

Mercy Afadzi was born in Sekondi, Ghana, in 1981. She attended the University of Cape Coast in Ghana and graduated in 2005 with a bachelor's degree in physics. She received the Dean of Science Award and Unilever Award for outstanding academic performance in 2002 and 2005, respectively. In 2008, she obtained her master's degree in medical technology (biophysics and medical physics) from the Norwegian University of Science and Technology (NTNU) in Trondheim, Norway, where she is pursuing a Ph.D. degree in medical technology (biophysics and medical physics). Her research interest includes improving the delivery of cytotoxic drugs to cancer tissues by combining ultrasound with drug delivery.

Sabina P. Strand was born in Rakovnik, Czech Republic, in 1970. She received her M.Sc. degree from the Institute of Chemical Technology in Prague, Czech Republic, in 1993, and her Ph.D. degree in biotechnology from the Department of Biotechnology at the Norwegian University of Science and Technology (NTNU), Trondheim, in 2001. From 2002 to 2011, she has been working as postdoctoral fellow in the Department of Biotechnology at NTNU, conducting research on drug and gene delivery focused on biopolymer-based nanoparticles. Since 2012, she has been employed at NTNU Technology Transfer.

Esben A. Nilssen was born in Tromsø, Norway, in 1967. He earned an M.Phil. degree in molecular virology from Cambridge University, England, in 1996 and a Ph.D. degree in molecular genetics from the University of Oslo in 2003. Dr. Nilssen was an equity analyst and patent attorney before he joined the biotech industry in 2006. For the last five years, he has headed the biotech company Epitarget AS (Oslo, Norway), where he has an active role in the company's research and development efforts. At Epitarget, Dr. Nilssen has focused on functional drug delivery, including ultrasound-mediated drug delivery by means of sonosensitive liposomes, as well as immunomodulatory liposomal peptides.

Svein-Erik Måsøy (M'07) was born in Halden, Norway, in 1975. He received his M.Sc. degree in applied mechanics, thermodynamics, and fluid dynamics from the Norwegian University of Science and Technology (NTNU), Trondheim, Norway, in 1999. In 2004, he received the Ph.D. degree with his dissertation entitled "Estimation and correction of aberration in medical ultrasound imaging." He is currently employed as a researcher in the Department of Circulation and Medical Imaging at NTNU. His current research interests are nonlinear acoustics, beamforming, contrast detection, and targeted drug delivery in medical ultrasound imaging.

Tonni F. Johansen was born in Asker, Norway, in 1960. He received the Siv.Ing. degree from the Department of Telecommunications at the Norwegian University of Science and Technology (NTNU), Trondheim, Norway, in 1984, and a Ph.D. degree from the same department in 1991. In 1998, he joined the Department of Circulation and Imaging at the Faculty of Medicine, NTNU, where he is currently employed as senior engineer/ assistant professor. His research interests include acoustics, numerical simulation, signal processing, transducer design, and laboratory development

Rune Hansen was born in Horten, Norway in 1974. He earned his M.Sc. degree from the Department of Mechanics, Thermodynamics, and Fluid Mechanics at the Norwegian University of Science and Technology (NTNU) in 1998 and his Ph.D. degree from the Department of Engineering Cybernetics at the Faculty of Information Technology, Mathematics, and Electrical Engineering, NTNU, in 2004. In 1999. he joined the Department of Circulation and Medical Imaging, Faculty of Medicine, NTNU, where he currently is employed in a part-time position as a Research Scientist. Since 2006, he has also been employed as a Research Scientist at the Department of Medical Technology at SINTEF in Trondheim, Norway. His research interests include acoustics and signal processing with special focus on nonlinear acoustics and ultrasound contrast agents.

Bjørn A. J. Angelsen was born 1946 in Vestvågøy, Norway. He obtained an M.S.E.E. degree in physical electronics from the Norwegian Institute of Technology (NTH) in 1971 and a Ph.D. degree from the same institution on ultrasound measurement of blood velocity in the heart and the large thorax vessels. He built an instrument (PEDOF) that was used by Dr. Jarle Holen and Dr. Liv Hatle in their groundbreaking use of ultrasound Doppler measurements for diagnosis of heart valves and other cardiac function. The work formed the basis for the company Vingmed Ultrasound, Horten, Norway, and Angelsen was central in the development of Vingmed's ultrasound equipment for cardiac diagnosis during the 1980s and the 1990s. The company was acquired by General Electric in 1998. He became an associate professor in 1981 and a full professor in 1985 in Medical Imaging at the Norwegian University of Science and Technology (NTNU), Trondheim. In 1982, he co-authored with Dr. Hatle a central text for cardiac diagnosis with Doppler ultrasound: *Doppler Ultrasound in Cardiology — Physical Principles and Clinical Applications* (Lea & Febiger, Philadelphia, PA) and in 2000 he published *Ultrasound Imaging—Waves, Signals, and Signal Processing in Medical Ultrasonics*, volumes I and II (http://www.ultrasoundbook.com). In 1979, he won the SINTEF Research Prize together with his colleague Kjell Kristoffersen, now VP of Technology at GE Ultrasound. In 2007, he won the Ian Donal Gold Medal for research contributions to medical ultrasound imaging, and NTNU and SINTEFs technology prize, together with his colleague Professor Hans Torp; in 2008 he won the year's prize from the National Society for Public Health together with Dr. Liv Hatle. Since about 2000, his research interest has been on new methods for improved ultrasound imaging, compensating for multiple scattering noise and wave-front aberrations, detection of ultrasound contrast agent micro-bubbles at higher frequencies, and ultrasound-mediated drug delivery using nanoparticle-encapsulated drugs. For technical developments, he has co-founded the company SURF Technology AS, Trondheim.

Catharina de Lange Davies was born in 1956 in Trondheim, Norway. She received her M.Sc. degree in biophysics and medical technology from the Norwegian University of Science and Technology in 1981 and her Ph.D. degree in biophysics from the University of Oslo in 1990. She has been an associate professor and later full professor in biophysics at the Norwegian University of Science and Technology since 1991. Her research interests includes the delivery of nanoparticles and macromolecules to tumor cells, and understanding the mechanism of drug delivery and how to improve the tumor uptake of therapeutic agents to improve cancer therapy.

Paper III

ULTRASOUND IMPROVES THE UPTAKE AND DISTRIBUTION OF LIPOSOMAL DOXORUBICIN IN PROSTATE CANCER XENOGRAPHS

Ultrasound Improves the Uptake and Distribution of Liposomal Doxorubicin in Prostate Cancer Xenografts

Siv Eggen (1), Mercy Afadzi (1), Esben A. Nilssen (2), Solveig Bjærum Haugstad (1), Bjørn Angelsen (3) and Catharina de L. Davies (1)

1: Department of Physics, Norwegian University of Science and Technology, Trondheim, Norway
2: Epitarget AS, Oslo, Norway
3: Department of Circulation and Diagnostic Imaging, Norwegian University of Science and Technology, Trondheim, Norway'

Corresponding author: Siv Eggen, Dept. of Physics, The Norwegian University of Science and Technology, 7491 Trondheim, Norway.
Phone: +47 73593465
Fax: +47 73597710
E-mail: siv.eggen@ntnu.no

Abstract

Combining liposomally encapsulated cytotoxic drugs with ultrasound exposure has improved the therapeutic response to cancer in animal models; however, little is known about the underlying mechanisms. This study focused on investigating the effect of ultrasound exposures (1 MHz and 300 kHz) on the delivery and distribution of liposomal doxorubicin in mice with prostate cancer xenografts. The mice were exposed to ultrasound 24 hours after liposome administration to study the effect on the release of doxorubicin and the penetration through the extracellular matrix. Optical imaging methods were used to examine the effects at both the microscopic subcellular and macroscopic tissue levels. Confocal laser scanning microscopy revealed that ultrasound-exposed tumors had increased levels of released doxorubicin compared with unexposed control tumors, and an improvement in the distribution of liposomes and doxorubicin through the tumor tissue. Whole animal optical imaging showed that liposomes were taken up by both abdominal organs and tumors.

Key words: Ultrasound exposure, liposomal doxorubicin, drug delivery, drug release, microdistribution, biodistribution

Introduction

Conventional treatment of solid tumors often includes the systemic administration of cytotoxic drugs to cancer patients. However, such treatment is not cancer specific, and the toxicity of the drugs also affects healthy cells. Encapsulating these drugs into nanoparticles improves their pharmacokinetics and reduces the systemic exposure due to the so-called enhanced permeability and retention (EPR) effect (Fang et al. 2011; Iyer et al. 2006; Maeda et al. 2000). The EPR effect is the passive accumulation of nanoparticles in tumors as a result of the hyperpermeability of tumor capillaries and the reduced lymphatic drainage of tumors. However, successful cancer therapy requires that the therapeutic agent reaches the cancer cells in sufficient amounts to inactivate the cells. Although encapsulation of the drugs reduces their toxicity and increases tumor accumulation, the nanoparticles and released drugs do not travel far from the blood vessels (Bae 2009; Davies et al. 2004). Thus, only a small population of cancer cells located close to the blood vessels is exposed to the cytotoxic drugs. One of the major obstacles for the tumor uptake of nanoparticles is the elevated interstitial fluid pressure (IFP) in tumors, compared with IFP in normal tissue, and the lack of pressure gradients (Boucher et al. 1990; Boucher et al. 1996; Eikenes et al. 2004). This implies that the transport through the extracellular matrix (ECM) by convection is reduced and diffusion becomes the major transport mechanism.

There are currently several types of nanoparticles being investigated for their potential as carriers of therapeutic agents (Allen 1997; Husseini and Pitt 2008a; Liu et al. 2006; Torchilin 2005), including so-called stealth liposomes. The layer of polyethylene glycol (PEG) used in stealth liposomes allows for their prolonged circulation (Gabizon et al. 2003; Lu et al. 2004) and the toxicity of drugs encapsulated within these liposomes towards healthy tissue is considerably reduced compared to free drugs (Immordino et al. 2006; Lu et al. 2004). A few stealth liposomes containing cytotoxic drugs have been approved for clinical use. However, clinical chemotherapy using liposomal drugs does not include any active action to release the contents of the liposomes or to improve their intratumoral distribution. In experimental settings, several methods to actively disrupt liposomes at the target site have been explored. During the latest years, the use of therapeutic ultrasound (US) as a strategy to improve the local delivery of liposomal drugs has received increasing attention (Frenkel 2008; Hagtvet et al. 2011; O'Neill and Li 2008; Pitt et al. 2004; Schroeder et al. 2007; Schroeder et al. 2009a).

Therapeutic US is non-invasive, can penetrate deep into tissue and can be focused to an area of interest without affecting the surrounding tissue. The effects of US can be classified

as either thermal or mechanical. The two most important mechanical effects are acoustic radiation forces and acoustic cavitation. Acoustic radiation forces are transfer of momentum from the US beam to a particle causing translation of the particle in the direction of the propagated sound beam, while acoustic cavitation is the formation and oscillation of gas bubbles. Cavitation can be divided into two classes: stable cavitation, i.e., the stable oscillation of gas bubbles, and inertial or collapse cavitation, which takes place at higher acoustic pressures, i.e., the oscillating gas bubbles violently collapse producing jet streams, radicals and high temperatures. US in combination with microbubbles is reported to increase the permeability of blood vessels (Lin et al. 2010) and cell membranes (Deckers et al. 2008) and the release of drugs from carrier systems (Afadzi et al. 2012; Husseini and Pitt 2008b; Kost and Langer 2001; Rapoport et al. 2003; Suzuki et al. 2008). Several *in vivo* studies have shown that the combination of encapsulated cytotoxic drugs and therapeutic US results in delayed tumor growth (Hagtvet et al. 2011; Myhr and Moan 2006; Pitt et al. 2011; Schroeder et al. 2009a) and increased tumor concentrations of the cytotoxic drugs (Staples et al. 2010) compared with non-insonated controls.

The degree of release of the liposomal contents under the influence of US also depends on the structure of the lipids. Phospholipids, e.g., disteraoyl-phosphatidylethanolamine (DSPE), dioleoylphosphatidylethanolamine (DOPE) or dierucoyl-phosphatidylcholine (DEPC), have a cone-shaped geometry that is more conductive to sonosensitivity compared with the cylindrical geometry of the saturated phosphatidylcholines often used in liposomes (Evjen et al. 2010; Evjen et al. 2011a).

Although US shows promise in improving the delivery of nanoparticles, little is known about its mechanism and the effect of US frequency on delivery. Thus, the purpose of the present work was to study the effect of low (300 kHz) and medium (1 MHz) frequency US exposures on the delivery and distribution of liposomal doxorubicin through the ECM in prostate cancer xenografts. Mice were exposed to US 24 hours after liposome administration to study the effect of liposomes that were present in the ECM at the time of US exposure rather than the effect on extravasation. The effect of US was investigated on a microscopic level using confocal laser scanning microscopy (CLSM), which enabled the determination of the microdistribution in the tumor tissue, and on a macroscopic level using whole animal optical imaging to study the liposome biodistribution. This study was performed using the sonosensitive DEPC-based liposomes.

Materials and Methods

Cells and Animals

PC-3 prostate adenocarcinoma cells (American Type Culture Collection, Manassas, VA, USA) were cultured in Dulbecco's Modified Eagle Medium (Life Technologies Corporation, Carlsbad, CA, USA) with 10 % FBS at 37 °C and 5 % CO_2.

Female Balb/c nude mice (C.Cg/AnNTac-*Foxn1*^{nu} NE9, Taconic, Denmark) were purchased at 6 weeks of age. The animals were housed in groups of 5 in individually ventilated cages (IVC) model 1284L (Tecniplast, France). The mice were housed under conditions that were free of specific pathogens according to the recommendations set by the Federation of European Laboratory Animal Science Association (Nicklas et al. 2002). The mice also had free access to food and sterile water and a controlled environment with temperatures kept between 19 - 22 °C and a relative humidity between 50 - 60 %. All experimental animal procedures were in compliance with protocols approved by the Norwegian National Animal Research Authorities.

Before tumor implantation, the mice were anesthetized with isoflurane, and a 50 µl suspension containing 3 x 10^6 PC-3 cells was slowly injected subcutaneously on the lateral aspect of one hind leg between the hip and the knee. Tumors were allowed to grow for 3-6 weeks until the diameter of the tumor was between 5 and 10 mm.

Liposomes

Liposomes (Epitarget AS, Oslo, Norway) based on DEPC phospholipids were produced as described by Afadzi et al. (2012). The liposomes had an average diameter of 90 nm and contained the cytotoxic drug doxorubicin at a concentration of 2.0 mg/ml. The mean intensity-weighted hydrodynamic liposome diameter was determined by photon correlation spectroscopy at 23 °C and a scattering angle of 90° (Nanosizer, Malvern Instruments, Malvern, UK). For CLSM and whole animal imaging, the liposomes were labeled with the lipophilic tracers carbocyanine fluorophore 1,1'-dioctadecyl-3,3,3',3'-tetramethylindodicarbocyanine,4'chlorobenzenesulfonate salt (DiD, Molecular Probes, Eugene, OR, USA) or 1,1'-dioctadecyl-3,3,3',3'-tetramethylindotricarbo-cyanine iodine (DiR, Molecular Probes, Eugene, OR, USA), respectively. The dye was dissolved in ethanol and added to the liposome solution to a final concentration of 15 µg/ml DiD or 30 µg/ml DiR. Incubation was performed at room temperature for 2 h. Free DiD or DiR was removed by dialysis (Float-A-Lyzer® G2, Spectrum Laboratories Inc., Fort Lauderdale, FL, USA) in HEPES for 12 hours during which the HEPES solution was changed 3 times. Dynamic light

scattering (Nanosizer, Malvern Instruments, Malvern, UK) was used to measure the size of the liposomes before and after labeling (24 h, 48 h and 168 h). No apparent change in the liposome mean size or polydispersity index (PDI) was observed after labeling.

Before administration of the liposomes to mice, the tumor-bearing mice were anesthetized with 0.15 ml of a solution of Hypnorm and Dormicum (VetaPharma Ltd., Leeds, UK, and Roche Norge AS, Oslo, Norway, respectively) and sterile water (1:1:2). The liposomes were administered intravenously (i.v.) through the lateral tail vein at a dosage of 16 mg doxorubicin per kg. For all experiments, the liposomes were allowed to circulate for 24 hours.

Ultrasound Setup and Exposure

Two custom-made transducers (Imasonic, Besancon, France) with frequencies of 300 kHz and 1 MHz, respectively, were connected to a signal generator (Hewlett Packard 33120A, San Jose, CA, USA), an oscilloscope (LeCroy LT262, Long Branch, NJ, USA) and a power amplifier (ENI 2100L, Rochester, NY, USA), as illustrated in Figure 1. The transducer was mounted inside a chamber with the transducer array facing up towards the water surface. The water in the chamber was deionized and degassed by boiling and was at room temperature at the time of US exposure. The surface of the water was covered with a fibrous filter to prevent reflections of the sound waves. The mice were given surgical anaesthesia by a subcutaneous injection of Hypnorm and Dormicum and placed in a holder, and the tumor-bearing leg was lowered into the sonication chamber so that the tumor was located in the area of maximum intensity of the sound waves, as illustrated in Figure 1. The distance from the transducer surface to the focus area was 69 mm for the 300 kHz transducer and 125 mm for the 1 MHz transducer. Thus, the mounting system for the transducer inside the chamber differed between the two transducers to ensure that the focal area corresponded with the location of the tumor in the chamber. The choice of acoustic intensities was based on settings that had shown promising effcts on liposomal drug release *in vitro* and, at the same time, did not cause a temperature increase. For the 1 MHz group (n = 5) the tumors were exposed to US with a peak negative pressure of 2.2 (I_{TA} of 13.35 W/cm^2), corresponding to a mechanical index (MI) of 2.2. The US was pulsed with one pulse consisting of 200 cycles and a pulse repetition frequency (PRF) of 250 Hz, corresponding to a duty cycle of 5 %. The total insonation time was 10 minutes, which gives an effective US exposure of 30 seconds. For the 300 kHz group (n = 5) the tumors were exposed to US with a peak negative pressure of 1.3 MPa (I_{TA} of 3.142 W/cm^2), corresponding to a MI of 2.4. One pulse consisted of 60 cycles and the PRF was 250

Hz, which gave a duty cycle of 5 %. The total insonation time was 10 minutes, and the effective US exposure was 30 seconds. For the control group (n = 5), the tumors were positioned in the insonation chamber similar to the exposure groups, but with no transducer active. In the biodistribution study, one group of mice (n = 4) was exposed to 300 kHz US with the same settings as described above, while the other group (n = 4) was not exposed.

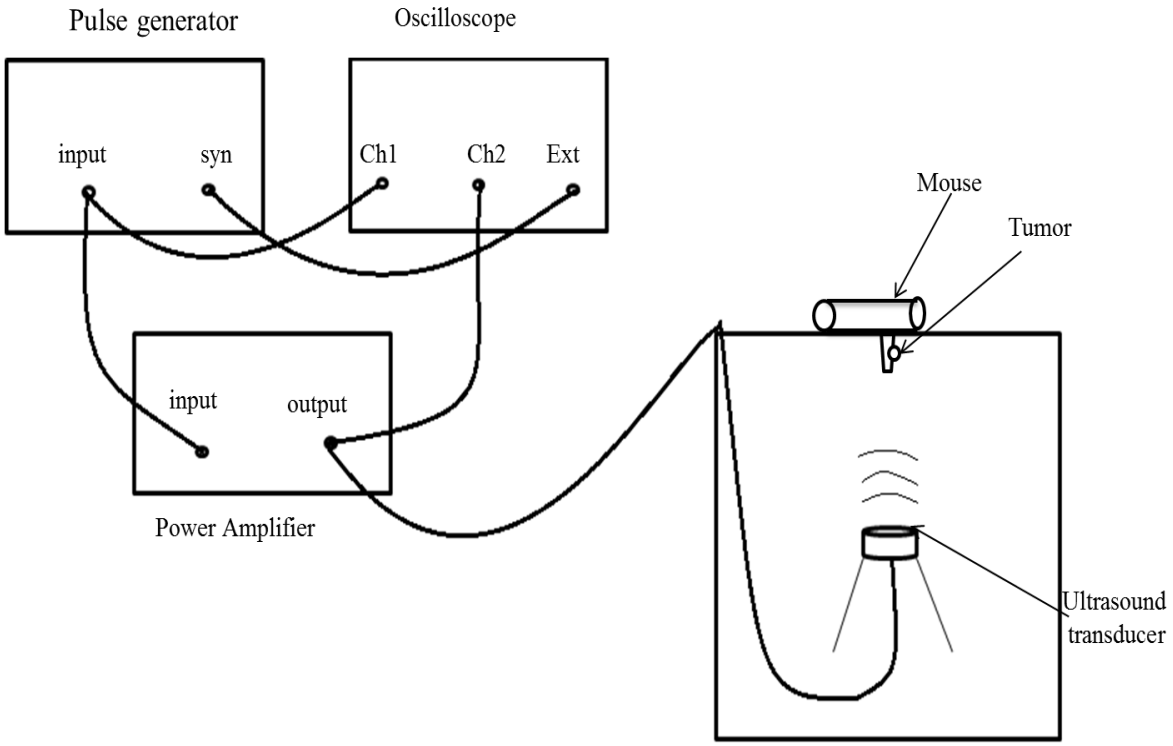

Figure 1: Schematic illustration of the experimental setup for ultrasound exposure.

Temperature Measurements

Separate experiments were performed to determine whether the US exposures caused a temperature increase in the tumor tissue. The temperature was measured in the tumor before and immediately after US exposure, but not during the exposure as the presence of the thermocoupler could affect the temperature measurements. The mice with PC3 xenografts were placed under surgical anesthesia with a subcutaneous injection of Hypnorm and Dormicum, and a K-TYPE thermocoupler (Testoon SAS, Chatillon, France) was placed in the center of the tumor for temperature registration. The tumor-bearing leg was then lowered into the water chamber and US (1 MHz or 300 kHz, respecticvely) was performed as described above. Immediately after the US exposure, the thermocoupler was placed into the tumor again and the temperature was remeasured. The mice were then euthanized by cervical dislocation.

Preparation of Tumor Sections

Following tumor insonation, mouse anesthesia was maintained for another 30 minutes before euthanasia using cervical dislocation. The tumor was excised, embedded in OTC Tissue Tec (Sakura, Alphen aan den Rijn, The Netherlands) and frozen in liquid N_2. Frozen sections with a thickness of 5 µm were prepared and mounted on objective glass slides with VECTASHIELD mounting medium (Vector Laboratories, Burlingame, CA, USA) for microscopic examination. Tumor sections were made at three depth levels, with 250 µm between each level.

Labeling of Blood Vessels

Two methods for labeling blood vessels in tumors were explored and then compared.

Immunofluorescence labeling of blood vessels: Tumor sections were rinsed in PBS and successively incubated in acetone and goat serum, followed by incubation with avidin for 15 minutes and biotin for 15 minutes (Abcam plc, Cambridge, UK) to prevent non-specific binding. Blood vessels were stained using 1 hour of incubation with Biotin Rat Anti-Mouse CD31 (BD Biosciences, Franklin Lakes, NJ, USA) diluted to 16.7 µg/ml in phosphate buffered saline (PBS) with 3 % goat serum and 0.05 % Tween20, and then 30 minutes of incubation with Streptavidin Alexa Fluor 488 (Molecular Probes, Eugene, OR, USA) diluted to 1 µg/ml in PBS with 3 % goat serum and 0.05 % Tween 20. All incubations took place at room temperature. The sections were rinsed thoroughly with PBS between the incubations.

In vivo *labeling of blood vessels:* Fluorescein labeled *Lycopersicon esculentum* (Tomato) lectin (FITC-lectin) (Vector Laboratories, Burlingame, CA, USA) diluted to 1 mg/ml with 0.9 % NaCl was injected i.v. at a volume of 100 µl and allowed to circulate for 5 minutes followed by euthanasia of the mice.

Confocal Laser Scanning Microscopy

The distribution of the released doxorubicin, liposomes and blood vessels was analyzed using CLSM (Zeiss LSM510, Jena, Germany). Doxorubicin was excited using the 488 argon laser line. To obtain tile scan images for quantitative measurements of doxorubicin, a 20x/0.5 objective was used. The tumor sections were imaged along a radial track from the periphery through the center and to the other periphery using the tile scan function. Each single image had a resolution of 512 x 512 pixels. The number of single images in the tile scan depended on the size of the tumor section. During image acquisition, the laser current, transmission,

detector gain, amplitude gain and amplitude offset were chosen to minimize noise and to utilize most of the grey scale. All images for quantitative analysis were acquired using the same microscopy settings. The co-localization of the released doxorubicin, blood vessels and liposomes was imaged in central and peripheral areas of the tumor sections using a 63x/1.4 oil objective. Doxorubicin was excited using the 533 nm helium/neon laser line, FITC-bound lectin and Streptavidin Alexa Fluor 488 were excited using the 488 nm argon laser line and DiD was excited using a 633 nm helium/neon laser line. For sections that had undergone immunofluorescent staining of blood vessels, the final images were generated by an overlay of pre- and post-staining images, as the immunofluorescence labeling process washed away the doxorubicin.

Biodistribution of Liposomes

The macroscopic distribution of the liposomes was investigated using a Pearl Impulse small animal imaging system (LI-COR Biosciences, Lincoln, NE, USA). Imaging of mice was performed with excitation at 785 nm and detection at 820 nm, and the image resolution was 85 µm. One mouse that did not receive any liposome injection served as a control. Tumor-bearing mice were imaged prior to the administration of DiR-labeled liposomes and again 30 minutes and 24 hours post-injection. The mice were then divided into two groups. One group (n = 4) was exposed to US at 300 kHz with the same exposure parameters as described above, while the other group (n = 4) served as the unexposed control group. Imaging of the exposed animals was also done immediately after the ultrasound exposure. All animals were imaged at 48, 72, 96 and 168 hours post-injection. After the last image acquisition, the animals were euthanized using cervical dislocation, and their organs (spleen, kidney, liver, heart, lungs and tumor) were excised for imaging. The images were analyzed using the Pearl Cam software. All images were linked to one lookup table (LUT) to allow for visual comparison. A circular background shape was drawn in a region outside the tumor, and then regions of interest (ROIs) were drawn along the tumor margins. The fluorescence signal in the ROI was calculated using equation 1:

$$S = TI - \left(\mu_B * Pc_B\right) \quad (1)$$

where S is the fluorescence signal, TI is the total intensity which is calculated as the sum of individual pixel intensities, μ_B is the mean background signal and Pc_B is the pixel count for the background.

Post-Processing of Images

Measuring the amount of doxorubicin: The amount of released doxorubicin was quantified using a custom-made Matlab (version R2007a, Natick, MA, USA) function. During this procedure, a threshold was manually set to exclude pixels with fluorescence intensities below 46. The threshold value was chosen to include fluorescent pixels originating from doxorubicin and to exclude pixels with autofluorescence. The Matlab function converted the original image into a binary image based on the threshold, and pixels were analyzed in areas along the tile scan with a step size of 200 µm. This resulted in numeric information about the area of fluorescence and the fluorescence intensity of pixels in defined areas along the tile scan images. This information was imported into a worksheet of Statistical Package for the Social Sciences (SPSS) (IBM, NY, USA). The uptake of doxorubicin was quantified by calculating the total fluorescence as the area with fluorescence multiplied by the pixel intensity. The overall tumor uptake of doxorubicin was quantified as the sum of the fluorescence along the tile scan image at each of the three depth levels.

Measuring the penetration of doxorubicin and liposomes from the blood vessels: The distance from the blood vessels through the area of doxorubicin fluorescence or DiD fluorescence was investigated by importing the CLSM images into the analysis program ImageJ (1.46m, National Institute of Health, USA). Lines were drawn from a selection of blood vessels through areas with doxorubicin fluorescence or DiD fluorescence, respectively. This was done in both periphery and center of the same tumor section. The length of the line was imported into a SPSS worksheet.

Comparison of blood vessel labeling methods: Tumor sections with blood vessels labeled using either the CD31 immunofluorescence staining method or the FITC-lectin circulation method were analyzed using a custom-designed Matlab function. This function converted the images into binary images based on a threshold value that was used to remove background signals. The number of fluorescent structures and the area of the fluorescent structures were registered and imported into a SigmaPlot worksheet (Systat Software Inc, San Jose, CA, USA).

Statistical Analysis

To test for differences across the exposure groups, Kruskal-Wallis tests were used. Pairwise comparisons were performed using Mann-Whitney U tests. A p-value of less than 0.05 was considered statistically significant.

Results

Comparison of Blood Vessel Labeling Methods

Visualization of blood vessels is important when studying the microscopic distribution of nanoparticles. Thus, the *in vitro* immunofluorescence staining of endothelial cells was compared with the *in vivo* labeling of blood vessels. The immunofluorescence staining marked all blood vessels, while the *in vivo* FITC-lectin labeling only detected functional vessels. An independent samples t-test was conducted to compare the mean number of fluorescent objects and the mean area of fluorescence per single image in each tile scan in sections with blood vessels labeled by CD31 immunofluorescence staining or *in vivo* circulation of FITC-lectin. The CD31 immunofluorescence staining method resulted in a larger number of fluorescent objects than the FITC-lectin circulation method ($p = 0.021$), whereas the FITC-lectin circulation method resulted in a larger area of fluorescence than the CD31 immunofluorescence staining method ($p = 0.001$) (data not shown).

Thermal Effects

No temperature increase was detected inside the tumor when the temperature was measured before and immediately after US exposure. For the 1 MHz exposure, the temperature inside the tumor was 35 °C both before and after the US exposure, while for the 300 kHz exposure, the temperature was reduced from 35 °C to 33 °C.

Increased Tumor Uptake of Doxorubicin

The amount of released doxorubicin in prostate tumor tissue was clearly enhanced in tumors exposed to US. The total fluorescence was increased in both insonation groups compared with the non-insonated controls. In the control group, the amount of doxorubicin fluorescence was largest at the periphery of the tumor sections and decreased towards the central areas. In the insonation groups, there were also strong fluorescent signals in central areas of the tumors (Figure 2). US exposure at both 300 kHz and 1 MHz induced large areas or clusters of cells with doxorubicin in both the periphery and central parts of the tumor sections. Figure 3 shows

the total fluorescence as a function of position along the tile scan images. The overall fluorescence in the tumors in each group is displayed in Figure 4. The amount of doxorubicin in the tumor tissue increased approximately 4-fold in the 1 MHz group and 5-fold in the 300 kHz group compared to the non-insonated group (Figure 4). Statistical analysis revealed a significant difference between the non-insonated group and both the 1 MHz group ($p = 0.009$) and the 300 kHz group ($p = 0.009$), but there was no significant difference between the 1 MHz group and the 300 kHz group ($p = 0.347$). In both exposure groups, there was a higher degree of variation in doxorubicin fluorescence than in the unexposed group. Standard deviations for the total fluorescence in each section ranged from 3.6 - 9.6 for the 1 MHz group, 4.6 - 17.3 for the 300 kHz group and 0.6 - 3.1 for the unexposed group (data not shown).

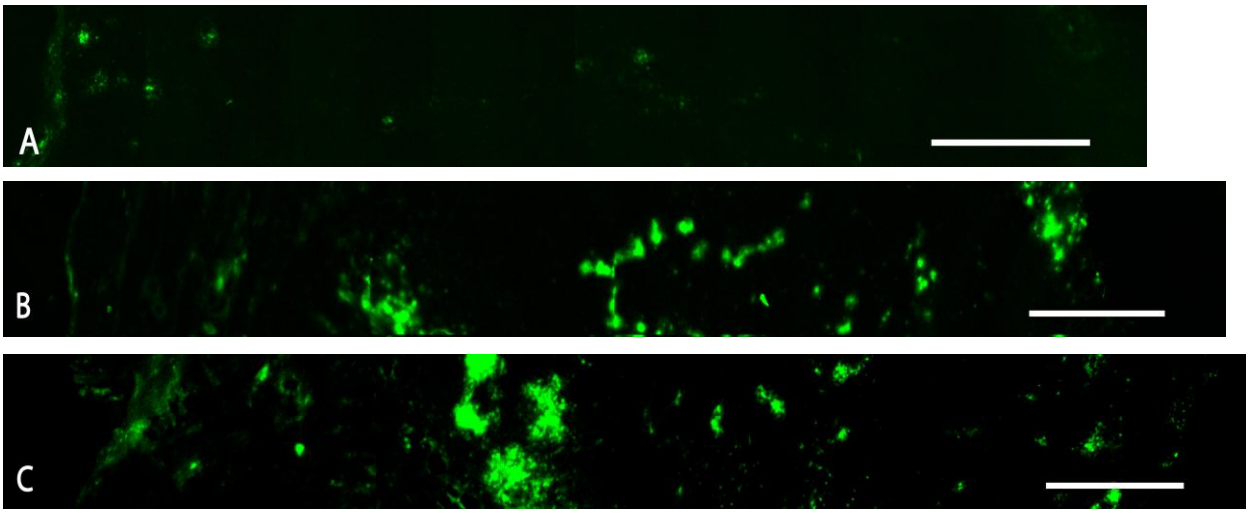

Figure 2: Representative confocal laser scanning microscopy (CLSM) tile scan images from sections of tumors not exposed to ultrasound (A), exposed to 1 MHz ultrasound (B) and exposed to 300 kHz ultrasound (C). The tile scan images were acquired by scanning the tumor sections from periphery to periphery to detect fluorescence from doxorubicin (green). Scale bar = 500 µm.

Improved Microdistribution of Liposomes and Released Doxorubicin

In non-insonated tumors, the fluorescence was located in clusters close to the blood vessels (Figure 5A). In contrast, the signals were more scattered and the distance between blood vessels and both the doxorubicin and DiD fluorescence increased after tumor insonation (Figure 5B and 5C).

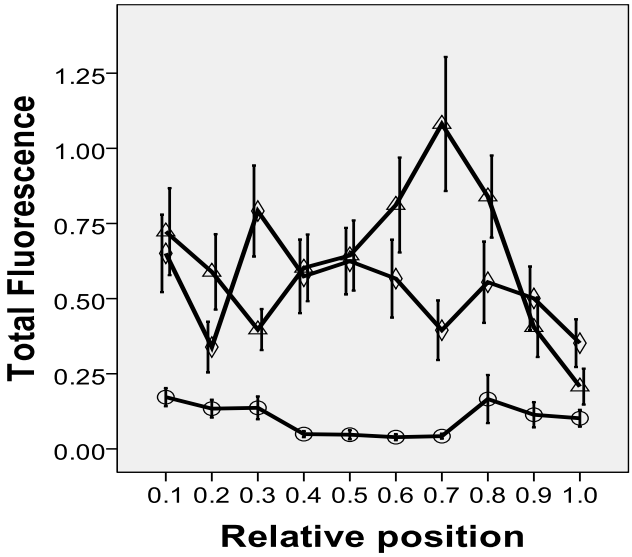

Figure 3: Doxorubicin fluorescence as a function of position in the tile scan images. Doxorubicin fluorescence was calculated as the area of fluorescence multiplied by intensity of the fluorescent pixels. The calculations were performed in steps of 200 µm along the tile scans. ○ = no ultrasound exposure, ◊ = 1 MHz ultrasound exposure, Δ = 300 kHz ultrasound exposure. Mean of 6 - 9 sections per mouse and 5 mice per group. Bars indicate standard error.

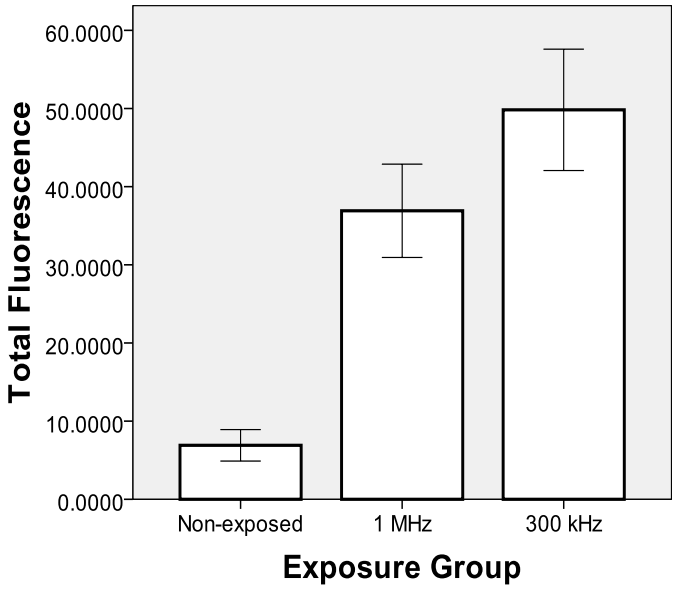

Figure 4. Total uptake of doxorubicin in the tumors, as quantified by calculating the total fluorescence across the tile scans at each of the three depth levels in the tumor and summarizing the values from the three levels in each tumor. Mean of 5 mice per group. Bars indicate standard error.

The distances between blood vessels and DiD or doxorubicin fluorescence were measured in both the periphery and central parts of the tumor (Figure 6). In the 1 MHz group, the degree of liposomal penetration, as measured by DiD fluorescence, increased approximately 2-fold

from both central (p = 0.040) and peripheral (p = 0.045) blood vessels compared to control tumors. In the 300 kHz group, the increase in liposome penetration was not significantly different from the controls (Figure 6A). The distance from the central blood vessels through the areas of doxorubicin fluorescence was increased in both the 1 MHz group (p = 0.022) and the 300 kHz group (p = 0.050) compared with the control group (Figure 6B). There was also an increase in doxorubicin displacement from peripheral vessels in the 1 MHz group (p = 0.043), but not in the 300 kHz group. In the 1 MHz group, the doxorubicin penetration from both central and peripheral blood vessels increased approximately 2-fold compared with the control group. In the 300 kHz group, the degree of doxorubicin displacement from central vessels was increased with approximately 20 %. Hence, the data strongly indicate that US causes a displacement of liposomes and doxorubicin away from blood vessels.

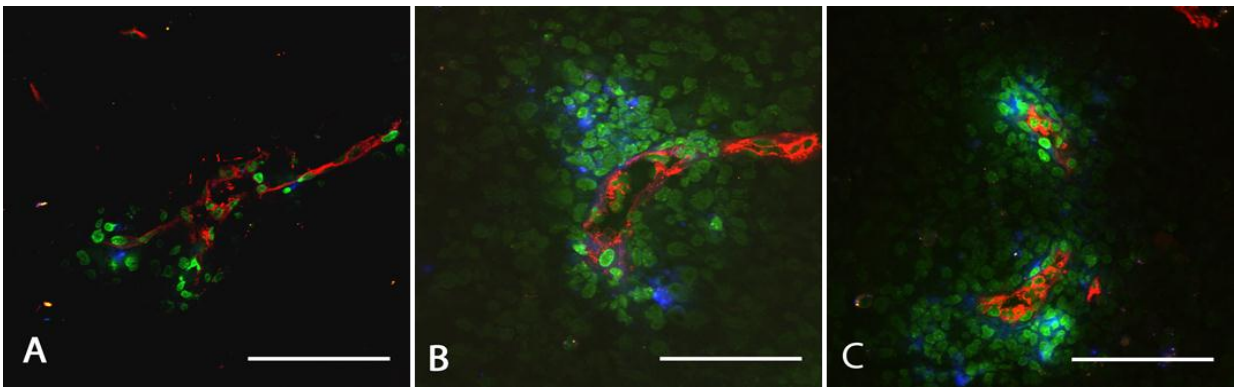

Fig. 5. Confocal laser scanning microscopy (CLSM) images from sections of tumors not exposed to ultrasound (A), exposed to 1 MHz ultrasound (B) and exposed to 300 kHz ultrasound (C). The images show the localization of DiD-labeled liposomes (blue) and released doxorubicin (green) relative to FITC-labeled capillaries (red). Scale bar = 100 µm.

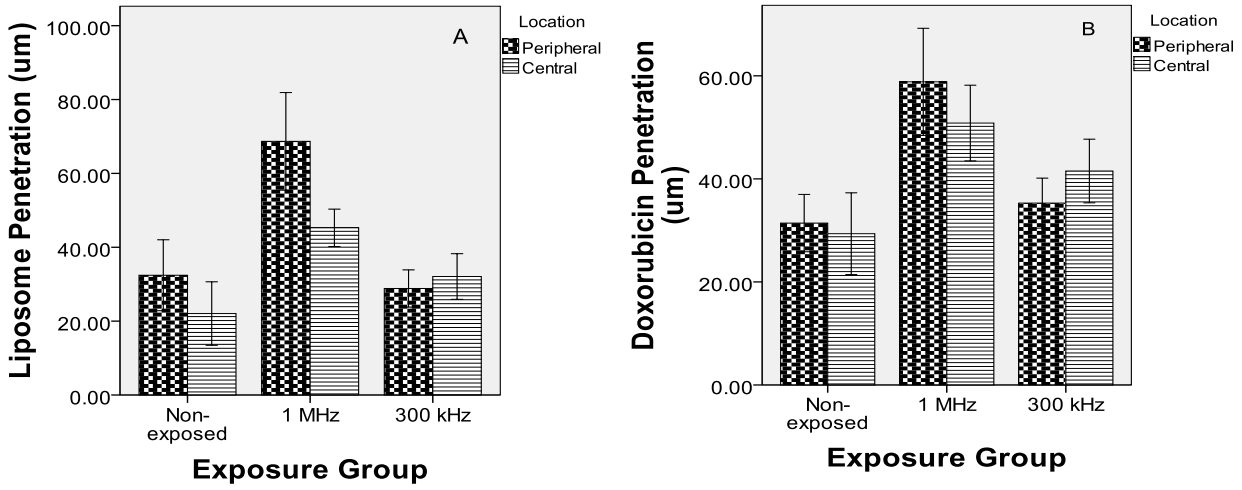

Figure 6: Measured distance from FITC-labeled blood vessels to areas with DiD fluorescence (A) or doxorubicin fluorescence (B). Measurements were performed from blood vessels in both central and peripheral areas of the tumor sections. Mean of 20 - 40 measurements per mouse in 4 mice per group. Bars indicate standard error.

Biodistribution of Liposomes

Image acquisitions of whole animals were performed to study the macroscopic biodistribution of liposomes labeled with DiR in tumors and normal organs. The highest fluorescence intensity was detected in the central abdominal region, and the images with organs show highest fluorescence in the liver, spleen, kidneys and tumor. Figure 7 shows an overlay of fluorescent images and white light images up to one week after liposome administration. The fluorescence from liposomes in the tumor reaches its maximal value at 24 - 48 hours after liposome injection (Figure 8). There was no significant difference in fluorescence intensity in the tumor between ultrasound-exposed and non-exposed animals ($p = 0.146$). Additionally, there was no significant difference when comparing groups at each individual time point (p-values ranging from 0.15 - 0.77).

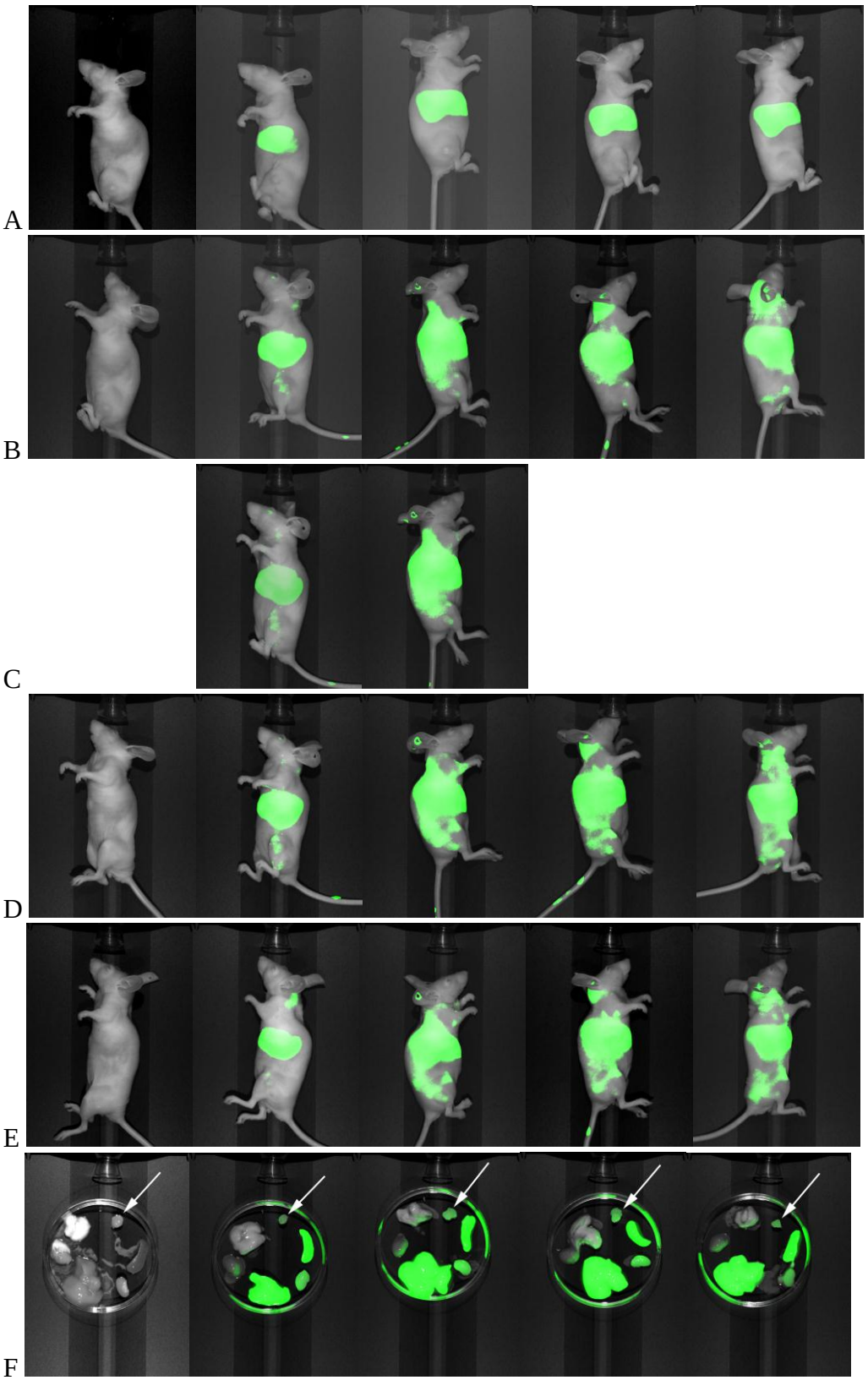

Figure 7: Mice with subcutaneous PC3 xenografts given DiR-labeled liposomes intravenously. The same animals are imaged at 30 minutes (A), 24 hours pre-US (B), 24 hours post-US(C), 48 hours (D) and 168 hours (E) post-injection. The animal to the left has not been given liposomes. After the image acquisition at 168 hours, the animals were euthanized and their tumor (arrow), spleen, kidney, liver, heart and lungs were excised for imaging (F).

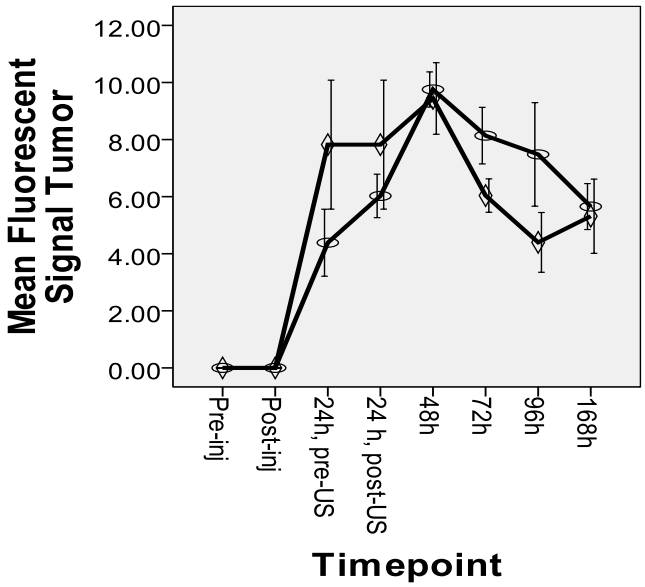

Figure 8: DiR fluorescence signal in tumors not exposed to ultrasound (◊) and exposed to 300 kHz ultrasound (○) at different time points after liposome administration. Mean of 4 measurements (4 animals per group) per time point. Bars indicate standard error.

Discussion

Blood Vessel Labeling Methods

The labeling of vessels *in vitro* using immunofluorescence with a CD31 antibody and *in* vivo using FITC-labeled lectin both generated good staining. The CD31 immunofluorescence staining method resulted in a larger number of fluorescent objects, whereas the labeling of vessels by *in vivo* circulation of FITC-lectin resulted in larger areas of fluorescence. These results are consistent with the fact that CD31 immunofluorescence stains all endothelial cells expressing the CD31 antigen irrespective of blood circulation through the vessels, whereas the circulation of FITC-lectin stains only functional vessels. FITC-lectin can also leak out through fenestrated capillaries and subsequently label the cells surrounding the capillaries, thus giving rise to a larger area of fluorescence. The labeling of only functional vessels corresponds better to the actual delivery of liposomes, and the analysis of the distribution of liposomes and released doxorubicin in the tumor tissue is therefore based on blood vessels labeled by the *in vivo* circulation of FITC-lectin.

Increased Doxorubicin Uptake by US

The US-mediated increase in doxorubicin fluorescence in the ECM in both exposure groups compared with the control group demonstrates that US triggers the release of doxorubicin from liposomes. Doxorubicin is quenched inside the liposomes, and the fluorescence intensity of encapsulated doxorubicin is approximately 5 % of the fluorescence intensity of free doxorubicin (Wu et al. 1997). Thus, the increase in doxorubicin fluorescence is due to the released doxorubicin and not an enhanced number of intact liposomes in the ECM. This increase in release occurred in both exposure groups, and no significant difference was observed between the two exposures, although there was a trend towards higher release in the 300 kHz group. The US exposure parameters were approximately the same at both frequencies, i.e., same duty cycle and insonation times, and there was only a small increase in MI at 300 kHz compared to 1 MHz. The release of doxorubicin from liposomes may be caused by either thermal or mechanical effects. Evjen and coworkers have demonstrated that lipid composition can influence the degree of ultrasound-mediated drug release from liposomes (Evjen et al. 2011b) and suggested that certain sonosensitive liposomes may release their contents due to destabilization of the lipid bilayer (Evjen et al. 2011a). A previous study using DEPC-based liposomes showed that these liposomes remain stable during incubation at 37 °C (Afadzi et al. 2012), indicating that the liposomes are not affected by the temperature in the tumors. The same *in vitro* study demonstrated that above a certain threshold of peak negative pressure, drug release increases with increasing MI at constant exposure times. The threshold values as given by MI were 1.9 and 1.6 for the 1 MHz and 300 kHz exposures, respectively, and the detection of OH radicals suggested that the drug release was caused by inertial cavitation. These threshold values are below the MI values used in our *in vivo* study. However, the *in vitro* study may not be directly comparable to *in vivo* conditions. One major difference is the presence of gas bubbles or small cavitation nuclei, which are required for acoustic cavitation to occur. During cavitation, bubble oscillations follow the compression and rarefaction phases of the ultrasound waves (stable cavitation). At higher ultrasound intensities, the amplitude of the oscillations increases above a certain threshold, and the bubble collapses (inertial cavitation). This causes a series of mechanical events, such as microstreaming, jet streams (Frenkel 2008; Pitt et al. 2004; Schroeder et al. 2009b) and local transient temperature and pressure increases (McNamara et al. 1999). In our system, no gas bubbles were added, and thus, gas bubbles or small gas nuclei must be present naturally in the tissue for cavitation to take place. The presence of gas inside the liposomes cannot be excluded, and small amounts of gas here could be a source for cavitation bubbles.

Additionally, it is not clear whether such gas bubbles or gas nuclei already exist in the ECM. However, the presence of pre-existing gas nuclei has been reported on some surfaces, such as endothelium in capillaries and skin epithelia (Blatteau et al. 2006). Gas bubbles may also be formed spontaneously in regions of tissue of very low interfacial tension, where they are produced during homogenous nucleation, in which inclusions of vapor grow to form a bubble under the mechanical influence of an acoustic wave (Church 2002). The behavior of pre-existing gas nuclei during exposure to an acoustic field is not completely understood but depends on viscosity and cell density (Apfel and Holland 1991). Thus, in cancer tissue as well as other solid tissues, the understanding of the underlying mechanisms by which acoustic cavitation occurs is still incomplete. For induction of drug release from liposomes to take place, the liposomes must be degraded or made permeable by events that destabilize their phospholipid layer. Whether this permeabilization is caused by acoustic cavitation or by other mechanical effects is not clear.

Increased amounts of doxorubicin in the ECM after insonation could also be due to enhanced liposome extravasation. In particular, US is reported to reduce the high IFP found in tumors (Watson et al. 2012) and may therefore increase the transcapillary pressure gradient and increase extravasation. However, when US was given 24 hours after liposome administration, only approximately 10 % of the liposomes were still in circulation (Cyril Lafon, personal communication). Thus, US-enhanced extravasation does not have any major effect on the improved uptake of doxorubicin. This notion was confirmed by whole animal optical imaging, as no difference in liposome uptake (DiR fluorescence) between insonated tumors and controls was observed.

Confocal laser scanning images revealed that doxorubicin was taken up by the cells and was not present extracellularly. This result is in accordance with our previous study in which the *in vitro* cellular uptake of DEPC liposomes and doxorubicin was measured after 300 kHz US. In this study, ultrasound caused extracellular liposomal release of doxorubicin and the liposomes were not internalized by the cells (Afadzi et al. 2013)

Improved Distribution of Liposomes and Doxorubicin in Tumor Tissue

The 1 MHz US exposure was more effective than the 300 kHz US exposure with respect to improving the distribution of both the liposomes and the released drug throughout the prostate tumor tissue. Several mechanisms may be involved in the transport process of drugs and particles through the ECM, and among these are acoustic radiation forces and acoustic streaming. In a liquid system, acoustic streaming may occur from the transfer of momentum

from the US beam to the fluid (Starritt et al. 1989). In less liquid systems, such as solid tissue, the transfer of momentum is classified as an acoustic radiation force. The transfer of momentum from the US beam to a particle may cause translation of the particle in the direction of the propagated sound beam. US-mediated radiation forces in tissue are proportional to the absorption coefficient of the tissue and increase with increasing US frequency. The radiation force created during the 1 MHz exposure is most likely an important contributor to the improved distribution of liposomes and doxorubicin, whereas at the lower 300 kHz frequency, the radiation force will be less pronounced.

The induction of hyperthermia increases blood flow and capillary permeability (Kong and Dewhirst 1999), and thus, the supply of fluids from the vasculature under this condition may contribute to the observed displacement of liposomes and released drug. However, no temperature increase was detected during the US exposure. In fact, a reduction of temperature was measured after the 300 kHz exposure. The water inside the exposure chamber remained at room temperature, which may have caused cooling of the tumor and the surrounding tissue. Any potential thermal effects of the US exposure would then be counteracted by cooling from the environment, and thus, hyperthermia can be excluded as a mechanism for the improved penetration of liposomes and doxorubicin.

The improved distribution may also be due to increase in the space available between the cells due to the US-induced apoptosis of cancer cells. Zhang and coworkers (2012) studied the induction of apoptosis in glioma cells exposed to US in the presence of gas bubbles and demonstrated alterations in the regulation of apoptosis-related proteins. A study on pancreatic cells exposed to different US parameters showed that apoptosis increased during the first hours after US exposure at 1.5 MHz and peaked at 24 h (Guo et al. 2012). Apoptotic cells shrink in size thereby causing a remodeling of the ECM, increasing the amount of space in the ECM and facilitating the transport of drugs and particles to target cells. This effect has also been reported in tumors given liposomes and exposed to ionizing radiation (Davies et al. 2004). Whether apoptosis occurs in all cancer cell types exposed to US and whether US-mediated apoptosis is a major contributor to improved chemotherapy have not been sufficiently explored.

A tumor in a living system is a 3-dimensional structure, and it is possible that some of the measured areas of DiD fluorescence or doxorubicin fluorescence did not originate from the blood vessels from which the measurements were performed. Similarly, drugs or particles could be displaced in another direction than the 2-dimensional sections of the tumors. Thus, this analysis is considered to be semi-qualitative, but because the same finding was present in

all exposed tumors, we postulate that a displacement of particles and released drugs actually occurs as a result of US exposure.

The enhanced release of doxorubicin from sonosensitive liposomes is consistent with another study that reports enhanced doxorubicin fluorescence from micelles after US exposure (Staples et al. 2010). However, in that study, US was given immediately after the administration of micelles and the increased level of doxorubicin in the tissue, which was measured spectroscopically, can also be attributed to enhanced extravasation. To our knowledge, our work is the first microscopic study of the effect of US exposure on the release of doxorubicin from liposomes and on the microdistribution and penetration of liposomes and doxorubicin through the ECM.

Biodistribution of Liposomes

Liposomes labeled with the infrared dye DiR was imaged in live mice. As expected, the uptake was higher in normal tissue, such as liver, spleen and kidneys, than in tumor tissue due to the mononuclear phagocyte system (MPS, also referred to as the reticulo-endothelial system) (Gabizon et al. 2003). The exposure of tumors to 300 kHz US took place 24 h after the administration of liposomes. No difference was observed in the accumulation of the liposomes in the exposed and non-exposed tumors, most likely because only a fraction of the liposomes remained in the circulation at the time of US exposure.

Conclusions

In this study, we demonstrated that the exposure of prostate tumor xenografts to US 24 hours after i.v. administration of PEGylated DEPC-based liposomes caused an increase in the release and tumor cell uptake of the liposomal drug. Both the 1 MHz and 300 kHz exposures caused a significant increase in the presence of free doxorubicin. US did not increase the extravasation of liposomes, most likely because only a minor fraction of the liposomes were in circulation at the time of the US exposure. Thus, the increased amount of doxorubicin appears to originate from liposomes that passively accumulated in the tumor tissue and were already present in the ECM at the time of the US exposure. The liposomes used have improved sonosensitivity compared to traditional liposomes; however, the mechanism of drug release is not fully understood. Whether acoustic cavitation is involved in the release process in tissue is not clear, although it has been shown to be an important mechanism *in vitro*. Another observation from this study is that the 1 MHz exposure caused an improved distribution of both liposomes and released doxorubicin throughout the tumor tissue, i.e., the

liposomes and released doxorubicin penetrated further away from the blood vessels. Because this improvement was present mainly in the 1 MHz-exposed tumors and not to the same extent in the 300 kHz-exposed tumors, we postulate that the generation of acoustic radiation forces caused a displacement of particles and drugs in the ECM. Our results demonstrate that the delivery of encapsulated drugs combined with US is highly relevant for clinical implementation.

Acknowledgements

The authors would like to thank Sibylla Røgnvaldsson for preparing the liposomes, Astrid Bjørkøy for developing and modifying the Matlab function, Madelene Ericsson for preparing the frozen sections and Kristin Sæterbø for technical assistance. This work was funded by the Norwegian Cancer Society and the Norwegian Research School in Medical Imaging.

References

Afadzi, M., Davies C. D., Hansen, Y. H., Johansen, T., Standal, O. K., Hansen, R., Masoy, S. E., Nilssen, E. A. & Angelsen, B. Effect of ultrasound parameters on the release of liposomal calcein. Ultrasound Med Biol 2012;38:476-86.

Afadzi, M., Strand, S. P., Nilssen, E. A., Masoy, S. E., Johansen, T. F., Angelsen, B & Davies C. D. Mechanisms of the intracellular delivery of liposomes and dextrans. UFFC (in press)

Allen, T. M. Liposomes. Opportunities in drug delivery. Drugs 1997;54Suppl 4:8-14.

Apfel, R. E. & Holland, C. K. Gauging the likelihood of cavitation from short-pulse, low-duty cycle diagnostic ultrasound. Ultrasound Med Biol 1991;17:179-85.

Bae, Y. H. Drug targeting and tumor heterogeneity. J Control Release 2009;133:2-3.

Blatteau, J. E., Souraud, J. B., Gempp, E. & Boussuges, A. Gas nuclei, their origin, and their role in bubble formation. Aviat Space Environ Med 2006;77:1068-76.

Boucher, Y., Baxter, L. T. & Jain, R. K. Interstitial pressure gradients in tissue-isolated and subcutaneous tumors: implications for therapy. Cancer Res 1990;50:4478-84.

Boucher, Y., Leunig, M. & Jain, R. K. Tumor angiogenesis and interstitial hypertension. Cancer Res 1996;56:4264-6.

Church, C. C. Spontaneous homogeneous nucleation, inertial cavitation and the safety of diagnostic ultrasound. Ultrasound Med Biol 2002;28:1349-64.

Davies C. D., Lundstrom, L. M., Frengen, J., Eikenes, L., Bruland, S. O., Kaalhus, O., Hjelstuen, M. H. & Brekken, C. Radiation improves the distribution and uptake of liposomal doxorubicin (caelyx) in human osteosarcoma xenografts. Cancer Res 2004;64:547-53.

Deckers, R., Rome, C. & Moonen, C. T. The role of ultrasound and magnetic resonance in local drug delivery. J Magn Reson Imaging 2008;27:400-9.

Eikenes, L., Bruland, O. S., Brekken, C. & Davies C. D. Collagenase increases the transcapillary pressure gradient and improves the uptake and distribution of monoclonal antibodies in human osteosarcoma xenografts. Cancer Res 2004;64:4768-73.

Evjen, T. J., Nilssen, E. A., Rognvaldsson, S., Brandl, M. & Fosseheim, S. L. Distearoylphosphatidylethanolamine-based liposomes for ultrasound-mediated drug delivery. Eur J Pharm Biopharm 2010;75:327-33.

Evjen, T. J., Nilsssen, E. A., Barnert, S., Schubert, R., Brandl, M. & Fosheim, S. L. Ultrasound-mediated destabilization and drug release from liposomes comprising dioleoylphosphatidylethanolamine. Eur J Pharm Sci 2011a;42:380-6.

Evjen, T. J., Nilssen, E. A., Fowler, R. A., Rognvaldsson, S., Brandl, M. & Fossheim, S. L. Lipid membrane composition influences drug release from dioleoylphosphatidylethanolamine-based liposomes on exposure to ultrasound. Int J Pharm 2011b;406:114-6.

Fang, J., Nakamura, H. & Maeda, H. The EPR effect: Unique features of tumor blood vessels for drug delivery, factors involved, and limitations and augmentation of the effect. Adv Drug Deliv Rev 2011;63:136-51.

Frenkel, V. Ultrasound mediated delivery of drugs and genes to solid tumors. Adv Drug Deliv Rev 2008;60:1193-208.

Gabizon, A., Shmeeda, H. & Barenholz, Y. Pharmacokinetics of pegylated liposomal Doxorubicin: review of animal and human studies. Clin Pharmacokinet 2003;42:419-36.

Guo, Q., Jiang, L. X. & Hu, B. Focused ultrasound induces apoptosis in pancreatic cancer cells. Chin Med J (Engl) 2012;125:2089-93.

Hagtvet, E., Evjen, T. J., Olsen, D. R., Fosseheim, S. L. & Nilssen, E. A. Ultrasound enhanced antitumor activity of liposomal doxorubicin in mice. J Drug Target 2011;19:701-8.

Husseini, G. A. & Pitt, W. G. Micelles and nanoparticles for ultrasonic drug and gene delivery. Adv Drug Deliv Rev 2008a;60:1137-52.

Husseini, G. A. & Pitt, W. G. The use of ultrasound and micelles in cancer treatment. J Nanosci Nanotechnol 2008b;8:2205-15.

Immordino, M. L., Dosio, F. & Cattel, L. Stealth liposomes: review of the basic science, rationale, and clinical applications, existing and potential. Int J Nanomedicine 2006;1:297-315.

Iyer, A. K., Khaled, G., Fang, J. & Maeda, H. Exploiting the enhanced permeability and retention effect for tumor targeting. Drug Discov Today 2006;11:812-8.

Kong, G. & Dewhirst, M. W. Hyperthermia and liposomes. Int J Hyperthermia 1999;15:345-70.

Kost, J. & Langer, R. Responsive polymeric delivery systems. Adv Drug Deliv Rev 2001;46:125-48.

Lin, C. Y., Huang, Y. L., Li, J. R., Chang, F. H. & Lin, W. L. Effects of focused ultrasound and microbubbles on the vascular permeability of nanoparticles delivered into mouse tumors. Ultrasound Med Biol 2010;36:1460-9.

Liu, Y., Miyoshi, H. & Nakamura, M. Encapsulated ultrasound microbubbles: therapeutic application in drug/gene delivery. J Control Release 2006;114:89-99.

Lu, W. L., Qi, X. R., Zhang, Q., Li, R. Y., Wang, G. L., Zhang, R. J. & Wei, S. L. A pegylated liposomal platform: pharmacokinetics, pharmacodynamics, and toxicity in mice using doxorubicin as a model drug. J Pharmacol Sci 2004;95:381-9.

Maeda, H., Wu, J., Sawa, T., Matsumura, Y. & Hori, K. Tumor vascular permeability and the EPR effect in macromolecular therapeutics: a review. J Control Release 2000;65:271-84.

McNamara, W. B., Y.T., D. & K.S., S. Sonoluminescence temperatures during multi-bubble cavitation. Nature 1999;401:772-775.

Myhr, G. & Moan, J. Synergistic and tumour selective effects of chemotherapy and ultrasound treatment. Cancer Lett 2006;232:206-13.

Nicklas, W., Baneux, P., Boot, R., Decelle, T., Deeny, A. A., Fumanelli, M. & Illgen-Wilcke, B. Recommendations for the health monitoring of rodent and rabbit colonies in breeding and experimental units. Lab Anim 2002;36:20-42.

O'Neill, B. E. & Li, K. C. Augmentation of targeted delivery with pulsed high intensity focused ultrasound. Int J Hyperthermia 2008;24:506-20.

Pitt, W. G., Husseini, G. A. & Staples, B. J. Ultrasonic drug delivery--a general review. Expert Opin Drug Deliv 2004;1:37-56.

Pitt, W. G., Husseini, G. A., Roeder, B. L., Dickinson, D. J., Warden, D. R., Hartley, J. M. & Jones, P. W. Preliminary results of combining low frequency low intensity ultrasound and liposomal drug delivery to treat tumors in rats. J Nanosci Nanotechnol 2011;11:1866-70.

Rapoport, N., Pitt, W. G., Sun, H. & Nelson, J. L. Drug delivery in polymeric micelles: from in vitro to in vivo. J Control Release 2003;91:85-95.

Schroeder, A., Avnir, Y., Weisman, S., Najajreh, Y., Gabizon, A., Talmon, Y., Kost, J. & Barenholz, Y. Controlling liposomal drug release with low frequency ultrasound: mechanism and feasibility. Langmuir 2007;23:4019-25.

Schroeder, A., Honen, R., Turjeman, K., Gabizon, A., Kost, J. & Barenholz, Y. Ultrasound triggered release of cisplatin from liposomes in murine tumors. J Control Release 2009a;137:63-8.

Schroeder, A., Kost, J. & Barenholz, Y. Ultrasound, liposomes, and drug delivery: principles for using ultrasound to control the release of drugs from liposomes. Chem Phys Lipids 2009b;162:1-16.

Staples, B. J., Pitt, W. G., Roeder, B. L., Husseini, G. A., Rajeev, D. & Schaalje, G. B. Distribution of doxorubicin in rats undergoing ultrasonic drug delivery. J Pharm Sci 2010;99:3122-31.

Starritt, H. C., Duck, F. A. & Humphrey, V. F. An experimental investigation of streaming in pulsed diagnostic ultrasound beams. Ultrasound Med Biol 1989;15:363-73.

Suzuki, R., Takizawa, T., Negishi, Y., Utoguchi, N., Sawamura, K., Tanaka, K., Namai, E., Oda, Y., Matsumura, Y. & Maruyama, K. Tumor specific ultrasound enhanced gene transfer in vivo with novel liposomal bubbles. J Control Release 2008;125:137-44.

Torchilin, V. P. Recent advances with liposomes as pharmaceutical carriers. Nat Rev Drug Discov 2005;4:145-60.

Watson, K. D., Lai, C. Y., Qin, S., Kruse, D. E., Lin, Y. C., Seo, J. W., Cardiff, R. D., Mahakian, L. M., Beegle, J., Ingham, E. S., Curry, F. R., Reed, R. K. & Ferrara, K. W. Ultrasound increases nanoparticle delivery by reducing intratumoral pressure and increasing transport in epithelial and epithelial-mesenchymal transition tumors. Cancer Res 2012;72:1485-93.

Wu, N. Z., Braun, R. D., Gaber, M. H., Lin, G. M., Ong, E. T., Shan, S., Papahadjopoulos, D. & Dewhirst, M. W. Simultaneous measurement of liposome extravasation and content release in tumors. Microcirculation 1997;4:83-101.

Zhang, Z., Chen, J., Chen, L., Yang, X., Zhong, H., Qi, X., Bi, Y. & Xu, K. Low frequency and intensity ultrasound induces apoptosis of brain glioma in rats mediated by caspase-3, Bcl-2, and survivin. Brain Res 2012;1473:25-34.

Paper IV

MULTIFUNCTIONAL PARTICLES FOR DRUG DELIVERY AND IMAGING: EFFECT OF PEGYLATION, SURFACTANT, SIZE AND ULTRASOUND EXPOSURE ON CELLULAR UPTAKE

Multifunctional particles for drug delivery and imaging: Effect of PEGylation, surfactant, size and ultrasound exposure on cellular uptake

Mercy Afadzi[1], Yrr Mørch[1,3], Per Stenstad[3], Rune Hansen[2,4], Bjørn Angelsen[2], Catharina de Lange Davies[1]

[1] Dept. of Physics, [2]Dept. of Circulation and Medical Imaging, Norwegian University of Science and Technology, [3] SINTEF Materials and Chemistry, [4] SINTEF Technology and Society. Trondheim, Norway.

Corresponding author: Mercy Afadzi, Dept. of Physics, Høgskoleringen 5, The Norwegian University of Science and Technology, 7491 Trondheim, Norway.
Phone: + 47 73593466
Fax: +47 73597710
E.mail: mercy.afadzi@ntnu.no

Abstract

Understanding the interaction between cells and nanoparticles (NPs) is crucial when designing NPs for improved drug delivery since the size, shape, morphology, surface chemistry etc. might influence the cell-NPs interaction. We investigated the effect of size (109 nm - 228 nm), PEGylation and surfactant on the kinetics of internalization of poly(butyl cyanoacrylate) (PBCA) NPs in prostate cancer cells. Secondly, we studied whether low frequency ultrasound (300 kHz) enhanced the uptake of the NPs in the presence and absence of air filled microbubbles (MBs) stabilized by PBCA NPs. PBCA NPs were prepared from miniemulsion polymerization and coated with polyethylene gylocol (PEG) in a single step. The NPs were then used to stabilize MBs forming a NPs shell around the MBs. Five NPs with three different types of PEG ("Long Jeffamine", "Short Jeffamine" and Tween80 (Polysorbate 80)) and surfactants (sodium dodecyl sulphate (SDS), Aerosol OT and Tween80) were used in this study. Cellular uptake was studied using flow cytometry xand confocal laser scanning microscope (CLSM). The cytotoxic effect of the NPs was measured using Alamar blue reagent with fluorescence–based method. Cellular uptake was affected by the type/length of PEG molecules on the NP surface and the surfactant used for emulsification with little effect on particle size. Thus, Jeffamine NPs were more efficient for cellular uptake than Tween80 NP. Also, cellular uptake of particles PEGylated with long Jeffamine was higher than particles with short Jeffamine PEG. NPs with SDS showed higher cellular uptake than NPs with AOT or Tween80. Internalization of nanoparticles was confirmed by CLSM, where nanoparticles were found mainly in the cytoplasm of cells with hardly any particle in the nucleus. PBCA NPs exhibited dose-response toxicity on PC3 cell line and toxicity was dependent on the surfactant used where Tween80 was less toxic than AOT and SDS. Ultrasound had no significant effect on cellular uptake of PBCA NPs in the presence and absence of NP-loaded MBs.

Keywords: PBCA nanoparticles, PEGylation, Multifunctional particles, ultrasound, cellular uptake

I. INTRODUCTION

The enhanced permeability and retention (EPR) effect increases the accumulation of nanoparticles (NPs) in tumor tissue because of the hyperpermeable capillaries [1, 2]. Thus, encapsulation of cytotoxic drugs reduces the toxic effect of healthy tissue. However, the distribution and cellular uptake of the NPs in tumor tissue are heterogeneous due to the distorted nature of the tumor blood vessels [1, 3], and the enhanced interstitial fluid pressure in tumors [4, 5]. Successful therapeutic response depends on the ability of the cytotoxic drug to reach the cancer cells and irradiate them. This calls for new strategies to overcome the delivery barriers. Such strategies may include; chemical treatment of tumor with enzymes [5, 6] or physical treatment with radiation [7] or ultrasound treatment [8-10].

Ultrasound exposure may improve delivery of NPs both through thermal and mechanical mechanisms depending on the frequency and acoustic pressures applied. High intensity focused ultrasound (HIFU) increases the temperature in the tissue and induces radiation forces [11], whereas lower frequency ultrasound can cause cavitation, *i.e.*, the formation and oscillation of gas bubbles [12-15]. Cavitation can be stable (oscillations with stable radius) or transient (inertial) depending on the amplitude of the ultrasound. Cavitation is reported to produce shear stresses and acoustic streaming, and inertial cavitation also forms jet streams which may form pore in the capillary wall as well as in the NPs and plasma membrane of cells, a process called sonoporation [12, 15]. Thus, cavitation may improve the transcapillary flux of NPs, as well as the release of drugs from the NPs and the cellular uptake. NPs integrated with gas microbubbles (MB) may therefore be used both for improving the delivery of NPs and the encapsulated drug, and for contrast enhanced ultrasound imaging. Such multifunctional particles may be applied both in ultrasound imaging for diagnosis and image-guided delivery of nanoparticles in cancer therapy.

Several approaches for designing multifunctional MBs have been suggested [16-21], such as loading therapeutic drugs in the shell of the MB [16, 22-24] or attaching NPs directly to microbubbles (NP-loaded MBs) [18, 19]. The shell may be based on phospholipids or polymers. Polymer shell MB is said to be more stable, than those with lipid shell and they also have an advantage of having longer circulation time and higher ligand density for efficient targeting to cells [20, 22]. Furthermore, higher amount of cytotoxic drugs can be encapsulated into the shell of polymeric MB than into lipid shell MB [22, 25]. However, the loading capacity of drugs into the shell of MBs is generally limited by the thickness of the MB, and there is a need to increase the drug payload for each MB. This can be done by using NPs containing drugs to stabilize the MB rather than a shell of polymer, as the NPs have a larger volume. The NP stabilizing and surrounding the MBs can also contain contrast agents for MRI or fluorescent probes for optical imaging which provide imaging of multiple modalities with additional spatial, temporal and depth resolution for improvement in the accuracy of disease diagnosis and local treatment of diseases [21]. Furthermore, it has been shown theoretically and experimentally that NP-loaded MB increases the contrast in ultrasound imaging due to the enhanced asymmetric bubble oscillations even at low excitation amplitudes [19-21, 26]. This is because close packing of the nanoparticles restricts bubble compression. Disruption of the MB can be done controllably to release the NPs at the targeted site under ultrasound image guidance. This may also minimize the destructive effect on nearby healthy cells caused by the acoustic cavitation while maintaining the uptake of NPs in the cells. The reason is that, the presence of NPs around the bubbles will increase the stiffness and attenuation compared with MBs without NPs [20]. Hence, with adequate amount of NPs, NP-loaded MB might reduce cell death whilst improving delivery efficiency.

The present work focuses on a newly developed multifunctional drug delivery system (manuscript in preparation), in this case the MBs are stabilized by NPs, *i.e.*, the shell only consist of NPs. The NPs stabilizing the MBs are made of a biocompatible and biodegradable [20, 27] synthetic polymer poly(butyl cyanoacrylate) (PBCA). PBCA NPs were prepared from miniemulsion polymerization and coated with polyethylene gylocol (PEG) in a single step. The NPs were then used to stabilize MBs forming a NPs shell around the MBs. A prerequisite for successful cancer therapy is that the cytotoxic drug is taken up by the cancer cells. Thus, we investigated first the effect of size, surfactant and PEGylation on the kinetics of internalization of the NP in prostate cancer cells. Secondly, we studied whether low frequency ultrasound (300 kHz) enhanced the uptake of the NPs alone and when integrated with the MB. The cellular uptake was studied using flow cytometry (FCM) and confocal laser scanning microscopy (CLSM) was used to confirm the distribution of the NPs in the cells. The cytotoxic effect of the NPs was measured using the Alamar blue reagent fluorescence assay.

II. MATERIALS AND METHODS

Materials

n-Butyl cyanoacrylate was supplied by Henkel Loctite (Dublin, Ireland). Jeffamine M-2070 (linear, with approx. 31 r.u.units of EO, polyether monoamine, PO/EO ratio 10/31, MW 2000, "long Jeffamine") and Jeffamine M-1000 (linear, with approx. 19 r.u.units of EO, polyether monoamine, PO/EO ratio 3/19, MW 1000, "short Jeffamine") was supplied by Huntsman (Antwerp, Belgium). Tween80 (Polysorbate 80; short branched with approximately 20 repeating units of ethylene oxide) supplied by Sigma-Aldrich.

Preparation of PEGylated PBCA NPs

Polymeric particles of various size and surface functionalities were prepared in one step using miniemulsion polymerization in acidic media. PEG was used both to functionalize the particle surface and as initiator of the polymerization. EGDMA (Ethylene glycol dimethacrylate, Fluka) was used to crosslink the polymer for increased stability. V65 (Azobisdimetyl valeronitril, Wako Chemicals) was used as initiator for the crosslinking reaction. To vary the surface functionalities of NPs, three different types of PEG were used: "Long Jeffamine", "Short Jeffamine" and Tween80. An oil-in-water emulsion was made by emulsifying the monomer phase consisting of 6g n-butyl cyanoacrylate, 0.39g EGDMA, 50mg V65, 120mg hexadecane and 2mg of the fluorescent dye Nile Red (Technical grade, Fluka) in an acidic solution containing surfactant.

The surfactant used for particles coated with Jeffamine-PEG was 0.1g SDS (sodium dodecyl sulphate, Merck) or 0.2g Aerosol OT (sodium dioctyl sulfosuccinate, AOT, Sigma) dissolved in 24 ml 0.1M HCl (pH 2). For particles coated with Tween80-PEG, 4.6g of Tween80 was dissolved in 60 ml water, adjusted to pH 2 with HCl, and used both as surfactant and PEG. The oil-in-water emulsion was sonicated for 3 min (9 x 20 sec intervals) on ice (Branson digital sonifier 450 CE). The particle size was varied by varying the amplitude of the power supply output voltage. For particles coated with Jeffamine PEG, 3.5g (short Jeffamine) or 7g (long Jeffamine) in 35 ml water (pH 6) was added immediately after emulsification to initiate the polymerization. The emulsion droplets were polymerized at 25°C over night under continuous stirring, the pH neutralized and crosslinking of the polymer initiated by increasing the temperature to 50°C for 8 hrs. The particles were thoroughly dialyzed against distilled water (8-9 shifts) using Spectra/Por MWCO 12-14000 kDa dialysis membrane to remove excess PEG and surfactant. Five different types of particles were made for the present work

and they were named based on the type of PEG, surfactant and the size of the particles. Thus; LoPEG/SDS/small (Long Jeffamine PEG and SDS with small NP size), LoPEG/SDS/large (Long Jeffamine PEG and SDS with large NP size), LoPEG/AOT (Long Jeffamine PEG and AOT), ShPEG/SDS (Short Jeffamine PEG and SDS) and Tween (Tween PEG and surfactant).

Preparation of microbubbles stabilized with NPs

Air-filled MBs stabilized by NPs were prepared by mixing the NP dispersion with bovine serum albumin (BSA) to a final concentration of 1% (w/v) PBCA NP and 1% (w/v) BSA and adjusting the pH to 7.4. Stable MBs were formed using ultra turrax (IKA-Werke T25) at 20,000 1/min for 2 min.

Physicochemical characterization of PBCA NPs and NP-loaded microbubbles

The particle size and zeta potential was determined using a Malvern Nano Series zetasizer. The final concentration of the particles was determined by dry weight. The morphology of the particles was studied with S(T)EM (Hitachi S-5500). The particles were air-dried directly on a sample holder at ambient temperature and sputtered with a 5 nm Au layer for enhanced surface conductivity. The particles were analyzed at 5-30 kV. The size and morphology of MBs was studied using an optical microscope (Carl Zeiss, Axioskop 20) connected to a CCD camera. ImageJ (version 1.44p) was used for determination of average MBs diameter (average of approximately 1,000 MBs, threshold: IsoData, circularity: 0.6-1.0). Confocal Laser Scanning Microscope (CLSM, Carl Zeiss LSM510 Meta) was used to verify that NPs loaded with Nile red were located on the bubble surface. The 514 nm Argon laser line was used to excite Nile red.

Cell culturing

The PC3 cell line (human prostatic carcinoma cell lines) was grown in Dulbecco's Modified Eagle Medium (DMEM) supplemented with 10% fetal bovine serum (FBS) (Sigma-Aldrich), 2 mM non-essential amino acids and 1 mM L-glutamine (Sigma-Aldrich,). The cell cultures were grown at 37°C and in 5% CO_2. Exponentially growing cells were harvested with 3 ml of trypsin (0.25%) and resuspended in growth medium.

Cellular uptake of PBCA-NPs

To study the kinetics of cellular uptake of the different types of NPs (see Table 1), 60,000 cells were seeded in a 24 well plate 48 h before incubation (37^oC, 5% CO_2) with the 5 different types of NPs (20μg/ml) at increasing times up to 24 h. After each time point, the cells were washed three times with 300 μl of warm PBS to remove surface associated NPs, trypsinized (150 μl trypsin per well) and then resuspended in 1ml (per well) of cell medium for FCM. When measuring cellular uptake by FCM it is critical to remove surface bound NP, and three times washing was found to be sufficient.

Cytotoxicity of NPs using Alamar blue assay

The cytotoxicity of the NPs was investigated with Alamar blue cell viability reagent (Molecular Probes, Invitrogen). Alamar blue is a cell health indicator which uses the reducing power of living cells to quantitatively measure the proliferation of cells. Viable cells are able to convert resazurin (active ingredient of Alamar blue which is non-fluorescent) to resorufin (red compound which is highly fluorescent) continuously thereby increasing the overall fluorescence and color of the cell media. Thus, Alamar blue measures the metabolic activity of cells.

Twenty four hours before the experiment, 20,000 cells were seeded in a 96 flat bottom well plate (Corning B.V. Life Sciences) in cell medium. The cells were incubated with varying concentrations (0 – 300 μg/ml) of 4 different types of NPs for 3 h or 24 h (37^{o}C, 5% CO_2). Four to eight replicas were used for each concentration and control samples. After incubation, cells were washed 3 times with 200μl of cell medium and then incubated with 110μl (per well) of cell medium with Alamar blue (diluted 10 times) (37^{o}C, 5% CO_2) for 2 h or 4 h. The fluorescence intensity of Alamar blue was measured using a microplate reader from the bottom (Tecan Group Ltd.) and the excitation and emission wavelengths were 550±9nm and 590±20nm, respectively. . Percentage of viable cells was calculated from equation 1;

$$Cell\ viability\ (\%) = \frac{(FL_{NP} - FL_B)}{(FL_C - FL_B)} \times 100 \qquad (1)$$

Where $FL_{NP,}$ FL_c and FL_B are the fluorescence intensity of samples treated with NPs, untreated samples (control) and fluorescence intensity of the medium (blank), respectively. To investigate the cytotoxic effect of the degradation products of PBCA NPs, the particles were dialyzed with Float-A-lyzer® G2 (Spectrum Laboratories, Inc.), before incubating the cells with the NPs.

Ultrasound exposure set-up and parameters

The ultrasound exposure set-up consisted of a signal generator (Hewlett Packard 33120A, San Jose, CA, USA), an oscilloscope (Lecroy waverunner, LT262, Long Branch, NJ, USA), a power amplifier (ENI 2100L, Rochester, NY, USA), custom-made single-element ultrasound transducers (Imasonic, Besancon, France) with a frequency of 300 kHz and an insonication chamber containing a sample chamber (Fig. 1). The geometric focus, active diameter and maximum intensity of the transducer are 90 mm, 55 mm and 69 mm respectively. The –3 dB

beam width in the lateral direction at the maximum intensity was 6.6 mm. The acoustic field was characterized using a hydrophone (Onda HGL-0200, Onda Corporation, Sunnyvale, CA, USA) with a tip diameter of 200 μm connected to a 20-dB pre-amplifier (Onda AH-2020). Rectangular Plexiglas water tank with dimensions of 150 mm by 350 mm was used as insonication chamber. The inside of the chamber was coated with a regular sponge with a thickness of 10 mm in order to avoid reflections of sound waves. The Plexiglas tank was filled with deionized and partially degassed water and was kept at room temperature. The sample chamber was made from the bulb of a disposable (polyethylene) 1-ml transfer pipette (Fig.1). The pipette was attached to a rotating motor at a position equivalent to the maximum intensity of the ultrasound beam. A rotating motor was used to maintain a uniform exposure of the ultrasound to the sample and recycle bubbles through the medium.

In the absence of MPs, mechanical indices (MI) of 0–2.7 (corresponding to peak negative pressures of 0–1.5 MPa) and a duty cycle of 20 % (*i.e.*, a 100-μs pulse length and PRF of 2 kHz) were used to treat the samples. In the presence of MPs, the exposure parameter was reduced in order to avoid too high cell killing. Hence, MI of 0–1.05 (corresponding to peak negative pressures of 0–0.58 MPa) and a duty cycle of 2.5% (*i.e.*, a 33-μs pulse length and a pulse repetition frequency (PRF) of 3 kHz) were used to treat the samples.

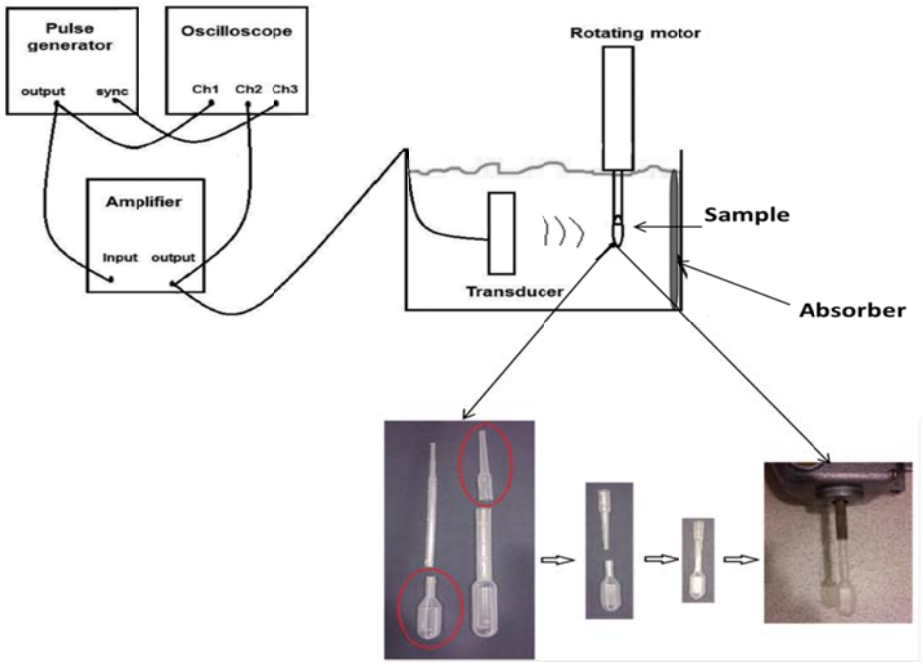

Fig. 1 A schematic diagram of the ultrasound exposure setup.

Cellular uptake of PBCA NP after ultrasound exposure

To investigate the effect of ultrasound and MBs on the cellular uptake and cell viability of the NPs, exponentially growing cells were harvested with trypsin and resuspended in growth medium. MP stabilized with LoPEG/SDS/small-NPs, ShPEG/SDS-NPs or Tween-NPs (see Table 1) were used. Just before ultrasound exposure, the sample chamber was filled with 1 or 1.5 ml of cell suspension (10^6cells/ml) and NP-loaded MBs at final concentration of approximately 4.5×10^7 bubbles/ml. When studying the effect of ultrasound on the cellular uptake of NP alone (without MB), the sample chamber was filled with 1 ml of cell suspension and 1.7µl of NPs (final concentration of 20µg/ml) and cell medium was added to a total volume of 2.5 ml. The sample chamber was then placed in the insonication chamber (Fig.1) and then the samples were exposed to the ultrasound wave for 120s or 180s in the presence or absence of MP, respectively, while the motor was rotating. Immediately after

ultrasound exposure, the samples were placed on ice and washed 3 times by spinning for 3 min at 1000 rpm before FCM.

Flow cytometetric measurements

The cellular uptake of PBCA-NPs was measured by FCM (Gallios, Beckman Coulter, Inc., Indianapolis, IN, USA). Sytox blue (Molecular Probes, Invitrogen, Grand Island, NY, USA) was used to distinguish live and dead cells. One micro liter of Sytox blue was added to 1 ml of each sample (final concentration of 1 μM) just before the flow cytometric measurements. Nile red was excited with the 488 nm laser line whereas the 405 nm laser line was used to excite Sytox blue. The fluorescence of Nile red and Sytox blue were detected in the spectral intervals of 630±30nm and 450±40nm respectively. To eliminate any spectral cross talk between the 2 dyes, cell stained with either Sytox blue or Nile red (NPs) were used. The percentage of electronic spectral compensation was determined based on these two single-labeled samples and hardly any compensation was necessary. To determine the cellular uptake of Nile red in live cells, *i.e*. Sytox blue-negative cells, a two-dimensional scatter plot of Nile red intensity versus Sytox blue intensity was used, and Nile red fluorescence was gated on Sytotox blue negative cells. The cells that exhibited a fluorescent intensity of Nile red higher than those of the unlabeled control (negative cells) were classified as positive cells.

The cellular uptake was calculated both as the percentage of fluorescent cells (positive cells) and as the amount of internalized fluorochrome, which was estimated based on the median fluorescence intensity (MFI) of the total live cell population. Relative MFI was also calculated as the ratio of MFI of cells treated with NPs and untreated cells. Data analysis was performed using Kaluza flow cytometry analysis software and SigmaPlot (Systat Software, Chicago, IL, USA).

Confocal laser scanning microscopy

Confocal laser scanning microscopy (Carl Zeiss LSM510 Meta) with a C-Apochromat 63x/1.2 water objective was used to confirm internalization of the PBCA-NPs. Thirty thousand cells were seeded in 8-well plate (ibidi GmBH, München, Germany) 48 h before the experiment. The cells were then incubated with LoPEG/SDS/small (final concentration of 20µg/ml in cell medium) for 3 h. After incubation, the cells were washed three times with 200 µl medium followed by 25 min incubation with 150µl of Hoechst 33452 (Molecular Probes, Invitrogen, Grand Island, NY, USA) (final concentration of 5µg/ml) to stain the cell nucleus. The cells were then washed twice with 200µl of cell medium before microscopy. Nile red was excited with the 543 nm laser whereas Hoechst was excited with a two–photon pulsed Ti-Sapphire laser at 800 nm. The fluorescence was detected in the spectral intervals of 548–644nm and 435–485nm, respectively. The frame size was 512 × 512. A z-stack of images through the cells was aquired to verify whether the NPs were intracellular or on the cell surface.

Mathematical fitting and statistical analysis

All the measurements were repeated 2 to 8 times, and the mean and standard deviations were calculated. Statistical analyses were conducted with Minitab software (Mintab Inc., Coventry, UK) using a one-way analysis of variance (ANOVA). A p value ≤ 0.05 was considered statistically significant. The relationship between percentage of positive cells (% Positive Cells) and incubation time was described using a first-order exponential model. The effective concentration ($EC_{50,}$ concentration where 50 % of the cells are not viable) was determined by fitting a Sigmoidal Dose Response curve (variable slope) to the data. SigmaPlot (Systat Software, IL, USA) was used for all fits. The goodness of the fit was determined by the square coefficient of correlation (R^2) and the p-value of the fit.

III. RESULTS

Characterization of PBCA –NPs and NP-loaded MBs

Physicochemical characteristics of NPs and MBs used in the present study are given in Table 1. The diameter of the NP ranged from 109 nm to 228 nm and the polydispersity index (PDI) was in most cases well below 0.2. The zeta potential was negative for all NPs. However, short -PEG NPs were less negatively charged compared to the other batches. The MBs had an average diameter of approximately 2 μm. There was no statistical difference between the sizes of the MB.

Table 1. Physicochemical characteristics of the various PBCA NPs and MBs[1].

PBCA NPs abbreviation	**PEG**	**Surfactant**	**z-average NP size (nm)**	**PDI[2]**	**ζpotential (mV)**	**Average MBs size (μm)**
Tween	Tween 80	Tween 80	119	0.27	-28	1.7±0.7
LoPEG/AOT	Long Jeffamine	AOT	228	0.13	-37	-
ShPEG/SDS-	Short Jeffamine	SDS	153	0.080	-19	2.7±1.4
LoPEG/SDS /small	Long Jeffamine	SDS	109	0.098	-32	2.4±1.4
LoPEG/SDS/ large	Long Jeffamine	SDS	172	0.089	-35	-

[1] The zetapotential of particles was measured in distilled water, pH 6. The size of MBs was measured using light microscope images and ImageJ and is given as the average diameter ± standard deviation of approximately 1,000 microbubbles. [2] Polydispersity index indicating the width of the size distribution

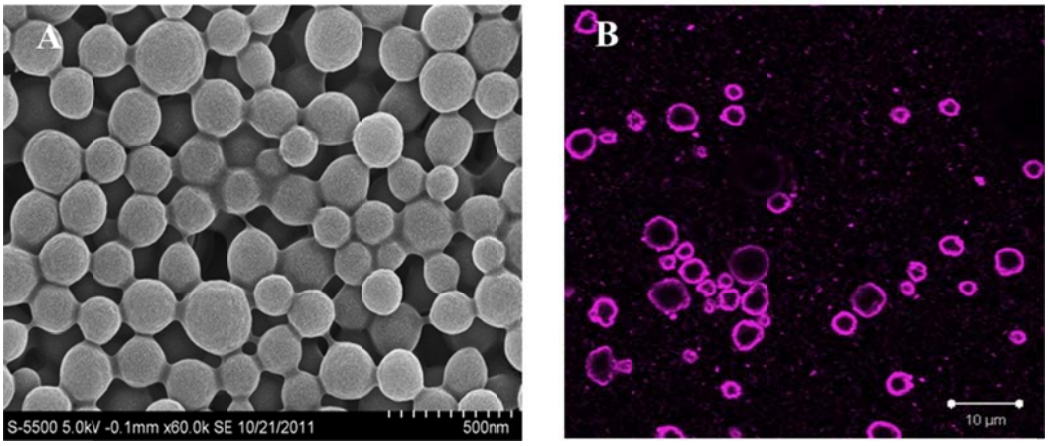

Fig 2: A: S(T)EM micrograph of densely packed PBCA nanoparticles (loPEG/SDS) and B: CLSM image of microbubbles loaded with the nanoparticles. The particles contain Nile red (purple color). The image is an optical slice of the bubble equator. Scale bar is 10 µm.

The morphology of the NPs was characterized by scanning electron microcsopy. Fig. 2A is a typical micrograph of PBCA nanopartices showing spherical shaped NP with a quite narrow size distribution. CLSM revealed a fluorescence ring of NPs surrounding the MBs (Fig. 2B) thus illustrating how the particles form a shell around the microbubbles. The sizes varied somewhat, but it should be empashized that the difference in size might also be due to the MBs being located in different planes along the optical axis.

Cellular cytotoxicity

The cytotoxic effect of the NPs was investigated by incubating PC3 cells with all four types of NPs using increasing concentrations (0, 5, 10, 20, 40, 60, 80, 100, 200 and 300 µg/ml) and the Alamar blue cell viability assay. Untreated cells were used as control cells and the percentage of viable cells were estimated using equation 1. Fluorescence intensity of Alamar blue was found to increase linearly with incubation time from 2 to 4 h; hence the percentage of cell viability was estimated after 4 h incubation with Alamar blue. The PBCA NPs exhibited a dose-response toxicity of PC3 cell line (Fig.3). Fig. 6 shows the viability after 3 h

of NP-incubation, and similar results were obtained after 24 h NP-incubation (data not shown). There was a steep decrease in viability at approximately 25 μg/ml. At concentrations of 40μg/ml and higher, the percentage of viable cells was below 20%, hence, a concentration of 20 μg/ml was chosen in further studies. The EC_{50} determined for Tween-NPs, LoPEG/AOT-NPs, ShPEG/SDS-NPs and LoPEG/SDS/small-NPs were approximately 45, 32, 29 and 26 μg/ml, respectively with R^2 value ≥ 0.9268 and $p < 0.0001$ for all fits. Hence, the toxicity was more dependent on the surfactant used than the type of PEG, Tween80 giving less toxicity than AOT and SDS. There was no significant difference between the EC_{50} values determined for these NPs before and after second dialysis, indicating that potentially harmful degradation products were not the main cause of cytotoxicity.

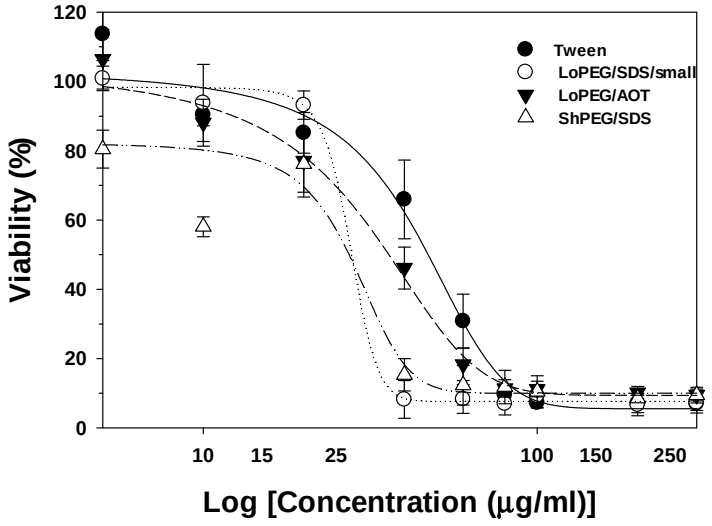

Fig 3. Percentage of viable cells as a function of NP concentration (Log). Cytotoxicity of PBCA NPs with different sizes (228 nm, 119 nm, 153 nm and 109 nm) for Tween (●), LoPEG/SDS/small (○), LoPEG/AOT (▼) and ShPEG/SDS (Δ) respectively), PEG (Jeffamine (LoPEG/AOT, ShPEG/SDS and LoPEG/SDS/small) and Tween-80 (Tween)) and surfactant (SDS (ShPEG/SDS and LoPEG/SDS/small)), AOT (LoPEG/AOT) and Tween-80 (Tween)). The data points are the mean of 4 to 8 measurements with standard deviation. The R^2 value ≥ 0.9268 and $p < 0.0001$ for all fits.

The results obtained by the Almar blue assay was supported by the morphological changes observed by the phase contrast light microscope. For all the four types of NPs, there were

extensive morphological changes in cells exposed to concentrations of 40μg/ml and higher. The cells were rounded but remained attached after 3 times rinsing.

Cellular uptake of NP

The ability of the various PBCA NPs to be internalized by endocytosis was compared. The optimal concentration of NPs showing high cellular uptake and low toxicity was first determined, and 20μg/ml was used. The kinetics of cellular uptake was determined by incubating the cells with NPs for increasing time up to 24 h. The uptake depended on the surface chemistry at all time points (Fig. 4). The percentage of positive cells as a function of incubation time demonstrated an initial steep slope before reaching a maximum value (Fig. 4A). There was no statistical difference between the cellular uptake of LoPEG/AOT-NPs (size of 228 nm) and Tween (size of 119 nm) at all incubation time points. Instantaneous addition and removal of NPs followed by three times washing led to about 6, 7, 10 and 21% of the cells being Nile red positive for Tween-NP, LoPEG/AOT-NP, ShPEG/SDS-NP and LoPEG/SDS/small-NPs respectively. Thus, the percentage of cells with surface bonded particles was dependent on the type of PEG and surfactant, Jeffamine PEG with SDS giving the highest.

All NPs reached half of their maximum cellular uptake values within less than 30 min. The percentage of cells internalizing LoPEG/SDS/small-NPs or ShPEG/SDS-NPs reached a maximum value (97 % and 66 % respectively) after 30 min of incubation, whereas those internalizing Tween-NPs or LoPEG/AOT-NPs reached a maximum value (45% and 53% respectively) after 2 h incubation. However, for all NPs, the amount of NPs that was internalized by the cells (*i.e.*, relative MFI) reached a maximum after 30 min of incubation (Fig. 4B) and the highest relative MFI was obtained by the LoPEG/SDS/small-NPs. The rate

constant determined by fitting a first-order kinetic curve to the experimental data of % positive cells was found to be 2.1 h^{-1}, 2.3 h^{-1}, 11. 9 h^{-1} and 66.4 h^{-1} for LoPEG/AOT-NPs, Tween-NPs, ShPEG/SDS-NPs and LoPEG/SDS/small-NPs respectively. The R^2 value ≥ 0.7868 and $p < 0.0001$ was obtained for all fits.

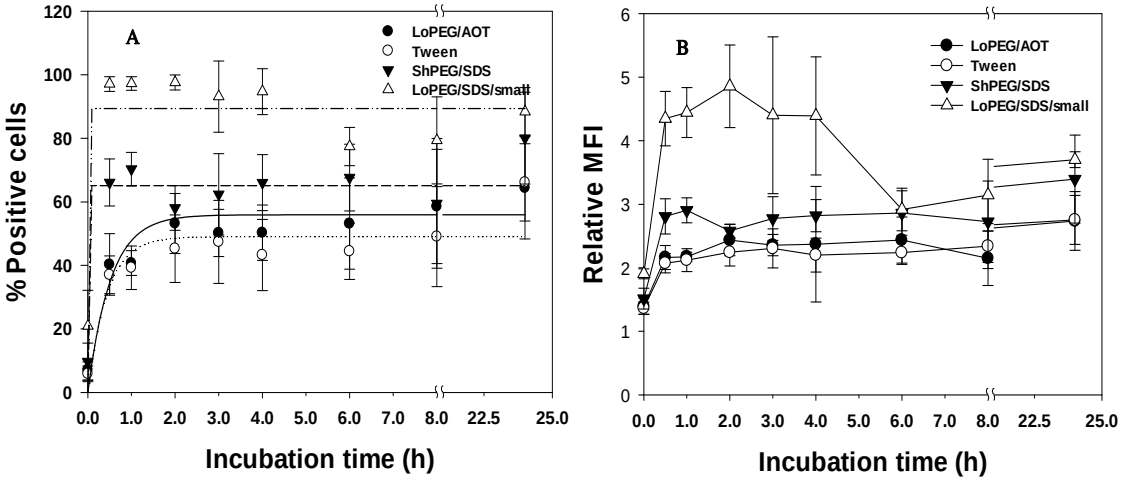

Fig. 4 Flow cytometric analysis of cells incubated with PBCA NPs with different sizes (228nm (LoPEG/AOT), 153-nm (ShPEG/SDS), 119-nm (Tween) and 109-nm (LoPEG/SDS/small)), PEG (Jeffamine (LoPEG/AOT, ShPEG/SDS and LoPEG/SDS/small) and Tween-80 (Tween)) and surfactant (SDS (ShPEG/SDS and LoPEG/SDS/small)), AOT (LoPEG/AOT) and Tween-80 (Tween)). (A) Percentage of nile red positive cells as a function of incubation time and (B) relative median fluorescence intensity (MFI) of the total live cell population. The data points are the means of 3 to 6 measurements with standard deviation. The R2 value ≥ 0.7868 for all fits.

To investigate the effect of size we included a NP with the same surface properties as LoPEG/SDS/small, *i.e*, SDS and long PEG but with larger diameter 172 nm (*i.e*., LoPEG/SDS/large). Cellular uptake was the same for the two NPs. Thus, surfactant and PEGylation seemed to be more important for the cellular uptake than NP size in the size range used here (Fig. 5). NPs with SDS showed higher cellular uptake than NPs with AOT or Tween 80 (Fig. 5). NP PEGylated with long Jeffamine demonstrated a higher cellular uptake

than NP with short Jeffamine (Fig. 5), and the linear Jeffamine PEG showed higher cellular uptake than the branched Tween80 PEG.

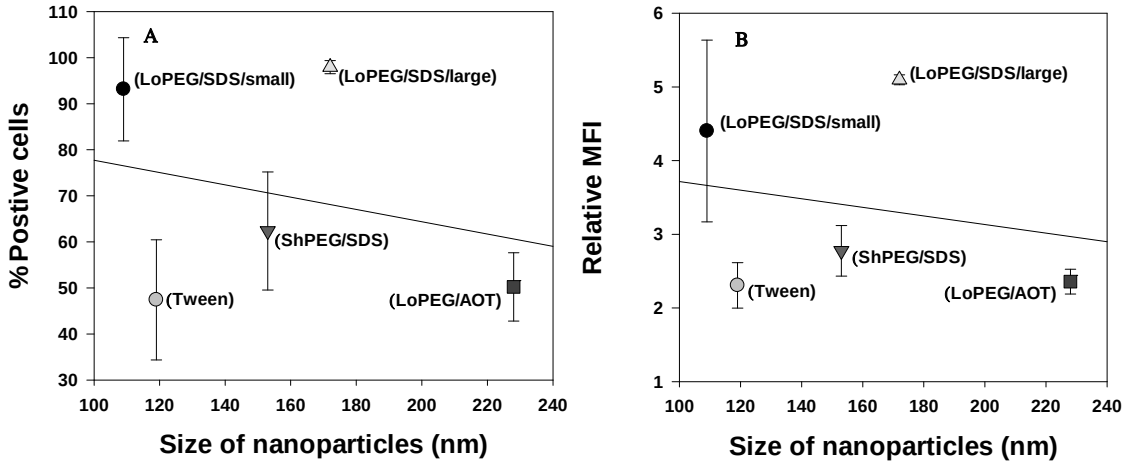

Fig. 5 Flow cytometric analysis of cells incubated (3 h) with PBCA NPs with different sizes (228 nm (LoPEG/AOT), LoPEG/SDS/large (172 nm), 153 nm (ShPEG/SDS), 119 nm (Tween) and 109 nm (LoPEG/SDS/small)), PEG (Jeffamine (LoPEG/AOT, ShPEG/SDS and LoPEG/SDS/small) and Tween 80 (Tween)) and surfactant (SDS (ShPEG/SDS and LoPEG/SDS/small)), AOT (LoPEG/AOT) and Tween 80 (Tween)). (A) Percentage of nile red positive cells for all NP types and (B) relative median fluorescence intensity (MFI) of the total live cell population. The data points are the means of 3 to 6 measurements with standard deviation. Asterisk indicates a significant increase (* $p < 0.001$).

Cellular uptake of PBCA NPs was confirmed using CLSM. PC3 cells were incubated with 20µg/ml of LoPEG/SDS/small-NPs for 3 h, washed three times and then incubated with Hoechst for 25 min to stain the nucleus. NPs were mainly found in the cytoplasm of all cells with hardly anything in the cell nuclei (Fig. 6). In some cells the NP seemed to be clustered, and this might be NP localized in endosomes or other vesicles.

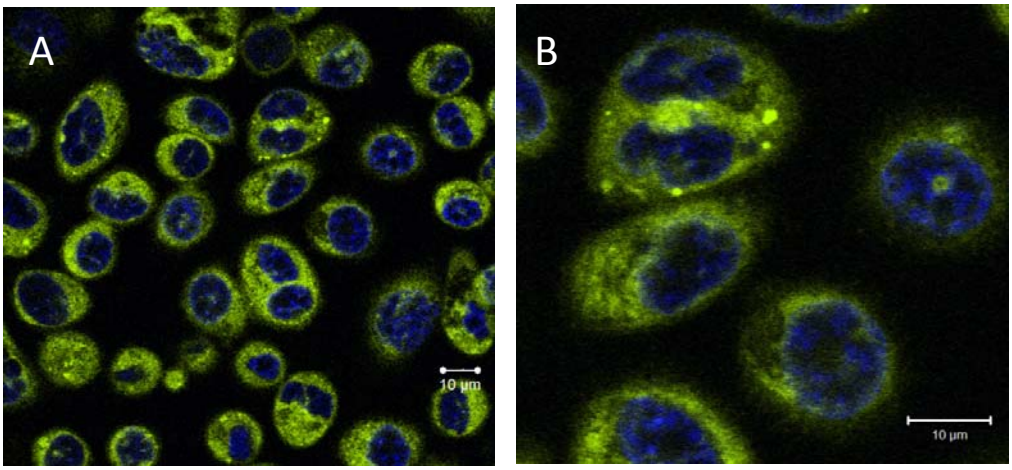

Fig. 6 Confocal images of PC3 cells incubated with LoPEG/SDS/small-NPs for 3 h. Image (A) shows the cellular uptake of Hoechst (blue) and Nile red (green) and image (B) is the zoomed version of image (A).

Cellular uptake of NP after ultrasound exposure

The effect of ultrasound alone and ultrasound plus NP-loaded MBs on cellular uptake of NPs was investigated using PC3 cells. Sham samples were treated with NPs or NP-loaded MBs but not with ultrasound. In general, ultrasound exposure at 300 kHz did not increase the uptake of the PBCA NP in live cells, neither NP given alone nor NP surrounding MB (Fig 7 A, B). Ultrasound exposure alone did not enhance the cellular uptake of NPs even when using higher ultrasound exposures than used in the presence of MBs. Ultrasound in combination with NP-loaded MBs (ShPEG/SDS-NPs or LoPEG/SDS/small-NPs) had no significant effect on cellular uptake in live cells with increase in MI up to 1.05 (Fig 7A and B). When MBs made with Tween-NPs were combined with ultrasound, cellular uptake in the live cell population increased from approximately 4 % to 20 % (Fig 8A) with increasing MI (0 to 1.05). Despite the increase in percent positive cells, there was no statistical difference between the relative MFI of ultrasound treated and untreated samples (Fig. 8B). Thus, there

was no difference in the amount of NPs in cells treated with ultrasound compared with those not treated with ultrasound.

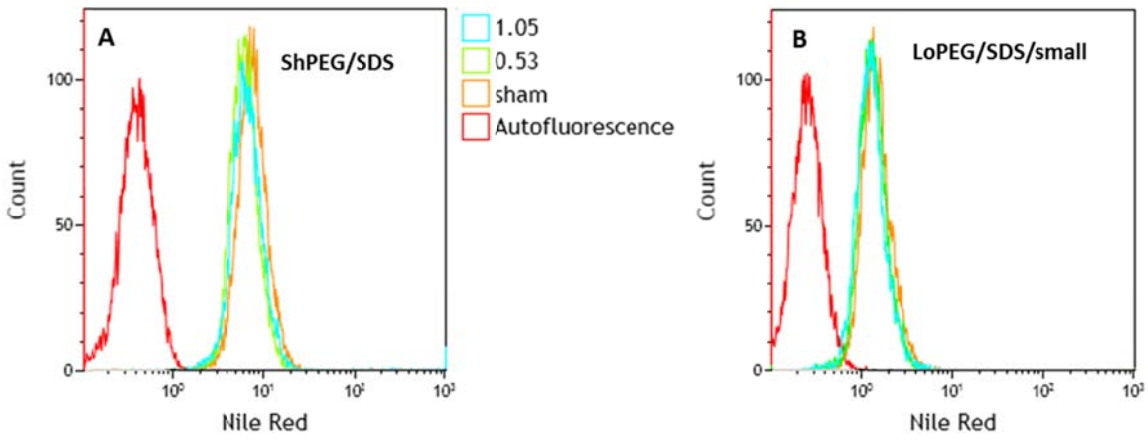

Fig. 7 The flow cytometric analysis of the cellular content of ShPEG/SDS and LoPEG/SDS/small PBCA NPs treated with different MI. (A) Cellular uptake of ShPEG/SDS NPs in live cells population. The cells were exposed to ultrasound and MB-loaded NPs with a pulse duration of 100 μs, 250-Hz PRF, an insonication time of 60 s and MI of 0.53 or 1.05. (B) Cellular uptake of LoPEG/SDS/small NPs in live cells. The cells were exposed to ultrasound and MB-loaded NPs with pulse duration of 100 μs, 250-Hz PRF, an insonication time of 120s and MI of 0.53 or 1.05

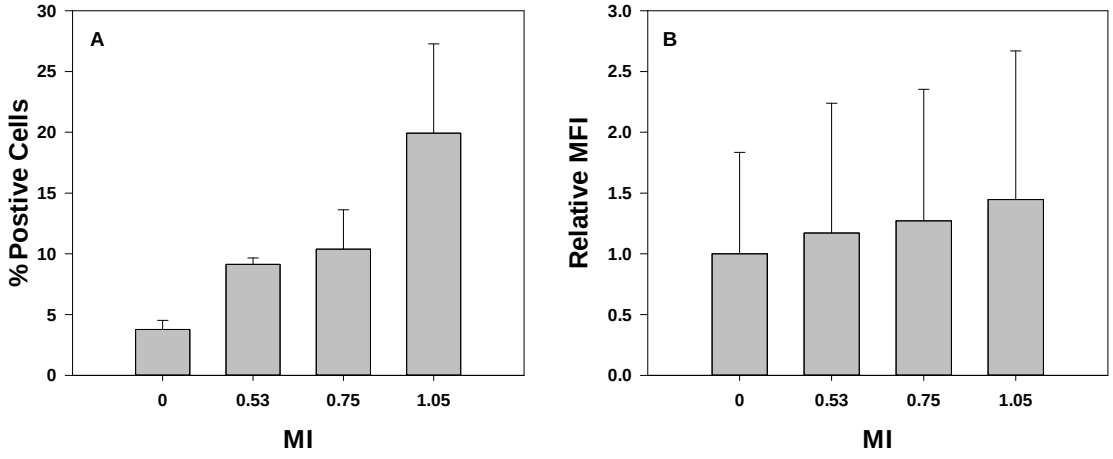

Fig. 8 The flow cytometric analysis of the cellular content of Tween-NPs. (A) Percentage of fluorescent cells as a function of MI. (B) Relative median fluorescence intensity (MFI) (relative to cells treated with NPs but not ultrasound) of the whole cell population as a function of the MI. The cells were exposed to ultrasound and MB-loaded NPs with pulse duration of 100 μs, 250-Hz PRF and an insonication time of 60 s. The data points are the mean of 2 measurements with standard deviation.

IV. DISCUSSION

Understanding the interaction between cells and NP is crucial to improve the delivery of NPs to intracellular targets. The interactions can be affected by the surface chemistry, size, shape, and morphology of the NPs. In the present study, the effect on cellular uptake of NP size, surface PEGylation and surfactant was studied. Two types of particles with the same surface properties and only differing in size (LoPEG/SDS/small, 109 nm and LoPEG/SDS/large, 178 nm) were found to be internalized into PC3 cells to the same extent. However, the difference in size might not be large enough to measure any effect of the size. From Fig. 5 it is evident that the cellular uptake rather depended on surface PEGylation and surfactant used. Generally, the kinetic study showed that NPs PEGylated with a linear PEG (Jeffamine) are taken up to a larger extent in PC3 cells compared to NPs PEGylated with a branched PEG (Tween80). Branched PEGs have, due to their larger hydrodynamic volume, been shown to cover a larger surface area compared to linear PEGs wherein the PEG will wrap around the NP more than the linear polymer [28-31].

This might explain why less Tween-NP was found on the surface of the cells compared to NPs covered with linear PEG when NPs were added to cells and washed immediately three times with PBS without incubation. Furthermore, NPs functionalized with long Jeffamine PEG were taken up to a larger extent compared to particles with short Jeffamine on the surface. The differences in the cellular uptake might be a result of differences in PEG density on the NP surface. The longer PEG chains might spatially hinder high amounts of this molecule from reacting with the monomer at the droplet surface upon polymerization. The grafting density of PEG has been shown to be highly dependent on the PEG molecular weight. Due to excluded volume effects, a large PEG chain cannot pack as tightly on the particle surface as a small PEG molecule [30]. Hence, the surface density of PEG might be

higher for particles with shorter PEG chains. This is also reflected in the zeta potential values (Table 1) where the NPs with short linear PEG are less negatively charged compared to NPs with longer PEG chains. Studies have shown that higher PEG density decreases cellular uptake [32-34]. The high negative zeta potential values are probably due to acid groups on the polymer particle surfaces, and may indicate that the PEGylation on the NP surface is not sufficient. The conformation and density of PEG on the particle surface is currently being investigated in our lab.

Finally, the influence of surfactant on the cellular uptake cannot be ruled out. Higher cellular uptake and higher uptake rate was demonstrated when SDS (anionic) surfactant was used for particle synthesis compared to those with Tween 80 (non-ionic) as surfactant (Fig. 3). This is in agreement with the result obtained by Musyanovych *et al* [35], where NPs with anionic surfactant were taken up at a higher rate than NP with non-ionic surfactant. Although excess surfactant should have been removed by the extensive dialysis, some surfactant might still be attached to the particle surface.

The cellular viability measurements show that PBCA NP concentration above 20µg/ml is toxic for the PC3 cell line. Although PBCA NPs have an advantage of being biocompatible and biodegradable, the data on toxicity is somewhat contradictory, and PBCA has in some studies shown to be toxic due to the degradation products (n-butanol and poly(cyanoacrylic acid) [27, 36-39]. Kreuter *et al* [36] demonstrated that at lower concentration (10-20µg/ml) of PBCA NPs there is little *in vivo* or *in vitro* evidence of toxicity on cerebral endothelial cells. This finding is in accordance with our results where little or no toxicity was found at concentration below 20µg/ml. Wessi *et al* [27] also reported that PBCA NPs exhibited cytotoxicity which is dependent on the polymer molar mass distribution. Apart from the degradation products, surfactant can also contribute to the level of toxicity since they are

known to influence cell permeability [39]. Finally, the density of the PEG coating can influence the degree of cytotoxicity [40].

Ultrasound exposure alone did not enhance the cellular uptake of NPs probably because of insufficient gas bubbles in the medium to cause cavitation to permeabilized the cells. However, exposing MB-loaded NPs (LoPEG/SDS/small or ShPEG/SDS) to ultrasound did not enhance cellular uptake either. The MBs stabilized with Tween80 NPs increased the number of cells internalizing NP to 20% at the highest MI applied, but the number of NP per cell was rather low and not significantly different from untreated cells. The mechanical strength of the MBs shell might be different depending on the type of NP used in forming the MB shell. This might also affect the acoustic properties of the MBs. Studies on the shell parameters of different NP-stabilized MBs is currently under investigation in our lab. Although up to 20% of the cells internalized the Tween-NP at the highest MI used, the number of NP per cell was rather low and not significantly different from untreated cells. The small uptake of NP might be caused by cavitation as also shown by others [41-45]. Thus, the oscillations or collapse of the MBs might have inflicted stress on the cells which in turn enhanced the permeability of the cell membrane. The main mechanisms involved in the US-induced uptake have been shown to be pore formation and enhanced endocytosis [41, 46]. The DLS measurements showed two distinct populations *i.e.*, 20 nm (perhaps micelles formed by Tween80 PEG) and 119 nm (Tween-NPs) and so, probably the smaller size NPs could be taken up by the cells, since ultrasound enhanced cellular uptake has been shown to favor smaller size molecules than larger size [41, 46]. Furthermore, the amount of molecules that can be internalized by the cell is reported to be dependent on the size and the number of pores [47]. This implies that the size of the pores that might have been created by the sonoporating bubbles was smaller than the size of the PBCA NP. In a previous study we found that ultrasound enhanced the uptake of dextrans of sized from 4kDa to 5MDa in the

presence of MB. Dextrans are smaller and might be more flexible and able to enter smaller pores than spherical NP. Our spherical NP might be too large to enter any pores formed by sonoporation. Also sonoporation is a reversible process [41, 42, 46-48], thus the pores created in the cell membrane is able to reseal or repair itself after few seconds to minutes. When the pore size is too big, resealing will not be possible and this can cause cell death.

V. CONCLUSION

In a nut shell, cellular uptake of PBCA NPs was found to be dependent on the type of PEG and surfactant on the surface of the NPs. Generally, NPs PEGylated with Jeffamine was taken up more than particles with Tween80. Also, NPs with long Jeffamine chain were found to have higher cellular uptake than particles with short Jeffamine. NPs with SDS surfactant demonstrated higher cellular uptake and higher uptake rate compared to those with AOT or Tween80. In addition, PBCA NPs exhibited dose-response toxicity on PC3 cell line and concentration above 20μg/ml was found to be toxic. The toxicity was dependent on the surfactant used, particles with Tween80 were found to be less toxic than those with SDS or AOT surfactant. Within the size range (rather small) studied in the current work, the size of particles had little effect on the uptake of nanoparticle and the effect was also influenced by effect of PEG and surfactant. Ultrasound exposure at 300 kHz did not increase the uptake of the NP in live cells, neither NP given alone nor NP surrounding MB.

ACKNOWLEDGEMENT

The authors wish to thank Kristin G. Sæterbø, Department of Physics, NTNU, for her assistance in the laboratory. This project is supported by the Schlumberger Foundation PhD Fellowship (Faculty for the Future).

REFERENCES

[1] Y. H. Bae, "Drug targeting and tumor heterogeneity," *Journal of Controlled Release,* vol. 133, pp. 2-3, 2009.

[2] F. Yuan*, et al.*, "Mirovascular Permeability and Interstitial Penetration of Sterically Stabilized (Stealth) Liposomes in a Human Tumor Xenograft," *Cancer Research,* vol. 54, pp. 3352-3356, July 1, 1994 1994.

[3] N. K. Reitan*, et al.*, "Characterization of tumor microvascular structure and permeability: comparison between magnetic resonance imaging and intravital confocal imaging," *J Biomed Opt,* vol. 15, p. 036004, May-Jun 2010.

[4] Y. Boucher and R. K. Jain, "Microvascular Pressure Is the Principal Driving Force for Interstitial Hypertension in Solid Tumors: Implications for Vascular Collapse," *Cancer Research,* vol. 52, pp. 5110-5114, September 15, 1992 1992.

[5] L. Eikenes*, et al.*, "Collagenase increases the transcapillary pressure gradient and improves the uptake and distribution of monoclonal antibodies in human osteosarcoma xenografts," *Cancer Res,* vol. 64, pp. 4768-73, Jul 15 2004.

[6] L. Eikenes*, et al.*, "Hyaluronidase induces a transcapillary pressure gradient and improves the distribution and uptake of liposomal doxorubicin (Caelyx) in human osteosarcoma xenografts," *Br J Cancer,* vol. 93, pp. 81-8, Jul 11 2005.

[7] L. Davies Cde*, et al.*, "Radiation improves the distribution and uptake of liposomal doxorubicin (caelyx) in human osteosarcoma xenografts," *Cancer Res,* vol. 64, pp. 547-53, Jan 15 2004.

[8] E. Hagtvet*, et al.*, "Ultrasound enhanced antitumor activity of liposomal doxorubicin in mice," *J Drug Target,* vol. 19, pp. 701-8, Sep 2011.

[9] W. G. Pitt*, et al.*, "Ultrasonic drug delivery--a general review," *Expert Opin Drug Deliv,* vol. 1, pp. 37-56, 2004.

[10] A. Schroeder*, et al.*, "Ultrasound, liposomes, and drug delivery: principles for using ultrasound to control the release of drugs from liposomes," *Chem Phys Lipids,* vol. 162, pp. 1-16, 2009.

[11] V. Frenkel, "Ultrasound mediated delivery of drugs and genes to solid tumors," *Adv Drug Deliv Rev,* vol. 60, pp. 1193-208, Jun 30 2008.

[12] T. G. Leighton, *The acoustic bubble*. London: Academic Press, 1994.

[13] T. G. Leighton, "What is ultrasound?," *Prog Biophys Mol Biol,* vol. 93, pp. 3-83, Jan-Apr 2007.

[14] W. L. M. Nyborg and J. Wu, *Emerging therapeutic ultrasound*. Hackensack, N.J.: World Scientific, 2006.

[15] F. R. Young, *Cavitation*. London: Imperial College Press, 1999.

[16] S. Fokong*, et al.*, "Image-guided, targeted and triggered drug delivery to tumors using polymer-based microbubbles," *Journal of Controlled Release*.

[17] T. Lammers*, et al.*, "Nanotheranostics and Image-Guided Drug Delivery: Current Concepts and Future Directions," *Molecular Pharmaceutics,* vol. 7, pp. 1899-1912, 2010/12/06 2010.

[18] I. Lentacker*, et al.*, "Design and evaluation of doxorubicin-containing microbubbles for ultrasound-triggered doxorubicin delivery: cytotoxicity and mechanisms involved," *Mol Ther,* vol. 18, pp. 101-8, Jan 2010.

[19] F. Yang, *et al.*, "Superparamagnetic iron oxide nanoparticle-embedded encapsulated microbubbles as dual contrast agents of magnetic resonance and ultrasound imaging," *Biomaterials,* vol. 30, pp. 3882-3890, 2009.

[20] F. Cavalieri, *et al.*, "Methods of preparation of multifunctional microbubbles and their in vitro / in vivo assessment of stability, functional and structural properties," *Curr Pharm Des,* vol. 18, pp. 2135-51, 2012.

[21] J. I. Park, *et al.*, "Microbubbles Loaded with Nanoparticles: A Route to Multiple Imaging Modalities," *ACS Nano,* vol. 4, pp. 6579-6586, 2010/11/23 2010.

[22] M. A. Wheatley, *et al.*, "Polymeric ultrasound contrast agents targeted to integrins: importance of process methods and surface density of ligands," *Biomacromolecules,* vol. 8, pp. 516-22, Feb 2007.

[23] M. S. Tartis, *et al.*, "Therapeutic effects of paclitaxel-containing ultrasound contrast agents," *Ultrasound in Medicine and Biology,* vol. 32, pp. 1771-1780, 2006.

[24] E. C. Unger, *et al.*, "Acoustically active lipospheres containing paclitaxel: A new therapeutic ultrasound contrast agent," *Investigative Radiology,* vol. 33, pp. 886-892, 1998.

[25] S. Fokong, *et al.*, "Image-guided, targeted and triggered drug delivery to tumors using polymer-based microbubbles," *Journal of Controlled Release,* 2012.

[26] E. Stride, *et al.*, "Increasing the nonlinear character of microbubble oscillations at low acoustic pressures," *J R Soc Interface,* vol. 5, pp. 807-11, Jul 6 2008.

[27] C. K. Weiss, *et al.*, "Cellular uptake behavior of unfunctionalized and functionalized PBCA particles prepared in a miniemulsion," *Macromol Biosci,* vol. 7, pp. 883-96, 2007.

[28] Y. Vugmeyster, *et al.*, "Pharmacokinetic, Biodistribution, and Biophysical Profiles of TNF Nanobodies Conjugated to Linear or Branched Poly(ethylene glycol)," *Bioconjugate Chemistry,* vol. 23, pp. 1452-1462, 2012/07/18 2012.

[29] J. B. Park, *et al.*, "PEGylation of bacterial cocaine esterase for protection against protease digestion and immunogenicity," *J Control Release,* vol. 142, pp. 174-9, Mar 3 2010.

[30] S. J. Sofia, *et al.*, "Poly(ethylene oxide) Grafted to Silicon Surfaces: Grafting Density and Protein Adsorption," *Macromolecules,* vol. 31, pp. 5059-70, Jul 28 1998.

[31] M. Wu, *et al.*, "Poly(n-butyl cyanoacrylate) nanoparticles via miniemulsion polymerization. 2. PEG-based surfactants," *Colloids and Surfaces B: Biointerfaces,* vol. 69, pp. 147-151, 2009.

[32] Y. Hu, *et al.*, "Effect of PEG conformation and particle size on the cellular uptake efficiency of nanoparticles with the HepG2 cells," *Journal of Controlled Release,* vol. 118, pp. 7-17, 2007.

[33] K. S. Soppimath, *et al.*, "Biodegradable polymeric nanoparticles as drug delivery devices," *Journal of Controlled Release,* vol. 70, pp. 1-20, 2001.

[34] J. V. Jokerst, *et al.*, "Nanoparticle PEGylation for imaging and therapy," *Nanomedicine (Lond),* vol. 6, pp. 715-28, Jun 2011.

[35] A. Musyanovych, *et al.*, "Criteria impacting the cellular uptake of nanoparticles: A study emphasizing polymer type and surfactant effects," *Acta Biomaterialia,* vol. 7, pp. 4160-4168, 2011.

[36] J. Kreuter, *et al.*, "Direct evidence that polysorbate-80-coated poly(butylcyanoacrylate) nanoparticles deliver drugs to the CNS via specific mechanisms requiring prior binding of drug to the nanoparticles," *Pharm Res,* vol. 20, pp. 409-16, 2003.

[37] J. C. Olivier, *et al.*, "Indirect evidence that drug brain targeting using polysorbate 80-coated polybutylcyanoacrylate nanoparticles is related to toxicity," *Pharm Res,* vol. 16, pp. 1836-42, 1999.

[38] J. C. Olivier, "Drug transport to brain with targeted nanoparticles," *NeuroRx,* vol. 2, pp. 108-19, 2005.

[39] V. Mailänder and K. Landfester, "Interaction of Nanoparticles with Cells," *Biomacromolecules,* vol. 10, pp. 2379-2400, 2009/09/14 2009.

[40] Y. Zhang*, et al.*, "Preparation, characterization and biocompatibility of poly(ethylene glycol)-poly(n-butyl cyanoacrylate) nanocapsules with oil core via miniemulsion polymerization," *European Polymer Journal,* vol. 44, pp. 1654-1661, 2008.

[41] M. Afadzi*, et al.*, "Mechanisms of the Ultrasound-mediated Intracellular Delivery of Liposomes and Dextrans," *IEEE Transactions on Ultrasonics, Ferroelectrics, and Frequency Control,* 2012.

[42] R. Karshafian*, et al.*, "Sonoporation by ultrasound-activated microbubble contrast agents: effect of acoustic exposure parameters on cell membrane permeability and cell viability," *Ultrasound Med Biol,* vol. 35, pp. 847-60, 2009.

[43] K. Kooiman*, et al.*, "Sonoporation of endothelial cells by vibrating targeted microbubbles," *Journal of Controlled Release,* vol. 154, pp. 35-41, 2011.

[44] Y. Qiu*, et al.*, "The correlation between acoustic cavitation and sonoporation involved in ultrasound-mediated DNA transfection with polyethylenimine (PEI) in vitro," *J Control Release,* vol. 145, pp. 40-8, Jul 1 2010.

[45] Y. Qiu*, et al.*, "Effect of microbubble-induced microstreaming on the sonoporation," *Shengxue Xuebao/Acta Acustica,* vol. 37, pp. 91-96, 2012.

[46] B. D. Meijering*, et al.*, "Ultrasound and microbubble-targeted delivery of macromolecules is regulated by induction of endocytosis and pore formation," *Circ Res,* vol. 104, pp. 679-87, Mar 13 2009.

[47] H. R. Guzman*, et al.*, "Equilibrium loading of cells with macromolecules by ultrasound: effects of molecular size and acoustic energy," *J Pharm Sci,* vol. 91, pp. 1693-701, 2002.

[48] A. Marin*, et al.*, "Drug delivery in pluronic micelles: effect of high-frequency ultrasound on drug release from micelles and intracellular uptake," *J Control Release,* vol. 84, pp. 39-47, 2002.

Addendum

After submitting the thesis, several experiments were conducted to investigate the fast uptake of nanoparticles by prostate cancer cells (fluorescence in cells). The results from these experiments show that free Nile red also was measured in the cellular uptake experiments presented in Paper IV. Thus, we think the percentage of cellular uptake measured was uptake of PBCA nanoparticles (containing Nile red) and free Nile red. This is because; Nile red could be transferred to the cells through contact-mediated transfer, *i.e.*, dissociation of Nile red from the nanoparticles as the particles come into contact with the cells [1] or directly from the cell culture medium.

References

1. Xu, P., et al., *Intracellular drug delivery by poly(lactic-co-glycolic acid) nanoparticles, revisited.* Mol Pharm, 2009. **6**(1): p. 190-201.